

RESEARCH ARTICLE

APETALA2 functions as a temporal factor together with BLADE-ON-PETIOLE2 and MADS29 to control flower and grain development in barley

Jennifer R. Shoesmith^{1,2}, Charles Ugochukwu Solomon^{3,4,*}, Xiujuan Yang^{5,*}, Laura G. Wilkinson^{5,6}, Scott Sheldrick¹, Ewan van Eijden¹, Sanne Couwenberg¹, Laura M. Pugh¹, Mhmod Eskan¹, Jennifer Stephens², Abdellah Barakate², Sinéad Drea³, Kelly Houston², Matthew R. Tucker^{5,‡} and Sarah M. McKim^{1,‡}

ABSTRACT

Cereal grain develops from fertilised florets. Alterations in floret and grain development greatly influence grain yield and quality. Despite this, little is known about the underlying genetic control of these processes, especially in key temperate cereals such as barley and wheat. Using a combination of near-isogenic mutant comparisons, gene editing and genetic analyses, we reveal that HvAPETALA2 (HvAP2) controls floret organ identity, floret boundaries, and maternal tissue differentiation and elimination during grain development. These new roles of HvAP2 correlate with changes in grain size and HvAP2-dependent expression of specific HvMADS-box genes, including the B-sister gene, *HvMADS29*. Consistent with this, gene editing demonstrates that *HvMADS29* shares roles with HvAP2 in maternal tissue differentiation. We also discovered that a gain-of-function *HvAP2* allele masks changes in floret organ identity and grain size due to loss of barley *LAXATUM.A/BLADE-ON-PETIOLE2* (*HvBOP2*) gene function. Taken together, we reveal novel pleiotropic roles and regulatory interactions for an AP2-like gene controlling floret and grain development in a temperate cereal.

KEY WORDS: Barley, AP2, Floret, Grain, CRISPR/Cas9, MADS-box, BOP1/2, B-sister, Nucellus, Integument

INTRODUCTION

Sex in angiosperms occurs in the flower, a complex structure of multiple organs, the coordinated growth of which leads to production of seed. Double fertilisation of the embryo sac within the ovary generates two filial seed tissues, the embryo and

endosperm, which proliferate and expand while enclosed by layers of maternal ovary tissue, including the proximal nutritive nucellus and the more distal integuments that form the protective seed coat (Wilkinson et al., 2018). The grass flower or ‘florete’ ovary is additionally encircled by the ovary wall or pericarp, which, with the underlying maternal and filial tissues, grows into the grain fruit or ‘caryopsis’. The caryopsis isotopically expands following fertilisation and then elongates and swells to fill the cavity between opposing floret hulls (Brinton and Uauy, 2019). Several genes that regulate ovary, nucellus, integument, pericarp and/or hull development also influence grain size (Song et al., 2007; Yin and Xue, 2012; Brinton et al., 2017; Ren et al., 2018; Zhao et al., 2018; Wilkinson et al., 2019). However, the mechanism used by these genes to influence grain size is poorly understood. This problem has major translational significance in cultivated cereal grasses, the endosperm of which provides more calories than any other source to the human diet.


Learning more about the genetic and functional networks in the floret and grain may help to dissect this problem. Each floret arises from a floret meristem made by the spikelet, the basic reproductive unit of grasses. Floret meristems form opposing lemma and palea hulls which enclose the stamens and single-ovary carpel (Schrager-Lavelle et al., 2017). Small sacs called lodicules develop between the lemma and stamens, which enlarge at anthesis (pollen shed), prising open the lemma to facilitate pollen transfer (Kellogg, 2015). Molecular patterns controlling floret morphogenesis appear to be partially conserved, with the ABCDE gene combinatorial model proposed to explain flower development in dicots such as *Arabidopsis thaliana* (Schrager-Lavelle et al., 2017). In the *Arabidopsis* flower, activity of class ‘A’ genes defines the outer perianth (sepals), ‘AB’ the inner perianth (petals), ‘BC’ the stamens, ‘C’ the carpel and ‘CD’ the ovule, with the ‘E’ class genes contributing to all other class functions (Theißen et al., 2016; Irish, 2017). Other than the ‘A’ class *APETALA2* (*AP2*) gene, the ABCDE genes encode MADS-box transcription factors. Orthologous MADS-box expression in rice suggests that the palea and lemma are analogous to sepals (Lombardo and Yoshida, 2015), whereas the lodicules are highly derived petals (Yoshida, 2012). Lemma formation also represents a commitment of the axillary meristem to floret fate (Arber, 2010; Kellogg, 2015). Thus, grass perianth development involves decisions about organ identity and spikelet versus floret fate.

Specific genes establishing floret and organ identity in grasses are not completely resolved, especially in temperate cereals such as barley and wheat that develop unbranched ‘spike’ inflorescences. However, the A-class *APETALA2*-like (*AP2L*) genes and their regulation by microRNA172 (*miR172*) appear to play a central role. In spikes, spikelets directly attach to the spike axis at alternating nodes

¹Division of Plant Sciences, School of Life Sciences, University of Dundee at the James Hutton Institute, Invergowrie DD2 5DA, UK. ²Cell and Molecular Sciences, The James Hutton Institute, Invergowrie DD2 5DA, UK. ³Department of Genetics and Genome Biology, University of Leicester, University Road, Leicester LE1 7RH, UK. ⁴Department of Plant Science and Biotechnology, Abia State University, PMB 2000, Uturu, Nigeria. ⁵Waite Research Institute, School of Agriculture, Food and Wine, University of Adelaide, Waite Campus, Urrbrae, SA, 5064, Australia. ⁶Crop Genetics, John Innes Centre, Norwich Research Park, Norwich NR4 7UH, UK.

*These authors contributed equally to this work

‡Authors for correspondence (smckim@dundee.ac.uk; matthew.tucker@adelaide.edu.au)

 J.R.S., 0000-0001-5178-6734; C.U.S., 0000-0002-6462-3384; X.Y., 0000-0001-9340-3551; L.G.W., 0000-0002-8379-7080; S.S., 0000-0002-0724-5348; E.V.E., 0000-0002-3429-6984; S.C., 0000-0002-6805-2806; J.S., 0000-0002-5761-9782; A.B., 0000-0002-7628-6741; M.R.T., 0000-0003-4661-6700; S.M.M., 0000-0002-8893-9498

flanked by two bract-like glumes. In wheat, *miR172*-resistant alleles of *TaAP2L5* (the *Q* domestication gene) or *TaAP2L2* cause glume-to-lemma transformations, ectopic florets and compact spikes, whereas overexpression of *miR172*, or loss of *TaAP2L5* or *TaAP2L2* function, leads to longer spike internodes, glume-like lemmas and reiterations of empty glumes (Simons et al., 2006; Sormacheva et al., 2015; Debernardi et al., 2017, 2020; Greenwood et al., 2017). These phenotypes suggest that *TaAP2Ls* promote lemma identity and floret establishment, a role partially conserved in rice based on loss-of-function phenotypes of the *SUPERNUMERARY BRACT* (*SNB*) and *INDETERMINATE SPIKELET1* (*IDS1*) AP2L-genes (Lee et al., 2007; Lee and An, 2012; Ji et al., 2019). In barley, a gain-of-function *HvAP2* allele called *Zeol1.b* disrupts *miR172*-directed *HvAP2* transcript cleavage, elevating *HvAP2* transcript levels and leading to small, non-swelling lodicules, semi-dwarfism and dense spikes (Houston et al., 2013; Patil et al., 2019). We do not know whether *HvAP2* fulfils similar roles as *TaAP2L5* or *TaAP2L2* in floret establishment or organ identity. The only gene currently identified that controls floret organ identity in barley is the *LAXATUM.A/HvBLADE-ON-PETIOLE2* (*HvBOP2*) gene encoding a transcription factor necessary for lodicule identity and repression of spike internode elongation (Jost et al., 2016). The regulatory mechanism(s) of *HvBOP2* and its relationship to *HvAP2* or the ABCDE model are unknown.

AP2L genes also regulate post-fertilisation development across different plants. In *Arabidopsis*, *AtAP2* restricts integument cell expansion, seed size and seed mass (Modrusan et al., 1994; Jofuku et al., 1994; Ohto et al., 2005) and in rice, *SNB* limits grain size and weight, a role associated with constraining floret hull cell expansion (Jiang et al., 2019; Ma et al., 2019). Whether AP2L genes also control post-fertilisation development in temperate cereals is unexplored. Here, we identify and characterise a new *HvAP2* allele in the barley Bowman Near-Isogenic Line (BWNIL) mutant population (Druka et al., 2011) and generate additional alleles by gene editing to reveal both conserved and novel roles for *HvAP2* in floret and grain development.

RESULTS

BW381 (*gigas1.a*) shows altered floret organ identity and growth

To learn more about *HvAP2*, we screened the BWNILs for loss-of-function *HvAP2* alleles, focusing on mutants with introgressions that overlapped *HvAP2* (Druka et al., 2011; Houston et al., 2013). We selected the BW381 line containing the *gigas1.a* locus (Greek for giant), originally isolated in the cultivar Golden Melon (Tsuchiya, 1962; Franckowiak, 1995; Druka et al., 2011; Table S1). BW381 (hereafter called *gigas1.a*) showed multiple elongated features compared with the recurrent parent cultivar Bowman (Fig. 1; Table S2). Spike internodes were longer ($P=0.036$), causing less dense, or laxatum, spikes, glumes were 20% longer ($P=0.028$) and lemmas and paleas were 50% longer ($P\leq 0.001$), shifting the *gigas1.a* spikelet shape from wedge to lance-shaped (Fig. 1A-D,F,G; Fig. S1A-C; Table S2). Adaxial lemma epidermal cell length in *gigas1.a* was increased 52% compared with Bowman ($P\leq 0.001$, Fig. S1D), suggesting that increased cell elongation explained longer *gigas1.a* lemmas, although these cells were also 16% wider compared with Bowman ($P\leq 0.001$; Fig. S1E). In Bowman and most cultivated barleys, lemma and glume tips have thin projections called awns; the lemma awn is longer, with a distinct boundary from the lemma (Fig. 1C,E). Glume awns in *gigas1.a* were 50% longer compared with those of Bowman ($P<0.001$; Fig. 1C,E,G; Table S2) yet lemma awns in *gigas1.a* were 23% shorter ($P\leq 0.001$), with a less

distinct lemma-awn boundary (Fig. 1C,E,F; Table S2), two glume awn-like features. Lodicules in *gigas1.a* developed ectopic distal lamina (Fig. 1H,I), associated with extreme open-flowering (Fig. S1F), and were decorated with glume-like hairs (Fig. 1J; Fig. S1G,H). We observed that *gigas1.a* stigmas had fewer, shorter papillae branches in contrast to feathery ‘plumose’ stigmas of Bowman (Fig. 1K), which may contribute to reduced seed set in *gigas1.a*, as previously reported (Tsuchiya, 1962). Grain length in *gigas1.a* mirrored the longer hulls and increased by 47% compared with Bowman ($P\leq 0.001$; Fig. 1L-N; Table S2). Pericarp epidermal cells in *gigas1.a* were only 16% longer compared with Bowman, as well as 23% wider ($P\leq 0.001$; Fig. S2B,C), suggesting that changes in grain length likely involves increases in cell size and cell number. However, *gigas1.a* thousand grain weight (TGW) increased only 7%, as *gigas1.a* grain was also narrower and thinner compared with Bowman ($P\leq 0.001$; Fig. 1M; Fig. S2; Table S2), although its lemma width was unchanged (Fig. S1A). Caryopses in *gigas1.a* were darker than Bowman (Fig. 1M), suggesting increased proanthocyanidins in the seed coat (Aastrup et al., 1984). We re-examined *Zeol1.b* for additional phenotypes, finding that *Zeol1.b* glumes often transform into lemmas (Fig. 1O) and that *Zeol1.b* grain is 8% wider compared with Bowman ($P\leq 0.001$; Fig. S2; Table S2). Although we did not observe differences in cell length or width in the adaxial lemma of *Zeol1.b*, the pericarp cells were 52% wider compared with Bowman ($P\leq 0.001$; Fig. S2C), suggesting that *HvAP2* promotes medial cell expansion in the barley pericarp. Taken together, elongated glume-like organs, expanded cells, lax spikes, open-flowering and longer grain of *gigas1.a* contrasted with the closed-flowering, compressed growth, glume-to-lemma transformation and wider grain of *Zeol1.b*.

gigas1.a phenotypes result from a deletion of *HvAP2*

Given the opposing phenotypes to *Zeol1.b*, we speculated that *gigas1.a* may be a loss-of-function *HvAP2* allele. To clone the locus, we first placed the BOPA2 markers associated with the *gigas1.a* introgression on the physical map (Mascher et al., 2017), which located a Golden Melon introgression on 2H between 710843099 bp and 758851055 bp (Fig. S3). Testing *gigas1.a* genomic DNA on the barley 50K iSelect SNP Array (Bayer et al., 2017) identified a slightly larger area on 2H from 710163110 bp to 760762651 bp (Fig. 2A; Table S3). SNPs starting after 729506693 bp and ending between 730687131 bp and 730852717 bp on 2H were present in Golden Melon and Bowman, but appeared as missing in *gigas1.a*, and demarked an area encompassing *HvAP2* (HORVU2Hr1G113880.23) and six other high-confidence genes (Fig. 2A; Tables S3,S4). Using *gigas1.a* genomic DNA, we successfully amplified two genes outside this region but could not amplify *HvAP2* or two other genes in this region (Fig. S3). We detected *HvAP2* transcripts in Bowman and *Zeol1.b* spikes but not in *gigas1.a* (Fig. 2B). Collectively, our evidence suggests that a deletion on 2H in *gigas1.a* removed *HvAP2* and at least six other genes.

To our knowledge, *gigas1.a* was the only available *gigas1* allele. To confirm that *gigas1.a* phenotypes do not result from the deletion of genes other than *HvAP2*, we targeted the *HvAP2* gene using CRISPR/Cas9 gene editing. We transformed Golden Promise with two binary vectors containing the barley codon optimised Cas9 (*bcoCas9*) sequence and one guide RNA sequence targeting *HvAP2* sequences upstream of those encoding the first AP2 DNA-binding domain (Fig. 2C). Screening 18 independent T₁ transformants identified two new *HvAP2* alleles, *hvap2-1* and *hvap2-2*, with 39 bp and 40 bp deletions, respectively, in the first exon (Fig. 2C). The *hvap2-1* deletion (175 bp to 214 bp relative to the coding sequence start) removed 13 amino acids (residues 60-73) before the first AP2 domain in the predicted protein but kept the remaining sequence in

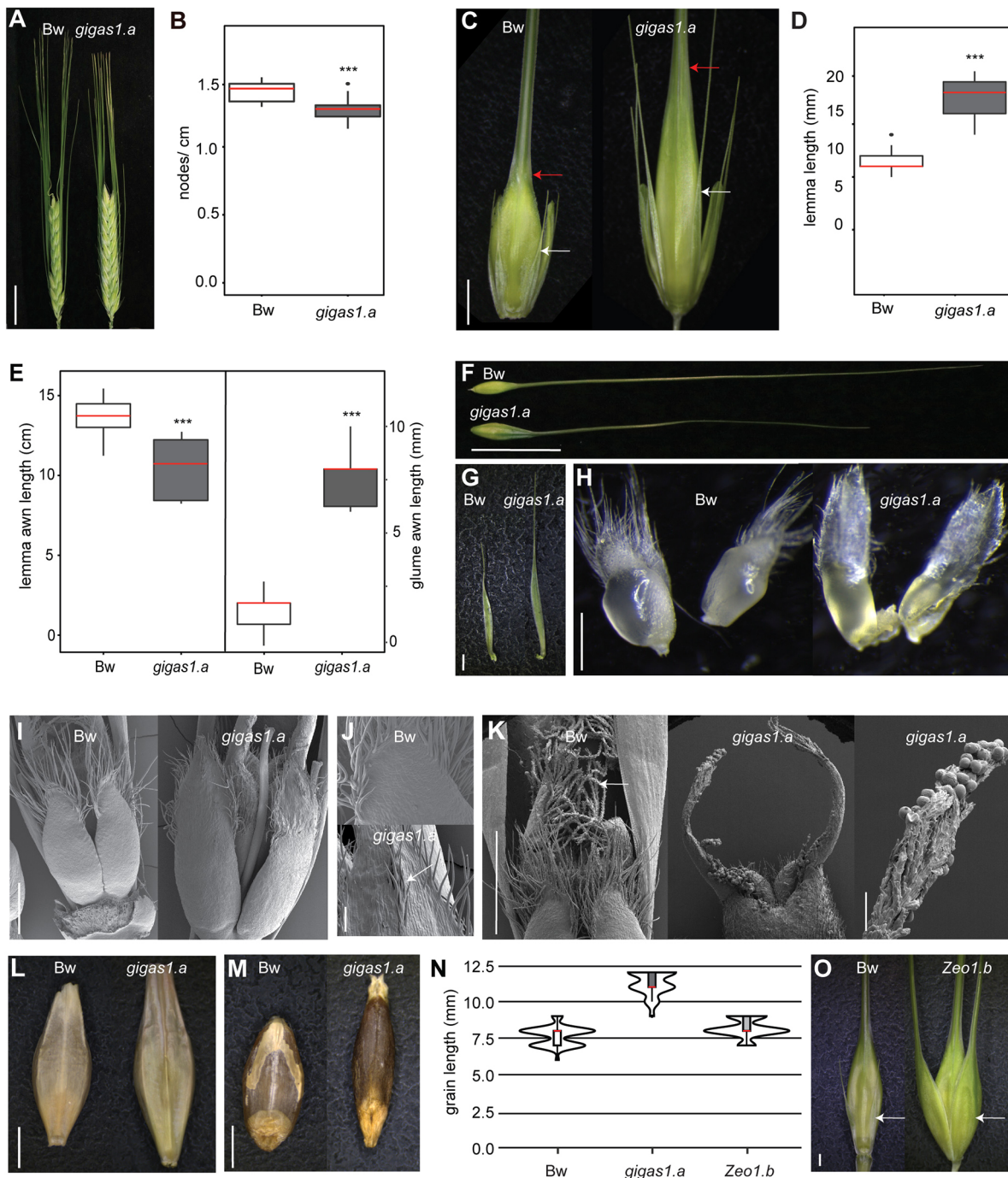


Fig. 1. *gigas1.a* mutants show altered reproductive organ and grain morphology. (A-H) Bowman (Bw) and *gigas1.a* spikes (A); spike density (nodes/cm) (B); spikelets (C; white arrows show distal end of the lemma and red arrows denote the awn-lemma boundary); lemma length (D); length of awn length on lemmas (left) and glumes (right) (E); lemmas (F); glumes (G); lodicules (H). (I) Scanning electron micrographs (SEMs) of Bowman and *gigas1.a* lodicules. (J) SEMs showing ectopic hairs on *gigas1.a* lodicules (arrow). (K) SEMs of Bowman and *gigas1.a* stigmas. Arrow points to stigma hairs on Bowman. Right panel shows a magnification of a single *gigas1.a* stigma lacking hairs. (L,M) Bowman and *gigas1.a* hull covered (L) and hull removed (M) grains. (N) Violin plots of Bowman ($n=97$), *gigas1.a* ($n=69$) and *Zeo1.b* ($n=72$) grains show the probability distribution of grain length. (O) *Zeo1.b* spikelets show glume-to-lemma conversion (white arrows indicate glume position organ). Box and violin plots (B,D,E,N) show 25th and 75th percentile, red line shows the median, whiskers show 1.5 \times the interquartile range. *** $P<0.001$ (t -test, two-tailed unpaired). (B,D,E) $n=8$ /genotype. Scale bars: 2 cm (A,F); 2 mm (C,G,L,M); 500 μ m [(I,J,K (left and centre)); 100 μ m (K, right); 1 mm (N)].

frame (Fig. 2C). We observed no obvious morphological differences in *hvp2-1* compared with Golden Promise (Fig. 2D-F). The *hvp2-2* deletion (175 bp-215 bp) removed the same 13 amino acids but also caused a frame shift and a premature stop codon in exon 5 (368 bp), predicted to significantly impair HvAP2 function (Fig. 2C). The

hvp2-2 mutant largely phenocopied *gigas1.a*, with longer lemmas ($P\leq 0.001$), lax spikes ($P=0.005$) and long, slender grain compared with Golden Promise (Fig. 2D,E; Fig. S4; Table S3). We note that, in this experiment, *gigas1.a* had marginally wider lemmas compared with Bowman ($P<0.05$; Fig. S4A). Lodicules in *hvp2-2* were larger,

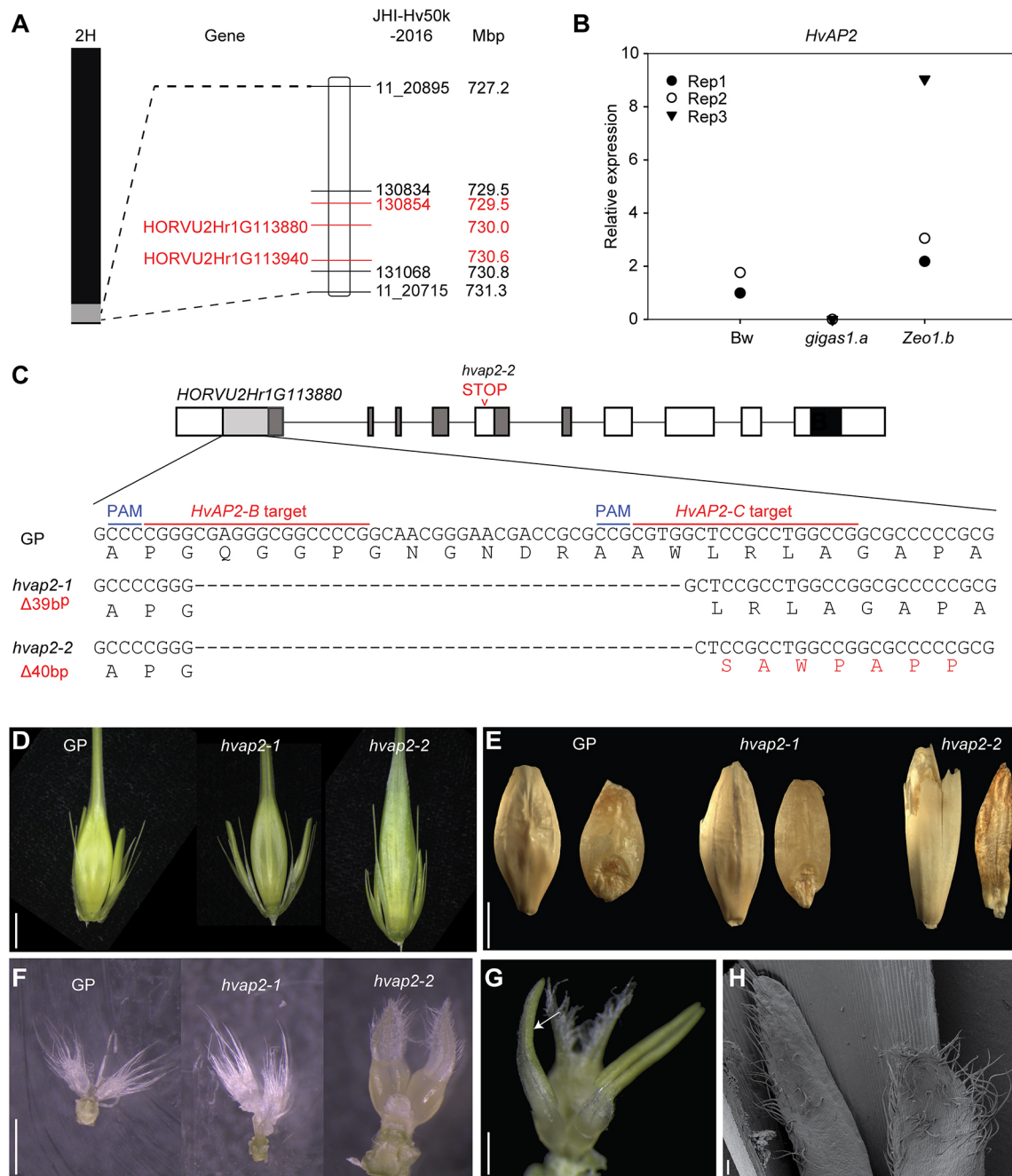


Fig. 2. Mapping of *gigas1.a* and gene editing of *HvAPETALA2*. (A) Grey block on chromosome 2H indicates introgression from Golden Melon in *gigas1.a* BW381. JHI-50k-2016 SNP markers and genes shown along with their physical position (Mbp). Missing markers (red) delineate a 1.3 Mbp deletion overlapping seven high confidence gene models, including *HORVU2Hr1G113880* (*HvAP2*) and *HORVU2Hr1G113940*. (B) RT-qPCR of *HvAPETALA2* (*HvAP2*) transcripts in Bowman, *gigas1.a* and *Zeo1.b* spikes. Individual points are independent biological replicates. (C) *HvAP2* gene model with sequences targeted by guide RNAs (light grey), those encoding the *APETALA2* DNA binding domains (dark grey) and *miR172* binding site (black). Nucleotides 167 to 239 and their corresponding protein sequences shown underneath for Golden Promise (GP), *hvacp2-1* and *hvacp2-2*. Lines over GP sequence indicate guide RNA target (red) and protospacer adjacent motif (PAM, blue). Dashes indicate deleted bases and triangles indicate deletion length in *hvacp2-1* and *hvacp2-2*. (D-H) Phenotypes of GP, *hvacp2-1* and *hvacp2-2*. (D) Spikelets. (E) Grains with hull on (left) and removed (right). (F) Lodicules. (G) Arrow shows transformation of lodicule to bract in *hvacp2-2*. (H) Scanning electron micrograph showing ectopic hairs on *hvacp2-2* lodicules. Scale bars: 2 mm (D,E); 1 mm (F); 100 μ m (H).

extended and swollen compared with the non-swelling lodicules of Golden Promise (Fig. 2F), a cleistogamous cultivar with the *Zeo2* allele (Houston et al., 2013). Green organs with a hybrid composition of stamen-like filaments and smooth and hairy bract-like regions replaced the lodicules in 3% of *hvacp2-2* florets (Fig. 2G,H), a more severe loss of lodicule identity compared with *gigas1.a*, potentially reflecting the different cultivar backgrounds. Overall *hvacp2-2* closely

phenocopied *gigas1.a*, corroborating that *gigas1.a* phenotypes result from deletion of *HvAP2* alone. Thus, we propose that *HvAP2* defines the boundary between the glume and lemma (outer perianth), promotes floret perianth identity, increases stigmatic papillae branching and widens grain, while also restricting longitudinal growth of spike internodes, spikelets, floret organs and grain.

HvAP2 functions during early floral development

We compared early spikelet development in Bowman, *Zeo1.b* and *gigas1.a* to understand when and how HvAP2 influences organ identity. We staged floret organ development using the Waddington (WD) stages (Waddington et al., 1983). WD4 stage *Zeo1.b* spikelets exhibited wider glumes than Bowman, leading to two interlocking lemma-like organs (Fig. 3A) which later overgrew the floret lemma (Fig. 3B). Lodicule primordia emerged similarly in Bowman, *gigas1.a* and *Zeo1.b* at WD4. By WD5.5, WD7 and later, Bowman lodicules displayed distinct proximal cushion and distal fringe tissues (Fig. 3C; Fig. S5). In contrast, *gigas1.a* lodicules were flatter

with distal extensions whereas *Zeo1.b* lodicules remained small, lacked cushions and formed hairs (Fig. 3C; Fig. S5). These data suggest that HvAP2 and its *miR172*-regulation between WD4 and WD7 influence early spikelet differentiation.

AtAP2 controls *Arabidopsis* floral organ development in part through regulating MADS-box gene expression (Drews et al., 1991; Yant et al., 2010; Dinh et al., 2012). We hypothesised that HvAP2 also controls floral development by modulating target gene(s) expression. We selected candidate HvMADS-box genes based on their predicted function, AP2-like binding motifs in their regulatory regions, expression in relevant tissues and whether they were

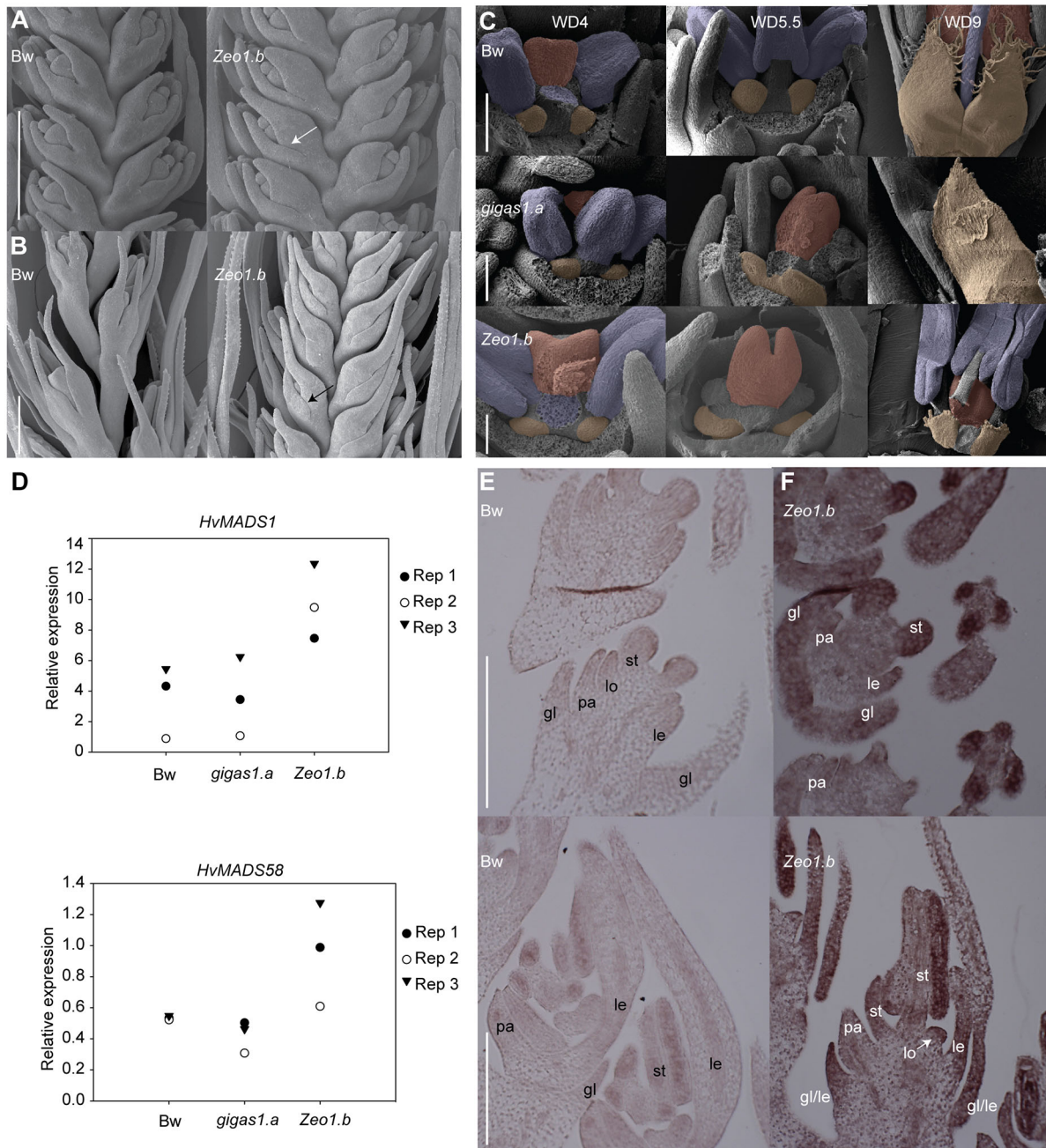


Fig. 3. HvAPETALA2 regulates early spikelet organogenesis and gene expression. (A,B) Scanning electron micrographs (SEMs) of Bowman and *Zeo1.b* spikelets at Waddington stage 4 (WD4; A) and WD5.5 (B). Arrows point to homeotic glume-to-lemma conversions in *Zeo1.b*. (C) SEMs of WD4, WD5.5 and WD9 Bowman, *gigas1.a*, and *Zeo1.b* with lemmas removed and inner floret primordia false coloured: lodicules, yellow; stamens, blue; carpel, red. (D) qRT-PCR of *HvMADS1* and *HvMADS58* mRNA in Bowman, *Zeo1.b* and *gigas1.a* spikelets. Individual points are independent biological replicates. (E,F) *In situ* hybridisation of *HvMADS1* probe at WD4 (E) and WD7 (F). gl, glume; le, lemma; lo, lodicule; pa, palea; st, stamen. Scale bars: 1 mm (A,E,F); 0.5 mm (B); 100 μ m (C).

differentially expressed in our earlier *Zeo1.b* microarray study (Figs S6,S7; Table S5; Patil et al., 2019). Our top candidate was *HvMADS1* (HORVU4Hr1G067680.2). The *HvMADS1* orthologue in rice, *OsMADS1* [*LEAFY HULL STERILE (LHS1)*] promotes lemma and lodicule identity and differentiation, transforms glumes into lemmas when overexpressed and causes glume-like lemmas and elongated bract-like lodicules when downregulated (Prasad et al., 2001, 2005). *HvMADS1* is expressed in differentiating spikelets, lemmas and lodicules (Fig. S7) and co-expressed with *HvAP2* in RNA-seq datasets of spikelet development (Digel et al., 2015). We sampled developing spikes in Bowman, *gigas1.a* and *Zeo1.b* genotypes, normalising expression to Bowman. *HvMADS1* expression increased in all genotypes between WD3.5 and WD4.0, suggesting this temporal pattern is independent from *HvAP2*. Overall, *HvMADS1* transcripts were little changed in *gigas1.a*, so factors other than *HvAP2* likely contribute to *HvMADS1* expression in *gigas1.a*. However, we detected increased *HvMADS1* expression in *Zeo1.b* WD4 and WD5.5 spikes compared with Bowman (Fig. 3D; Fig. S8). *In situ* hybridisation with an antisense *HvMADS1* probe gave a strong signal in young and older *Zeo1.b* spikelets compared with Bowman, especially within developing glumes, lemma/palea, lodicule and stamen primordia (Fig. 3E,F). These data support the suggestion that ectopic *HvAP2* promotes *HvMADS1* expression, potentially explaining the glume-to-lemma transformations in *Zeo1.b*.

Other potential *HvAP2* targets include *HvMADS2* (HORVU3Hr1G091000.8) and *HvMADS4* (HORVU1Hr1G063620.2), the orthologue of which, the ‘B’ class *PISTILLATA (PI)* gene, is a direct target of *Arabidopsis AtAP2* (Krogan et al., 2012). *HvMADS2* expression increased in *gigas1.a* at WD5, and *HvMADS4* expression showed no *HvAP2*-dependent differences (Fig. S8). We also examined the expression of *HvMADS3* (HORVU3Hr1G026650.1) and *HvMADS58* (HORVU1Hr1G029220.1), two *AGAMOUS-like* genes, the orthologues of which in *Arabidopsis* are direct targets of *AtAP2* (Zhao et al., 2007; Yant et al., 2010; Ripoll et al., 2011). *HvMADS3* was lower in *Zeo1.b* at WD5 and *HvMADS58* expression was lower in *gigas1.a* at WD4 compared with Bowman and *Zeo1.b* (Fig. 3D; Fig. S8). Reduced *HvMADS58* expression could contribute to *gigas1.a* lodicule and pistil phenotypes, as *OsMADS58* is essential for carpel and lodicule identity in rice (Yamaguchi et al., 2006; Dreni et al., 2011). Altogether, our comparative gene expression analyses link *HvAP2*-dependent changes in floral organ development with a specific MADS-box gene misexpression. Whether this relationship is direct is unknown.

HvAP2 promotes maternal tissue degeneration during caryopsis development

To learn when *HvAP2* alters grain parameters, we tracked changes in pre-anthesis ovary and caryopsis dimensions at days post anthesis (DPA). Depth was measured along the dorsal:ventral axis. Compared with Bowman, *gigas1.a* ovaries were 12% longer, 20% wider, 24% deeper (all $P < 0.001$) and 70% lighter ($P < 0.01$; Fig. 4A,B; Fig. S9; Table S6). Post-fertilisation, *gigas1.a* caryopses became 36% and 55% longer at 10 and 30 DPA, respectively, ($P < 0.001$) and remained narrower during most growth ($P < 0.05$; Fig. 4A,B; Table S6). Caryopses in *gigas1.a* were 9–16% shallower at 15–25 DPA ($P < 0.05$) and 10–50% lighter ($P < 0.01$) compared with Bowman until final stages (Fig. S9; Table S6). Pre-anthesis, *Zeo1.b* ovaries were 16% deeper ($P < 0.001$), 6% shorter ($P < 0.001$) and 36% lighter ($P < 0.01$) and, following fertilisation, *Zeo1.b* caryopses at 5 DPA were 30% shorter ($P < 0.05$) and afterwards showed no clear length or depth trend but became progressively heavier (Fig. 4A; Table S6). *Zeo1.b*

caryopses were 20% wider ($P < 0.001$) and 10% heavier ($P < 0.01$) than Bowman by 30 DPA (Table S6). Overall, *HvAP2* activity positively correlated with wider and heavier grain during grain fill, whereas loss of *HvAP2* function lengthened and narrowed grain.

We examined transverse sections of developing caryopses to explore potential causes of *HvAP2*-dependent differences. Bowman caryopses showed a dumbbell-shaped embryo sac with dorsal indentations at 5 DPA, whereas the *gigas1.a* embryo sac was rectangular-shaped and the *Zeo1.b* embryo uniformly oval (Fig. 4C). Variation in embryo sac shape correlated with differences in the lateral and dorsal mesocarp provascular strands, structures that supply nutrients to the pericarp before degenerating (Fisher, 1990). Caryopses from *gigas1.a* displayed provascular strands, Bowman showed remnants of provascular strands and *Zeo1.b* lacked any trace of provascular strands (Fig. 4C), suggesting that *HvAP2* accelerates provascular degeneration, potentially influencing the shape of the expanding embryo sac. The nucellar projection, a specialised structure that differentiates from the nucellus, also differed amongst alleles. Flanked by a pigment strand and vascular bundle, the nucellar projection transports nutrients from maternal to filial tissues before undergoing programmed cell death (PCD), leaving a large cavity (Radchuk et al., 2006; Thiel et al., 2008; Domínguez and Cejudo, 2014; Lu and Magnani, 2018). At 10 DPA, nucellar projection degeneration was least noticeable in *gigas1.a*, whereas *Zeo1.b* showed more breakdown compared with Bowman, with corresponding differences in cavity size (Fig. 4D). Thus, *HvAP2* may promote breakdown of nucellar tissues. We also detected differences in the integuments across *HvAP2* alleles. Grass ovules have outer and inner integuments, and the outer integument degrades rapidly following fertilisation (Kellogg, 2015). At 5 DPA, Bowman and *Zeo1.b* showed the two-layered inner integument, whereas *gigas1.a* had inner integuments plus multiple layers of enlarged integument-like cells, which may be a non-degraded outer integument (Fig. 4E). By 10 DPA, the inner integuments of Bowman and *Zeo1.b* were crushed, along with most of the nucellar epidermis, to form the seed coat (Fig. 4F). At 10 DPA, the inner integuments and nucellar epidermis of *gigas1.a* also compressed into the seed coat, but the extra integument-like layers persisted, separated from the pericarp by a prominent cuticle (Fig. 4F). Altogether, loss of *HvAP2* function inhibited or profoundly delayed the degradation of multiple maternal tissues while gain of *HvAP2* function promoted the degradation of multiple maternal tissues. We propose that *HvAP2* is a crucial negative regulator of maternal tissue growth and survival during grain development.

We asked whether *HvAP2* expression correlated with its proposed roles in the grain. *HvAP2* transcripts localise to lodicule primordia as well as the lemma and glume (Nair et al., 2010; Anwar et al., 2018) but the *HvAP2* expression pattern in grain has yet to be reported. We detected *HvAP2* mRNA in the lemma and pre-anthesis ovary, and concentrated expression in the vascular bundle, pigment strand and nucellar projection at 2 DPA (Fig. 4G; Fig. S10). By 5 and 10 DPA, *HvAP2* transcripts persisted in remaining nucellar tissues, seed coat and pericarp (Fig. 4G). Taken together, *HvAP2* transcripts accumulate in tissues altered owing to *HvAP2* allelic variation.

We used qPCR to examine expression levels of potential downstream genes in the developing grain. We were particularly interested in *HvMADS29* (HORVU6Hr1G032220), a gene almost exclusively expressed in young grain (Fig. S7) and the orthologue of a B-sister gene (the closest relatives of B-class genes) in rice called *OsMADS29*. Downregulation of *OsMADS29* in rice inhibits degradation of all maternal tissues, including the nucellus and

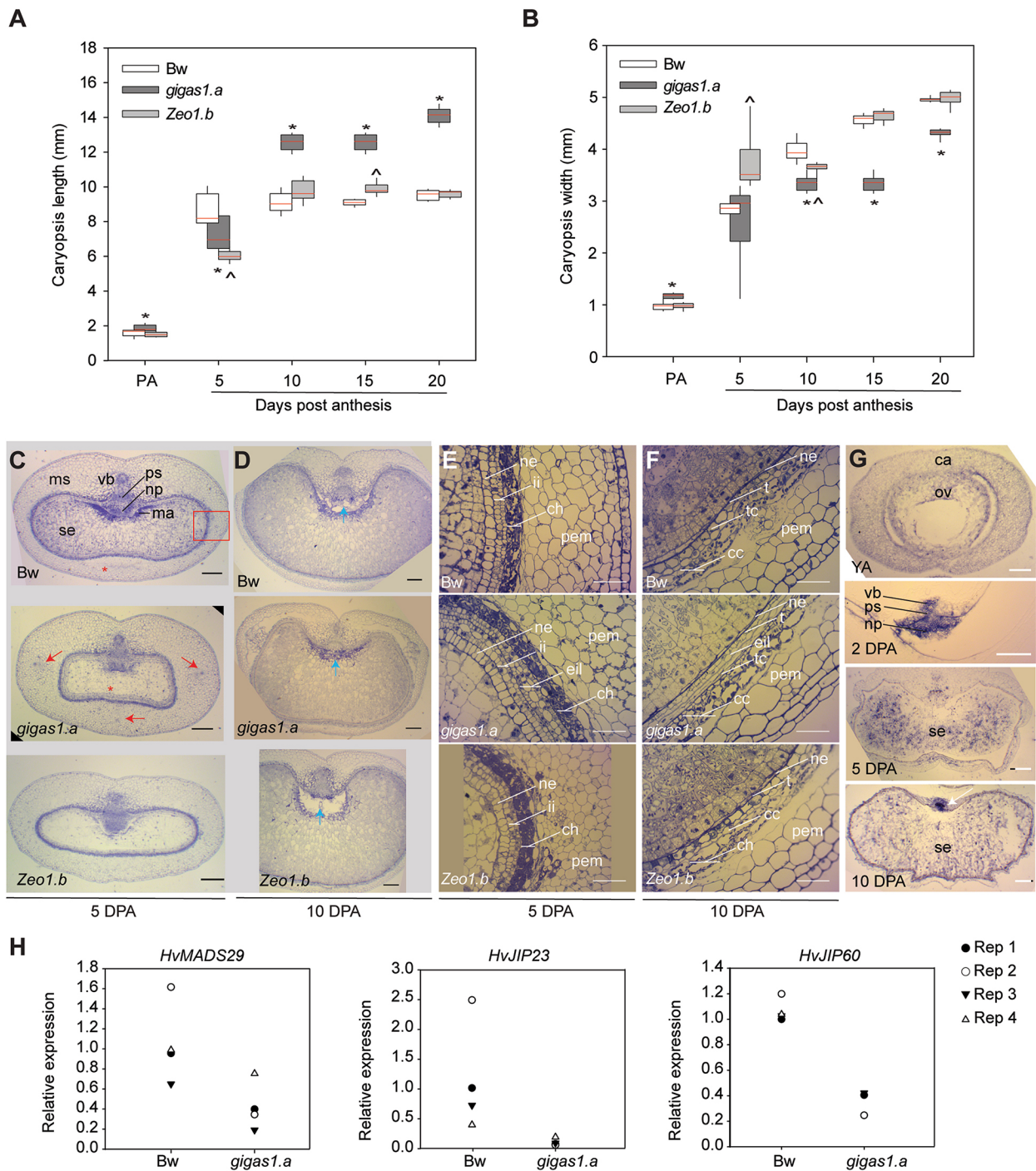


Fig. 4. *HvAPETALA2* alleles influence grain maturation and gene expression. (A,B) Bowman, *gigas1.a* and *Zeo1.b* caryopses parameters measured at pre-anthesis (PA) and days post anthesis (DPA), showing caryopsis length (A) and width (B). (C-F) Grain ultrastructure in Bowman, *Zeo1.b* and *gigas1.a* at 5 DPA (C,E) and 10 DPA (D,F). Red arrows show provascular strands, red asterisks show provascular strands, red box indicates region at higher magnification in D (C) and blue arrows show degradation of the nucellar projection (D). (G) *HvAP2* *in situ* hybridisation in pre-anthesis spikelets (top panel) and caryopses. (H) qRT-PCR of *HvMADS29*, *HvJIP23* and *HvJIP60* mRNA in Bowman and *gigas1.a* caryopses at 5 DPA. Individual points are independent biological replicates. ca, carpel; cc, cross cells; ch, chlorenchyma; eil, extra integument layer; ii, inner integument; ma, maternal aleurone; ms, mesocarp; ne, nucellus epidermis; np, nucellar projection; ov, ovary; pem, pericarp mesocarp; ps, pigment strand; se, starchy endosperm; t, testa; tc, tube cells; vb, vascular bundle; YA, young pre-anthesis. (A,B) $n=5$ /genotype. Box plots show the median (red line), 25th and 75th percentile, whiskers show $1.5\times$ the interquartile range. $P<0.05$ (Dunn's post-hoc test); *Significant difference between *gigas1.a* and Bowman; ^Significant difference between *Zeo1.b* and Bowman. Scale bars: 200 μm (C,D,G); 50 μm (E,F).

nucellar projection, leading to shrunken seeds (Yin and Xue, 2012; Yang et al., 2012). *HvMADS29* expression was reduced to 37% of the Bowman level in *gigas1.a* grain at 5 DPA (Fig. 4H). Although the 'C' class *HvMADS3* and *HvMADS58* are also highly expressed in grain (Figs S7,S11), neither were differentially regulated in

gigas1.a 5 DPA grain (Fig. S12). Jasmonate (JA) positively regulates nucellus PCD in tomato (Schubert et al., 2019) and is associated with PCD in barley grain (Sreenivasulu et al., 2006). Our previous work suggested that *HvAP2* promotes JA-associated gene expression to suppress growth (Patil et al., 2019). Here, we show

that transcripts encoding two JA-induced proteins (JIP), JIP23 and JIP60, expressed during barley grain development (Figs S7,S11), were strongly downregulated in *gigas1.a* caryopses at 5 DPA compared with Bowman (Fig. 4H). In sum, lower levels of *HvMADS29* and JIP transcripts agree with the reduced maternal PCD in *gigas1.a* and is consistent with being putative targets of direct or indirect regulation by *HvAP2*.

***HvMADS29* contributes to the formation of nucellus projection and vascular bundle**

To assess the relationship between *HvAP2* and *HvMADS29* in greater detail, we addressed the role of *HvMADS29* in caryopsis development. RNA-seq data from unfertilised pistils and developing grain staged by days after pollination (DAP) (Aubert et al., 2018) indicated that *HvMADS29* expression increases during pre-anthesis stages before peaking at around 9 DAP and subsequently decreasing

during grain development (Fig. 5A). Before fertilisation, *HvMADS29* expression overlaps with *HvAP2* (in addition to *HvMADS1*, *HvMADS3* and *HvMADS58*), although *HvMADS29* is subsequently maintained during grain development when *HvAP2* levels decrease (Fig. S11). *In situ* hybridisation showed *HvMADS29* expression in the developing ovule, predominantly in the nucellus, integuments and embryo sac (Fig. S11), in agreement with previous microarrays showing *HvMADS29* expression in maternal tissues (Thiel et al., 2008). After fertilisation, *HvMADS29* showed weak expression in the integuments and strong signals in the vascular bundles overlying the nucellar projection and in peripheral vascular bundles (Fig. 5B), overlapping with the pattern observed for *HvAP2*.

To directly demonstrate the importance of *HvMADS29* for caryopsis development, we edited the *HvMADS29* gene using the CRISPR/Cas9 system (Ma et al., 2015). Screening of 25 T0 transformants in Golden Promise revealed five lines (*hvmads29*)

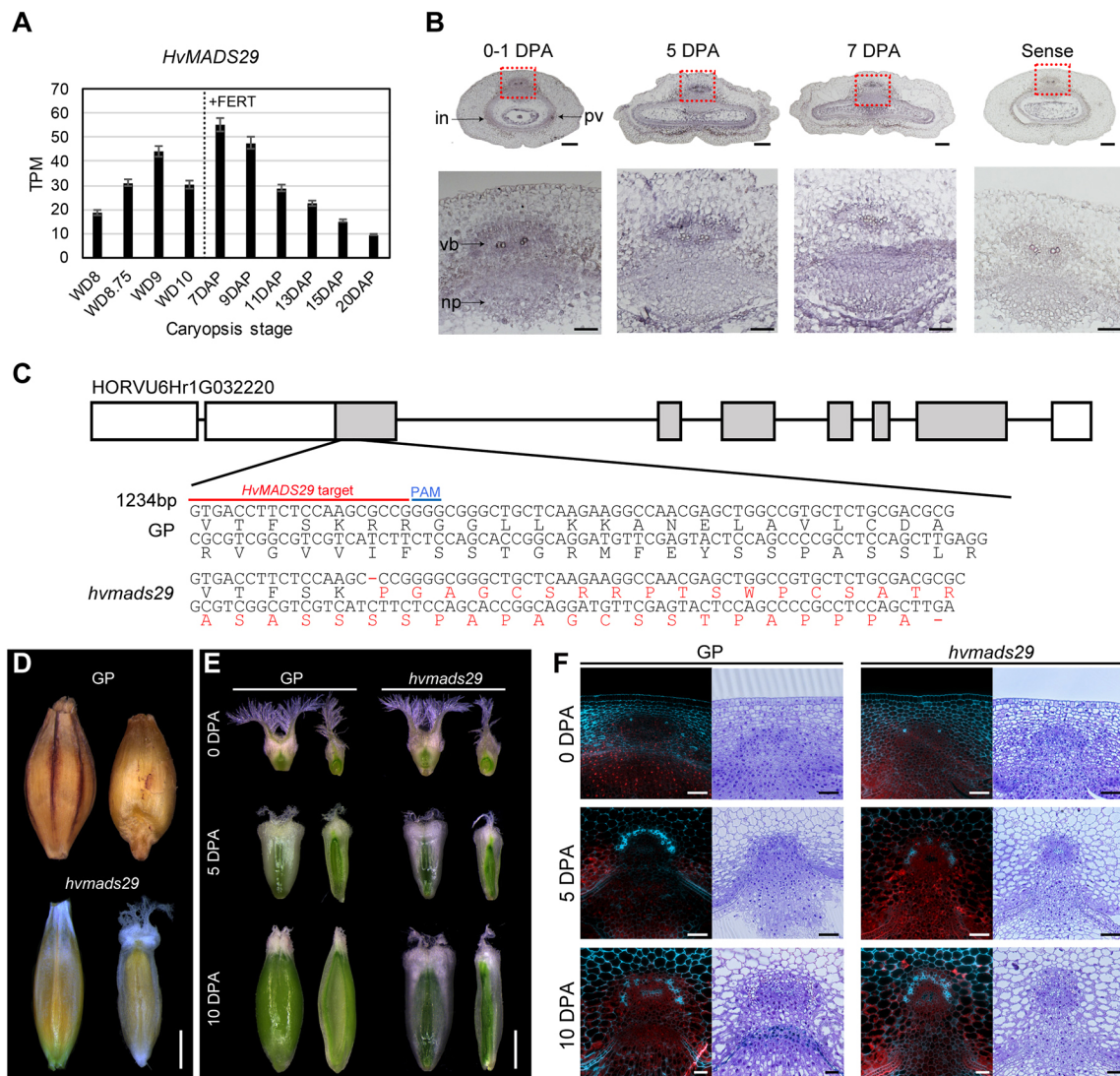


Fig. 5. *HvMADS29* controls post-fertilisation development. (A) *HvMADS29* expression in ovary and caryopses based on RNA-seq. TPM, transcripts per million. (B) *HvMADS29* *in situ* hybridisation on developing caryopses. Upper panel shows caryopsis section and lower panel shows higher magnification of the nucellar projection in the boxed region. (C) *HvMADS29* gene model shows coding region sequence between nucleotides 55-195 and corresponding protein sequence for Golden Promise (GP) and *hvmads29-2*. Lines over GP sequence indicate guide RNA target (red) and protospacer adjacent motif (PAM, blue). Dash in *hvmads29* indicates the deleted base. (D) Mature GP and *hvmads29* caryopses. (E,F) GP and *hvmads29* caryopses at 0, 5 and 10 days post anthesis (DPA). (E) Whole. (F) Sections show vascular bundles in the nucellus projection. For each genotype: left lane shows Calcofluor White staining (cyan) and auto fluorescence (red); right lane shows Toluidine Blue staining. Scale bars: 100 μ m (B, upper panel); 50 μ m (B, lower panel, F); 2 mm (D,E).

with a 1 bp deletion in *HvMADS29*, leading to a frame shift, early stop codon, and predicted complete loss of function (Fig. 5C). Caryopses of *hvmads29* were malformed and shrivelled compared with Golden Promise, with differences in ovule development already evident at anthesis (Fig. 5D; Fig. S12). In particular, the two layers of inner integument cells showed similar morphology to Golden Promise but with an overall misshapen structure, possibly due to reduced nucellus growth. In addition, the outer integument cells in *hvmads29* were abnormally enlarged and occasionally exhibited three cell layers rather than the two cell layers detected in Golden Promise (Fig. S13). Defects in caryopsis development were particularly obvious at 5 DPA, when *hvmads29* grain appeared thinner and unfilled, suggesting defective transport tissues including the nucellar projection and vascular bundle (Fig. 5E). Transverse sections of developing caryopses revealed that 5 DPA Golden Promise contained a well-developed nucellar projection, and a vascular bundle from the ventral pericarp joining the nucellar projection (Fig. 5F). Notably, the phloem cells intensely stained by Calcofluor White highlighted the vascular bundle in a semi-circle pattern. By 10 DPA, the nucellar projection increased in size and differentiated various cell types. In *hvmads29*, the nucellus failed to degrade, the nucellar projection did not differentiate, no transport tissue was formed and the vascular bundle was shrunken with fewer phloem fibres, compared with wild type (Fig. 5F). Importantly, *hvmads29* mutants failed to produce endosperm or viable seed. Collectively, the putative *hvmads29-2* null allele showed several tissue-specific defects similar to *gigas1.a* in terms of defective integument development and an under-developed nucellar projection. Along with the qPCR, RNA-seq and *in situ* data, this provides additional evidence that *HvAP2* and *HvMADS29* both influence the development and differentiation of transport tissues, particularly in the nucellar projection. We speculate that *HvAP2* may contribute to upstream control of *HvMADS29* expression, but this relationship remains to be tested.

HvAP2 interacts with HvBOP2 to control lodicule identity and grain length

Although *HvMADS29* and *HvMADS1* may mediate some *HvAP2* functions, we know little about other factors interacting with *HvAP2* beyond *miR172*. Deletion of the transcription factor-encoding gene *HvBOP2* in *laxatum.a* (*lax.a*, BW419) causes lax spikes, elongated narrow paleas and lemmas, an impaired lemma-awn boundary, skinny grain, and transforms lodicules into stamens, leading to open-flowering (Jost et al., 2016; Fig. 6A–I). We noted that *lax.a* also develops needle-like glumes, elongated narrow ovaries and shorter lemma awns ($P < 0.04$; Fig. 6C,D; Fig. S14). As *lax.a* and *gigas1.a* share some phenotypes, we speculated that *HvAP2* and *HvBOP2* may interact. To explore this hypothesis, we generated *gigas1.a lax.a* and *Zeo1.b lax.a* double mutants (Table S13). Most double mutant phenotypes suggested independent, additive roles of *HvAP2* and *HvBOP2*. The *gigas1.a lax.a* double mutant displayed more extreme open-flowering than either parent, needle-like *lax.a* glumes equivalent in length to *gigas1.a* ($P = 0.86$), lemma length equivalent to *lax.a* ($P = 0.31$) and lemma awns shorter than either parent ($P < 0.02$), and with a more impaired awn-lemma boundary, as well as narrow ovaries lacking stigmatic papillae and extremely narrow grain ($P \leq 0.001$; Fig. 6A–I; Figs S14, S15; Table S7). *Zeo1.b lax.a* lemmas had shorter awns ($P \leq 0.001$) similar to *Zeo1.b*, and defective awn-lemma boundaries similar to *lax.a* (Fig. 6E,F; Fig. S14; Table S7). The *Zeo1.b lax.a* mutant also retained *Zeo1.b* glume-to-lemma transformation but these organs were extremely thin with longer awns, indicating that loss of *HvBOP2*

influences lemma morphology regardless of position, ($P \leq 0.001$; Fig. 6C,D; Table S7). Grain of *gigas1.a lax.a* appeared narrower than either parent, suggesting an additive effect ($P \leq 0.05$; Fig. 6I; Fig. S15). Interestingly, the *Zeo1.b lax.a* mutant showed both *lax.a* elongated lemmas while also displaying *Zeo1.b* shortened grain ($P < 0.05$; Fig. 6I,J; Fig. S15, S16), suggesting that these two traits can be uncoupled. However, *Zeo1.b lax.a* double mutants also showed striking epistasis in other features. Double mutants showed *Zeo1.b*-like spike density ($P \leq 0.001$) and a recovery of lodicule identity with *Zeo1.b*-like morphology (Fig. 6A,B,G,H; Figs S14, S15, Table S6), whereas *Zeo1.b/+ lax.a* plants showed lodicule/stamen mosaic-like structures (Fig. S16). Thus, we propose that *HvAP2* may act downstream of *HvBOP2* in the control of spike density, grain length and lodicule identity. To explore the molecular nature of this interaction, we analysed *HvAP2* and *Hvmir172* expression in Bowman and *lax.a* mutant plants. We detected no difference in *HvAP2* mRNA levels in entire seedlings at 2 weeks after planting or developing spikes; however, we detected slightly elevated levels of *Hvmir172* in *lax.a* as well as lowered levels in *Zeo1.b*, suggesting that *HvAP2* suppresses levels of *Hvmir172* and that *HvBOP2* may enhance *Hvmir172* expression (Fig. S17).

DISCUSSION

Cereal yield depends upon multiple factors including floret number, coordinated growth of floral organs, fertilisation and relocation of maternal nutrients to the developing seed (Brinton et al., 2017; Wilkinson et al., 2019; Sakuma and Schnurbusch, 2020; Ren et al., 2020; Paul et al., 2020). Targeted modification of individual factors is challenging because they typically have both direct and indirect impacts on grain size, number and quality (Wang et al., 2012; Xie et al., 2015; Si et al., 2016; Bull et al., 2017; Wilkinson et al., 2018; Li et al., 2019). One way to dissect pleiotropic effects is to characterise key regulatory modules and genes that contribute to tissue-specificity. Here, we show via analysis of the *gigas1.a*, *hvp2* and *Zeo1.b* mutants that *HvAP2* is a major regulator of barley reproductive development that influences tissue-specific factors in the flower and seed (Fig. 7).

HvAP2 promotes and accelerates the transition to floret identity

Effects on the perianth from gain and loss of *HvAP2* function alleles (Figs 1 and 2) and restored lodicule identity in *Zeo1.b lax.a* (Fig. 6) show that *HvAP2* promotes perianth organ identity and defines the outer perianth boundary, suggesting that *HvAP2* participates in the commitment to floret fate. Barley lacking *Hvmir172* expression and wheat with strong overexpression of *TaAP2L5* show a complete conversion of glumes to florets (Brown and Bregitzer, 2011; Debernardi et al., 2017; Greenwood et al., 2017; Song et al., 2019). As homeotic lemmas in *Zeo1.b* did not enclose floret organs, we suggest that gain of *HvAP2* function in *Zeo1.b* is insufficient for ectopic florets and instead gives rise to ‘sterile lemmas’ – intermediate organs normally found in cultivated rice, and in wheat with moderate overexpression of *TaAP2L5* (Debernardi et al., 2017; Greenwood et al., 2017; Song et al., 2019). Our interpretation supports previous suggestions that glumes, sterile lemmas and lemmas develop on an ontogenetic gradient that determines the fate of their axillary meristem, from glumes subtending spikelet meristems, to empty sterile lemmas, and finally to fertile lemmas subtending floret meristems (Lee et al., 2007; Chuck et al., 2008; Lee and An, 2012; Song et al., 2019; Debernardi et al., 2020). We propose that the gradient shifts towards fertile lemma identity with increasing AP2L function, making AP2L genes master regulators of floret establishment in grasses.

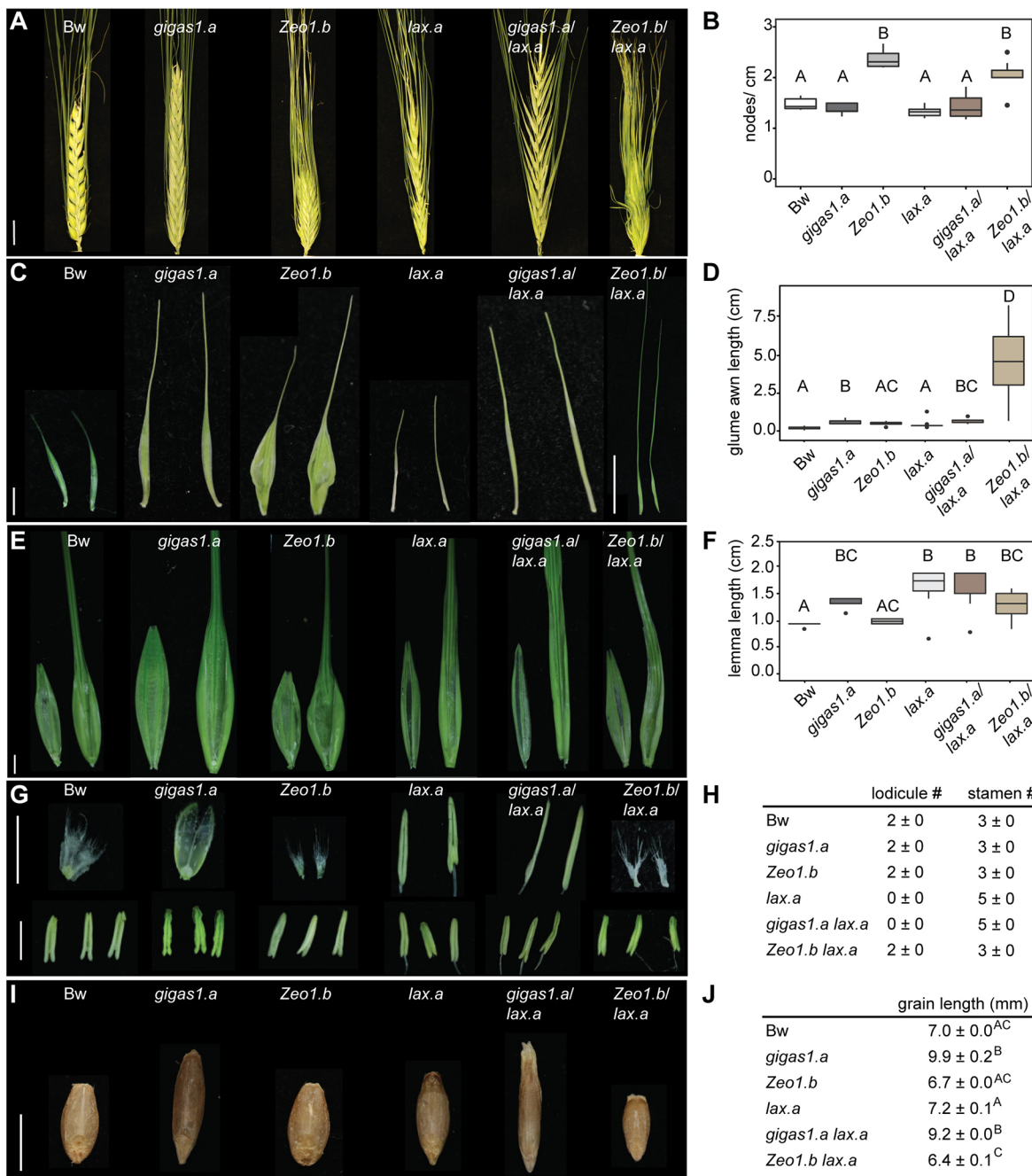


Fig. 6. Genetic analyses between *gigas1.a*, *lax.a* and *Zeo1.b*. (A–J) Spike (A,B), spikelet (C–H) and grain (I,J) phenotypes in Bowman, *gigas1.a*, *Zeo1.b*, *lax.a*, *gigas1.a lax.a* and *Zeo1.b lax.a*. Panels show spikes (A), spike density (B), glume position organs (C), glume awn length (D), palea/lemma position organs (E), lemma length (F), lodicule and stamen position organs (G), lodicule and stamen organ counts per spikelet (H), grain (I) and grain length (J). Box plots show the median (red line), 25th and 75th percentile, whiskers show 1.5× the interquartile range and outliers as dots. For multiple comparisons (ANOVA), letters are used to label means, such that bars bearing different letters are statistically different from one another with a minimum *P* value of <0.05 (Tukey HSD). *n*=8/genotype. Scale bars: 2 mm (A,C,E,G); 2 cm (*Zeo1.b lax.a* in C); 0.5 cm (I).

Control of floral fate by AP2Ls likely involves the *LHS1*-like subclade of the ‘E’ class SEPALLATA genes considered central for the evolution of the floret-bearing grass spikelet (Malcomber and Kellogg, 2004). The rice APL2s SNB and IDS1 promote the expression of the *LHS1*-like *OsMADS1* which confers perianth organ identity and accelerates the transition from spikelet to floret meristem fate (Jeon et al., 2000; Prasad et al., 2001, 2005; Ohmori et al., 2009; Lee and An, 2012; Khanday et al., 2013; Dai et al., 2016). HvAP2-dependent changes in *HvMADS1* expression

(Fig. 3D,F; Fig. S5B), suggest that *HvMADS1* also promotes perianth and floret identity in barley. Elevated JA-signalling in *Zeo1.b* (Patil et al., 2019) may also contribute to *HvAP2* regulation of *HvMADS1* as JA-signalling upregulates *OsMADS1* expression in rice (You et al., 2019). *OsMADS1* inhibits *miR172* accumulation and possibly directly regulates AP2Ls (Khanday et al., 2016; Dai et al., 2016). We propose that *HvMADS1* and *HvAP2* co-expression (Digel et al., 2015), and our data showing *HvAP2*-responsive *HvMADS1* expression, reflect positive feedback that may coordinate

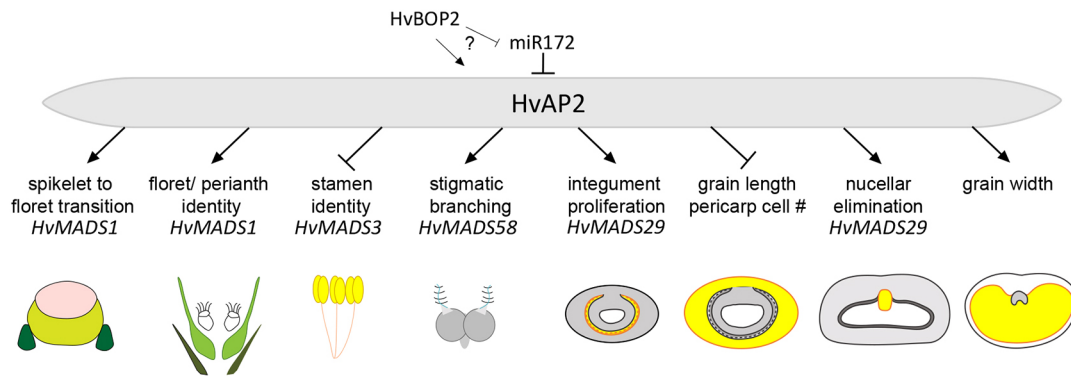


Fig. 7. Model of HvAP2 function with putative up- and downstream regulators. HvAP2 has multiple roles in pre- and post-fertilisation development. Diagrams underneath each role show the tissue involved. HvAP2 promotes the transition from spikelet to floret identity and perianth formation. *miR172* regulation of HvAP2 is necessary to exclude floret/perianth identity from the glume primordia. These roles may be mediated by HvAP2 upregulation of *HvMADS1*. Elevated HvAP2 function represses stamen formation in the lodicule whorl, potentially by downregulating *HvMADS3*. HvAP2 promotes stigmatic branching, associated with *HvMADS58* expression. HvAP2 inhibits integument layer proliferation and promotes integument degradation. HvAP2 limits final grain length by restricting pericarp cell number and length. HvAP2 promotes nucellar tissue elimination, associated with *HvMADS29* expression, associated with endosperm growth and grain widening. HvBOP2 may promote HvAP2 function in the lodicule and grain through unknown mechanisms. Yellow colour in integument proliferation, grain length, nucellar elimination and grain width diagrams indicates integuments, pericarp, nucellar projection and endosperm, respectively.

identity switches and hormone signalling to ensure a sharp transition from spikelet to floret fate. However, as substantial *HvMADS1* levels persist in *gigas1.a* (Fig. 3D), factors besides HvAP2 must also upregulate *HvMADS1* expression.

HvAP2 promotes lodicule identity

AP2 was first described in *Arabidopsis* as a class ‘A’ gene conferring sepal and petal identity (Bowman et al., 1989, 1991; Kunst et al., 1989; Drews et al., 1991). Weak *ap2* alleles develop stamenoid petals and stronger *ap2* alleles show carpel-like transformation in the sepal and petal whorl, phenotypes associated with loss of ‘B’ and ‘E’ class function and expanded ‘C’ class function (Kunst et al., 1989; Drews et al., 1991; Jack et al., 1992; Modrusan et al., 1994; Goto and Meyerowitz, 1994). In wheat, loss of both *TaAPL2* and *TaAPL5* function leads to carpel-like structures on lodicules, consistent with increased ‘C’ class *MADS3/MADS58* (*TaAG1/TaAG2*) expression and reduced ‘B’ class gene expression at WD3.5-WD4.25 stages (Debernardi et al., 2020). We did not observe carpelloidly in *gigas1.a* or *hvac2-2* lodicules, which instead showed bract and filament-like transformations (Fig. 1J-L; Fig. 2F-H). This may reflect reduced HvAP2 activation of *HvMADS1*, as *SNB/OsIDS1*-dependent expression of *OsMADS1* is important for lodicule formation development (Jeon et al., 2000; Prasad et al., 2001, 2005; Lee and An, 2012), rather than HvAP2 regulation of B or C class genes. However, *Zeol.b* WD5.5 spikelets showed reduced *HvMADS3* mRNA abundance (Fig. S8). In rice, ectopic expression of *OsMADS3* converted lodicules to stamens (Kyozuka and Shimamoto, 2002), an identical phenotype to *lax.a* (Jost et al., 2016; Fig. 6G). Thus, *Zeol.b*-dependent reductions in *HvMADS3* expression may help suppress homeotic stamen identity in *Zeol.b lax.a* lodicules (Fig. 6G). Thus, we propose that HvAP2 may control lodicule differentiation through regulating both ‘C’ and ‘E’ class genes. Nonetheless, lodicules in *gigas1.a* or *hvac2-2* usually retained lodicule features, so other genes must confer lodicule identity either along with *HvAP2* or when *HvAP2* function is impaired, consistent with redundant control of lodicule identity amongst wheat AP2Ls (Debernardi et al., 2020). In *Arabidopsis*, *AtBOP* promotes *AtAP2* function via the *miR172*-AP2 network (Khan et al., 2015). Although we did not detect changes in *HvAP2* expression in *lax.a*, we speculate that *HvBOP2* could regulate *HvAP2* at a protein level or that *HvBOP2* may promote the function

of other *miR172*-regulated HvAP2L genes to regulate lodicule identity.

HvAP2 elongates hulls and caryopses

Hulls are proposed to physically limit grain size in rice (Li and Li, 2016; Li et al., 2019) and multiple rice grain size quantitative trait loci control hull cell number and/or expansion (Song et al., 2007; Wang et al., 2012; Zhang et al., 2012; Si et al., 2016; Ren et al., 2016, 2018; Lyu et al., 2020; Ruan et al., 2020). Here, we found that hulls and grain in *gigas1.a* and *hvac2-2* equally elongated (Fig. 1C,D,L-N; Fig. 2D-E; Fig. S4), suggesting that HvAP2 limits both hull and grain length. Interestingly, the mechanism differs between these tissues, with HvAP2-dependent repression of cell expansion underlying changes in lemma length, whereas HvAP2 is required to suppress both cell length and number in the pericarp. Caryopses in *gigas1.a* extended longer than Bowman at 10 DPA, corresponding with the timing of pericarp cell expansion in barley (Radchuk et al., 2011). As pericarp cell number and length were increased in *gigas1.a*, HvAP2 could limit this final cell longitudinal expansion event as well as earlier proliferation, similar to its role in the internode (Patil et al., 2019). The role of HvAP2 in ovary wall cell length control appears to be conserved in grasses, where the rice *SNB* shortens both hull cell length and pericarp epidermis cell length (Jiang et al., 2019; Ma et al., 2019), as well as in *Arabidopsis* where *miR172*-resistant AP2 represses cell expansion in the replum valves (Ripoll et al., 2011). However, although multiple genes, including *HvAP2*, may modulate grain length by influencing hull length, how the hull mechanically limits caryopsis growth is largely unexplained. For example, do changes in grain length occur in direct response to the hull, such as surface-surface contact and/or mechanical pressure? Uncoupling of hull from grain length in the *Zeol.b lax.a* double mutant suggests that HvAP2 and *HvBOP2* may be key nodes in this communication. Learning the identity of putative hull ‘signals’ and how they might synchronise caryopsis development with hull proportions would advance our understanding of the control of cereal grain size.

HvAP2 and maternal degradation transitions

Although increased grain length can lead to heavier grain (Zhang et al., 2012; Brinton et al., 2017), TGW increased by only 7% in

gigas1.a as its grain is narrower and shallower (Figs 1,4; Figs S2,S8). Our data links HvAP2-dependent variation in grain width and depth to an altered balance between maternal versus filial growth and survival. Most strikingly, multiple maternal tissues in *gigas1.a* show defective and/or delayed degradation (Fig. 4), which may reduce remobilisation of nutrients and/or space to enlarge, both considered crucial for endosperm growth (Radchuk et al., 2006; Thiel et al., 2008; Domínguez and Cejudo, 2014; Wilkinson et al., 2019). Impaired maternal elimination correlates with defective endosperm development across plants (Radchuk et al., 2011; Yin and Xue, 2012; Domínguez and Cejudo, 2014; Xu et al., 2016), with nucellar degradation playing a major role in promoting endosperm growth (Lu and Magnani, 2018). We show here that *HvMADS29* expression is significantly reduced in *gigas1.a* (Fig. 4H) and demonstrate for the first time in temperate cereals that *MADS29* function is essential for nucellar differentiation and degradation, control of integument growth and endosperm development. We propose that HvAP2 controls grain width and weight in part by influencing the rate of maternal degradation via *MADS29*-driven processes, suggesting that coordination of filial endosperm expansion with the maternal tissue degradation and differentiation is at least partially under phase change *miR172/AP2* control. In rice and *Arabidopsis*, the B-sister genes *OsMADS29* and *TRANSPARENT TESTA16 (TT16)*, respectively, promote the degeneration of nucellar and other maternal tissues in response to auxin produced from the endosperm following fertilisation (Yin and Xue, 2012; Yang et al., 2012; Nayar et al., 2013; Xu et al., 2016; Lu and Magnani, 2018). Whether HvAP2 directly regulates *HvMADS29* and/or other activators of nucellar elimination in response to filial signals remains a pressing question.

In *Arabidopsis*, signals from the endosperm transform integuments into the seed coat (Figueiredo et al., 2016), a process sustained by mechanical pressure from the expanding endosperm (Creff et al., 2015). This in turn limits endosperm growth (Garcia et al., 2005), highlighting a developmental interdependency which may underlie *ap2* mutant seed phenotypes. AtAP2 appears necessary to restrict integument cell expansion, promote seed coat epidermal differentiation, accelerate endosperm cellularisation and constrain endosperm cell expansion, roles linked to limits on seed weight and size, embryo size, storage protein accumulation and sugar metabolism (Jofuku et al., 1994; Ohto et al., 2005, 2009). Our data suggest that HvAP2 limits integument number in barley, potentially by promoting the degradation of the outer integument, showcasing a role for an AP2L gene in cereal integument development. This role may relate to regulation of *HvMADS29*, as anthesis-stage *hvmads29* ovules showed abnormally enlarged cells in disorganised integument layers. In *Arabidopsis*, TT16 coordinates communication between the integuments and endosperm (Xu et al., 2016), promotes inner integument flavonoid deposition and differentiation (Nesi et al., 2002) and controls outer integument thickness (Fiume et al., 2017), while a recently duplicated B-sister gene, *GORDITA (GOA)* contributes to outer integument differentiation (Prasad et al., 2010). Although *HvMADS29* is clearly not relevant to all functions of HvAP2, tissue-specific regulation of one or more of the three barley B-sister genes (Yang et al., 2012) by HvAP2 may explain the darker seeds and persistence of the outer integuments in *gigas1.a*, in addition to alterations in the rate of nucellar degradation. Increased proanthocyanidins in the seed coat of barley are associated with increased dormancy (Himi et al., 2012). We observed that germination of *gigas1.a* grain was less efficient compared with wild type, suggesting that HvAP2 may influence seed germination through its effects on the seed coat.

Spikelet and grain traits and domestication

Changes in lemma and palea dimensions control the overall shape of the floret, influencing final grain size while lodicule size and swelling leads to open flowering. Similar to *gigas1.a*, spikelets of wild barley (*Hordeum spontaneum*) have elongated lance-shaped hulls and show open flowering compared with the wedge-shaped form of cultivated barley (Abdel-Ghani et al., 2004; Clayton et al., 2006). Although wild barley populations show large variation in seed size (Chen et al., 2004), cultivated barley grain tends to be shorter, wider and heavier (Fuller, 2007; Hughes et al., 2019) with more uniform germination (Fuller and Allaby, 2018). Our data suggest that HvAP2 controls multiple traits which differ between wild and cultivated barley. In wheat and rice, selection of allelic variation in AP2L genes was associated with improved grain traits (Xie et al., 2018; Jiang et al., 2019). It is tempting to speculate that changes in HvAP2 function and/or *HvMADS* regulation contributed to selection for changes in spikelet and grain during barley cultivation.

MATERIALS AND METHODS

Plant material, growth conditions and BWNIL genotyping

Parent cultivars and mutant germplasm are listed in Table S1. Plants were grown in the glasshouse under 16 h light/8 h dark and day/night temperatures of 18/15°C. Plants were grown in plastic pots filled with universal compost [1200 l of peat, 100 l of sand, 2.5 kg of magnesium limestone, 2.5 kg of calcium limestone, 1.5 kg of Osmocote® Start (ICL Speciality Fertilizers), 3.5 kg of Osmocote® Exact Standard 3-4M (ICL Speciality Fertilizers), 0.5 kg of Celcote, 100 l of Perlite, 390 g of Intercept insecticide (active ingredient: imidacloprid)]. Golden Promise and *hvmads29* plants were grown in controlled environment reach-in chambers in The Plant Accelerator, the University of Adelaide, Australia, under the same conditions as all other plant materials which were grown in the UK. gDNA from the *gigas1.a* (BW381), Bowman and Golden Melon were genotyped using the Barley 50K SNP chip (Bayer et al., 2017).

Phenotyping, microscopy and *in situ* hybridisation

Whole plant phenotypic measurements were taken from mature plants. Spikelet length was measured from the base of the spikelet to the lemma-awn boundary on the fourth spikelet from the base of the spike. Awns were measured from awn tip to the top of the glume or lemma body. Spike length was the length from the collar node to the top of the rachis (spike axis). Spikelet width was measured at the widest part of the lemma. Culm height was measured from the top of the soil to the collar at the base of the spike. Mature and developing Bowman, *Zeo1.b* and *gigas1.a* spikes were harvested at 21, 23, 25, 30 and 35 days after germination, their length recorded and stages assigned based on Waddington et al. (1983) (Table S8). Scanning electron microscopy was performed as previously described (Houston et al., 2013). Mature grain width and length were analysed using MARVIN-Universal (GTA Sensorik GmbH). Developing caryopses ($n=5$ independent replicate grains per genotype) were sampled on their respective DPA. For Golden Promise and *hvmads29* samples, caryopses were collected at anthesis, 5 and 10 DPA, photographed by stereo microscope (Leica, MZ FLIII) or fixed in FAA solution, dehydrated in an ethanol series and embedded in Technovit 7100 resin (Kulzer Technique). Transverse 1.5 µm sections were stained with Calcofluor White (Sigma-Aldrich) or 1% Toluidine Blue. Sections were photographed using a Zeiss AxioImager M2 for cell wall (excitation, 335-383 nm; emission, 420-470 nm) and auto fluorescence (excitation, 538-562 nm; emission, 570-640 nm).

HvAP2 in situ hybridization was performed as previously described (Hands et al., 2012) and *HvMADS29 in situ* hybridisation was performed automatically using an InsituPro VSi robot (Intavis), following a standard protocol (Javelle et al., 2011). cDNA fragments of 2225 bp and 319 bp were amplified from Bowman cDNA using primers fused to the T7 promoter as a template for *HvAP2* and *HvMADS1 in situ* probes, respectively (Table S9). Digoxigenin-labelled antisense and sense probes were transcribed using T7 polymerase (Thermo Fisher Scientific) according to the manufacturer's instructions.

CRISPR/Cas9 vector cloning

CRISPR/Cas9 technology was used to generate mutations in *HvAP2* at the University of Dundee (Garcia-Gimenez et al., 2020 preprint). Two guide RNAs (gRNAs) were designed (Table S9) using the Broad Institute sgRNA Designer and the Zhao Bioinformatics Laboratory pssRNAit (Noble Foundation). Each gRNA was cloned into pC95-gRNA entry vector downstream of the rice small nuclear RNA (snRNA) U6 promoter (OsU6p) by Gibson Assembly[®]. Each sgRNA cassette was then released and inserted into the pBract214m-bcoCas9-HSPT expression vector which contains a bcoCas9 under the control of maize ubiquitin promoter and *Arabidopsis* heat shock protein 18.2 terminator. The resultant construct was transformed by electroporation into *Agrobacterium* strain AGL1 containing replication helper pSoup. Transformed *Agrobacterium* clones from each CRISPR construct were combined and co-transformed into Golden Promise immature embryos (Bartlett et al., 2008) in the FUNGEN facility at The James Hutton Institute, Dundee, UK. Transgenic plants containing CRISPR constructs were regenerated under hygromycin selection. Of the 174 T0 plants, 143 were transformed with a single gRNA from 35 separate calli and 31 plants transformed with the two gRNAs from 12 different calli. No mutations were found in the single gRNA transformation lines and one was detected in the double transformation lines. We examined 16 individuals from 18 T1 lines (originating from 10 different T0 calli) which still contained the *Cas9* gene. We detected three homozygous mutations in these T1, including a 39 bp deletion (*hvac2-1*) in nine different lines from three different calli and a 40 bp deletion (*hvac2-2*) in four lines from two different calli. In the T2 generation, following segregation of *Cas9*, *hvac2-1*, *hvac2-2* and Golden Promise were phenotyped ($n=8$ per genotype).

We used a monocot-optimised CRISPR/Cas9 system (Ma et al., 2015) to create the *hvmads29* mutant at the University of Adelaide. The selected target of *HvMADS29* was sequenced before the sgRNA expression cassette was amplified from vector pYLsgRNA-OsU6a and cloned into a binary vector pYLCRISPR/Cas9Pubi-H using *Bsa*I sites as previously described (Ma et al., 2015). The CRISPR construct was transformed into Golden Promise by AGL1 as previously described (Harwood et al., 2009). A total of 25 T0 transformants were analysed in greater detail.

CRISPR/Cas9 screening and genotyping

For *HvAP2* CRISPR lines, genotyping conditions are described in the Supplementary Materials and Methods and primers are listed in Table S10. Genomic DNA (gDNA) was isolated from young leaf tissue using the Qiagen DNA easy plant mini kit. *Cas9* was detected using *Cas9* primers. A region spanning 1 kb around the gRNA target region was amplified using external primers followed by a nested PCR using FAM-labelled internal primers. This product was analysed using a capillary sequencer, and genotypes were determined using GeneMapper[®] Software 5. Samples predicted to contain insertions and/or deletions (indels) were re-amplified without FAM-labelling and sequenced. T0 and T1 plants from *HvMADS29* CRISPR transformation events were genotyped using a Phire Plant Direct PCR Kit (Thermo Fisher Scientific) to amplify a 588 bp fragment that was directly sequenced by Sanger sequencing (AGRF, Australia).

qRT-PCR

RNA extraction and qRT-PCR were performed as in Patil et al. (2019) with the following modifications: RNA was isolated from entire spikes harvested at 23, 25, 30, 35 and 40 days after sowing. cDNA was synthesised using ProtoScriptII kit (New England Biolabs) using random primers. The qPCR was normalised using RQ values calculated by the Pfaffl method $2^{-\Delta\Delta CT}$ (Pfaffl, 2001). One replicate of Bowman at the earliest timepoint was normalised to 1.0 and each other sample replicates normalised to this value. We used *ACTIN2* (*HvACT2*) and *PROTODERMAL FACTOR7* (*HvPDF7*) as endogenous controls as in Patil et al. (2019). The SYBR Green Power Up kit (Thermo Fisher Scientific) was used to detect *HvJIP23*, *HvJIP60*, *HvmiR172* and *HvsnoR101* transcripts. Primers for qPCR are listed in Table S11.

Double mutant generation

Double mutants between *gigas1.a* or *Zeo1.b* with *lax.a* were generated by crossing. Double *Zeo1.b lax.a* and *Zeo1.b/+heterozygote lax.a* mutants

were isolated by screening a segregating *Zeo1.b/lax.a* F2 population which showed the expected ratio of double homozygotes of 1:16 (Table S12). An F3 population from a *Zeo1.b/lax.a* F2 individual was grown and segregated as expected. The *gigas1.a lax.a* F2 population was screened by genotyping with CAPS markers to isolate double mutants (Supplementary Materials and Methods; Table S10).

Statistical analysis

Data were modelled in R 3.5.1 using ANOVA. Models were checked visually for normality in variance and any non-significant terms dropped from the model. Where only two genotypes were compared, a two-tailed unpaired *t*-test was performed. Multiple genotypes were compared using a Tukey honestly significant difference (HSD) test on the modelled data. Grain dimensions over time were analysed by ANOVA followed by a Dunn's post-hoc test.

Acknowledgements

S.D. acknowledges support from the University of Leicester and from Natalie Allcock and Ania Straatman-Iwanowska in the Electron Microscopy Facility. M.R.T. and X.Y. acknowledge technical support from Mr Chao Ma for operation of the *in situ* robot and plant maintenance.

Competing interests

The authors declare no competing or financial interests.

Author contributions

Conceptualization: S.M.M.; Methodology: S.M.M.; Formal analysis: J.R.S., C.U.S., S.M.M.; Investigation: J.R.S., C.U.S., X.Y., S.S., E.v.E., S.C., L.M.P., M.E., S.D., K.H., S.M.M.; Resources: L.G.W., J.S., A.B., M.R.T., S.M.M.; Writing - original draft: J.R.S., S.M.M.; Writing - review & editing: J.R.S., X.Y., S.D., K.H., M.R.T., S.M.M.; Supervision: S.D., K.H., M.R.T., S.M.M.; Project administration: M.R.T., S.M.M.; Funding acquisition: M.R.T., S.M.M.

Funding

This work was supported by the Biotechnology and Biological Sciences Research Council (BBSRC) grant (BB/L001934/1) to S.M.M., and an Australian Research Council grant (DP180104092) to M.R.T. S.M.M. also acknowledges support from the University of Dundee and a Personal Research Fellowship from the Royal Society of Edinburgh. J.S. and K.H. acknowledge funding from the Scottish Government RESAS strategic research programme. J.R.S. and L.M.P. are supported by the BBSRC EASTBIO PhD program (BB/J01446X/1). C.U.S. was supported by the Tertiary Education Trust Fund, Nigeria. M.E. is supported by a Cara Research Fellowship and by the University of Dundee. E.v.E. and S.C. were supported by the Erasmus+ programme and their home institutes, Hogeschool van Arnhem en Nijmegen and De Leijgraaf, respectively. A.B. is funded by the European Research Council (Shuffle Project ID: 669182).

Supplementary information

Supplementary information available online at <https://dev.biologists.org/lookup/doi/10.1242/dev.194894.supplemental>

Peer review history

The peer review history is available online at <https://dev.biologists.org/lookup/doi/10.1242/dev.194894.reviewer-comments.pdf>

References

- Aastrup, S., Outtrup, H. and Erdal, K. (1984). Location of the proanthocyanidins in the barley grain. *Carlsberg Res. Commun.* **49**, 105-109. doi:10.1007/BF02913969
- Abdel-Ghani, A. H., Parzies, H. K., Omary, A. and Geiger, H. H. (2004). Estimating the outcrossing rate of barley landraces and wild barley populations collected from ecologically different regions of Jordan. *Theor. Appl. Genet.* **109**, 588-595. doi:10.1007/s00122-004-1657-1
- Anwar, N., Ohta, M., Yazawa, T., Sato, Y., Li, C., Tagiri, A., Sakuma, M., Nussbaumer, T., Bregitzer, P., Pourkheirandish, M. et al. (2018). miR172 downregulates the translation of cleistogamy 1 in barley. *Annals of Botany* **122**, 251-265. doi:10.1093/aob/mcy058
- Arber, A. (2010). *The Gramineae*. Cambridge: Cambridge University Press.
- Aubert, M. K., Coventry, S., Shirley, N. J., Betts, N. S., Würschum, T., Burton, R. A. and Tucker, M. R. (2018). Differences in hydrolytic enzyme activity accompany natural variation in mature aleurone morphology in barley (*Hordeum vulgare* L.). *Sci. Rep.* **8**, 11025. doi:10.1038/s41598-018-29068-4
- Bartlett, J. G., Alves, S. C., Smedley, M., Snape, J. W. and Harwood, W. A. (2008). High-throughput *Agrobacterium*-mediated barley transformation. *Plant Methods* **4**, 22. doi:10.1186/1746-4811-4-22

- Bayer, M. M., Rapazote-Flores, P., Ganal, M., Hedley, P. E., Macaulay, M., Pleske, J., Ramsay, L., Russell, J., Shaw, P. D., Thomas, W. et al.** (2017). Development and evaluation of a barley 50k iSelect SNP array. *Front. Plant Sci.* **8**, 1792. doi:10.3389/fpls.2017.01792
- Bowman, J. L., Smyth, D. R. and Meyerowitz, E. M.** (1989). Genes directing flower development in Arabidopsis. *Plant Cell* **1**, 37-52. doi:10.2307/3869060
- Bowman, J. L., Smyth, D. R. and Meyerowitz, E. M.** (1991). Genetic interactions among floral homeotic genes of Arabidopsis. *Development* **112**, 1-20.
- Brinton, J. and Uauy, C.** (2019). A reductionist approach to dissecting grain weight and yield in wheat. *J. Integr. Plant Biol.* **61**, 337-358. doi:10.1111/jipb.12741
- Brinton, J., Simmonds, J., Minter, F., Leverington-Waite, M., Snape, J. and Uauy, C.** (2017). Increased pericarp cell length underlies a major quantitative trait locus for grain weight in hexaploid wheat. *New Phytol.* **215**, 1026-1038. doi:10.1111/nph.14624
- Brown, R. H. and Bregitzer, P.** (2011). A Ds insertional mutant of a barley miR172 gene results in indeterminate spikelet development. *Crop Sci.* **51**, 1664-1672. doi:10.2135/cropsci2010.09.0532
- Bull, H., Casao, M. C., Zwirek, M., Flavell, A. J., Thomas, W. T. B., Guo, W., Zhang, R., Rapazote-Flores, P., Kyriakidis, S., Russell, J. et al.** (2017). Barley SIX-ROWED SPIKE3 encodes a putative Jumonji C-type H3K9me2/me3 demethylase that represses lateral spikelet fertility. *Nat. Commun.* **8**, 936. doi:10.1038/s41467-017-00940-7
- Chen, G., Suprunova, T., Krugman, T., Fahima, T. and Nevo, E.** (2004). Ecogeographic and genetic determinants of kernel weight and colour of wild barley (*Hordeum spontaneum*) populations in Israel. *Seed Sci. Res.* **14**, 137-146. doi:10.1079/SSR2004163
- Chuck, G., Meeley, R. and Hake, S.** (2008). Floral meristem initiation and meristem cell fate are regulated by the maize AP2 genes *ids1* and *sid1*. *Development* **135**, 3013-3019. doi:10.1242/dev.024273
- Clayton, W.D., Vorontsova, M.S., Harman, K.T. and Williamson, H.** (2006). GrassBase - The Online World Grass Flora. <http://www.kew.org/data/grasses-db.html>
- Creff, A., Brocard, L. and Ingram, G.** (2015). A mechanically sensitive cell layer regulates the physical properties of the Arabidopsis seed coat. *Nat. Commun.* **6**, 6382. doi:10.1038/ncomms7382
- Dai, Z., Wang, J., Zhu, M., Miao, X. and Shi, Z.** (2016). OsMADS1 represses microRNA172 in Elongation of Palea/Lemma development in rice. *Front. Plant Sci.* **7**, 1891. doi:10.3389/fpls.2016.01891
- Debernardi, J. M., Lin, H., Chuck, G., Faris, J. D. and Dubcovsky, J.** (2017). microRNA172 plays a crucial role in wheat spike morphogenesis and grain threshability. *Development* **144**, 1966-1975. doi:10.1242/dev.146399
- Debernardi, J. M., Greenwood, J. R., Jean Finnegan, E., Jernstedt, J. and Dubcovsky, J.** (2020). APETALA 2-like genes AP2L2 and Q specify lemma identity and axillary floral meristem development in wheat. *Plant J.* **101**, 171-187. doi:10.1111/tpj.14528
- Digel, B., Pankin, A. and von Korff, M.** (2015). Global transcriptome profiling of developing leaf and shoot apices reveals distinct genetic and environmental control of floral transition and inflorescence development in barley. *Plant Cell* **27**, 2318-2334. doi:10.1105/tpc.15.00203
- Dinh, T. T., Girke, T., Liu, X., Yant, L., Schmid, M. and Chen, X.** (2012). The floral homeotic protein APETALA2 recognizes and acts through an AT-rich sequence element. *Development* **139**, 1978-1986. doi:10.1242/dev.077073
- Domínguez, F. and Cejudo, F. J.** (2014). Programmed cell death (PCD): an essential process of cereal seed development and germination. *Front. Plant Sci.* **5**, 366. doi:10.3389/fpls.2014.00366
- Dreni, L., Pilatone, A., Yun, D., Erreni, S., Pajoro, A., Caporali, E., Zhang, D. and Kater, M. M.** (2011). Functional analysis of all AGAMOUS subfamily members in rice reveals their roles in reproductive organ identity determination and meristem determinacy. *Plant Cell* **23**, 2850-2863. doi:10.1105/tpc.111.087007
- Drews, G. N., Bowman, J. L. and Meyerowitz, E. M.** (1991). Negative regulation of the Arabidopsis homeotic gene AGAMOUS by the APETALA2 product. *Cell* **65**, 991-1002. doi:10.1016/0092-8674(91)90551-9
- Druka, A., Franckowiak, J., Lundqvist, U., Bonar, N., Alexander, J., Houston, K., Radovic, S., Shahinnia, F., Vendramin, V., Morgante, M. et al.** (2011). Genetic dissection of barley morphology and development. *Plant Physiol.* **155**, 617-627. doi:10.1104/pp.110.166249
- Figueiredo, D. D., Batista, R. A., Roszak, P. J., Hennig, L. and Köhler, C.** (2016). Auxin production in the endosperm drives seed coat development in Arabidopsis. *eLife* **5**, e20542. doi:10.7554/eLife.20542
- Fisher, D. B.** (1990). Persistence of non-crease protophloem strands in the developing wheat grain. *Funct. Plant Biol.* **17**, 223. doi:10.1071/PP9900223
- Fiume, E., Coen, O., Xu, W., Lepiniec, L. and Magnani, E.** (2017). Developmental patterning of sub-epidermal cells in the outer integument of Arabidopsis seeds. *PLoS ONE* **12**, e0188148. doi:10.1371/journal.pone.0188148
- Franckowiak, J.** (1995). Notes on linkage drag in Bowman backcross derived lines of spring barley. *Barley Genet News* **24**, 63-70.
- Fuller, D. Q.** (2007). Contrasting patterns in crop domestication and domestication rates: recent archaeobotanical insights from the old world. *Ann. Bot.* **100**, 903-924. doi:10.1093/aob/mcm048
- Fuller, D. Q. and Allaby, R.** (2018). Seed dispersal and crop domestication: shattering, germination and seasonality in evolution under cultivation. *Annu. Plant Rev. Online* **38**, 238-295. doi:10.1002/9781119312994.apr0414
- Garcia, D., Fitz Gerald, J. N. and Berger, F.** (2005). Maternal control of integument cell elongation and zygotic control of endosperm growth are coordinated to determine seed size in Arabidopsis. *Plant Cell* **17**, 52-60. doi:10.1105/tpc.104.027136
- Garcia-Gimenez, G., Barakate, A., Smith, P., Stephens, J., Khor, S. F., Doblin, M. S., Hao, P., Bacic, A., Fincher, G. B., Burton, R. A. et al.** (2020). Targeted mutation of barley (1,3;1,4)- β -glucan synthases reveals complex relationships between the storage and cell wall polysaccharide content. *Plant J.* **104**, 1009-1022. doi:10.1111/tpj.14977
- Goto, K. and Meyerowitz, E. M.** (1994). Function and regulation of the Arabidopsis floral homeotic gene PISTILLATA. *Genes Dev.* **8**, 1548-1560. doi:10.1101/gad.8.13.1548
- Greenwood, J. R., Finnegan, E. J., Watanabe, N., Trevaskis, B. and Swain, S. M.** (2017). New alleles of the wheat domestication gene Q reveal multiple roles in growth and reproductive development. *Development* **144**, 1959-1965. doi:10.1242/dev.146407
- Hands, P., Kourmpetli, S., Sharples, D., Harris, R. G. and Drea, S.** (2012). Analysis of grain characters in temperate grasses reveals distinctive patterns of endosperm organization associated with grain shape. *J. Exp. Bot.* **63**, 6253-6266. doi:10.1093/jxb/ers281
- Harwood, W. A., Bartlett, J. G., Alves, S. C., Perry, M., Smedley, M. A., Leyland, N. and Snape, J. W.** (2009). Barley transformation using Agrobacterium-mediated techniques. *Methods Mol. Biol.* **478**, 137-147. doi:10.1007/978-1-59745-379-0_9
- Himi, E., Yamashita, Y., Haruyama, N., Yanagisawa, T., Maekawa, M. and Taketa, S.** (2012). Ant28 gene for proanthocyanidin synthesis encoding the R2R3 MYB domain protein (Hvmyb10) highly affects grain dormancy in barley. *Euphytica* **188**, 141-151. doi:10.1007/s10681-011-0552-5
- Houston, K., McKim, S. M., Comadran, J., Bonar, N., Druka, I., Uzek, N., Cirillo, E., Guzy-Wrobelska, J., Collins, N. C., Halpin, C. et al.** (2013). Variation in the interaction between alleles of HvAPETALA2 and microRNA172 determines the density of grains on the barley inflorescence. *Proc. Nat. Acad. Sci. USA* **110**, 16675-16680. doi:10.1073/pnas.1311681110
- Hughes, N., Oliveira, H. R., Fradgley, N., Corke, F. M. K., Cockram, J., Doonan, J. H. and Nibau, C.** (2019). μ CT trait analysis reveals morphometric differences between domesticated temperate small grain cereals and their wild relatives. *Plant J.* **99**, 98-111. doi:10.1111/tpj.14312
- Irish, V.** (2017). The ABC model of floral development. *Curr. Biol.* **27**, R887-R890. doi:10.1016/j.cub.2017.03.045
- Jack, T., Brockman, L. L. and Meyerowitz, E. M.** (1992). The homeotic gene APETALA3 of Arabidopsis thaliana encodes a MADS box and is expressed in petals and stamens. *Cell* **68**, 683-697. doi:10.1016/0092-8674(92)90144-2
- Javelle, M., Marco, C. F. and Timmermans, M.** (2011). In situ hybridization for the precise localization of transcripts in plants. *J. Vis. Exp.* **57**, e3328. doi:10.3791/3328
- Jeon, J.-S., Jang, S., Lee, S., Nam, J., Kim, C., Lee, S.-H., Chung, Y.-Y., Kim, S.-R., Lee, Y. H., Cho, Y.-G. et al.** (2000). *leafy hull sterile1* is a homeotic mutation in a rice MADS box gene affecting rice flower development. *Plant Cell* **12**, 871-884. doi:10.1105/tpc.12.6.871
- Ji, H., Han, C.-D., Lee, G.-S., Jung, K.-H., Kang, D.-Y., Oh, J., Oh, H., Cheon, K.-S., Kim, S. L., Choi, I. et al.** (2019). Mutations in the microRNA172 binding site of SUPERNUMERARY BRACT (SNB) suppress internode elongation in rice. *Rice* **12**, 62. doi:10.1186/s12284-019-0324-8
- Jiang, L., Ma, X., Zhao, S., Tang, Y., Liu, F., Gu, P., Fu, Y., Zhu, Z., Cai, H., Sun, C. et al.** (2019). The APETALA2-Like transcription factor SUPERNUMERARY BRACT controls rice seed shattering and seed size. *Plant Cell* **31**: 17-36. doi:10.1105/tpc.18.00304
- Jofuku, K. D., den Boer, B. G., Van Montagu, M. and Okamoto, J. K.** (1994). Control of Arabidopsis flower and seed development by the homeotic gene APETALA2. *Plant Cell* **6**, 1211-1225. doi:10.1105/tpc.6.9.1211
- Jost, M., Taketa, S., Mascher, M., Himmelbach, A., Yuo, T., Shahinnia, F., Rutten, T., Druka, A., Schmutzer, T., Steuernagel, B. et al.** (2016). A homolog of Blade-On-Petiole 1 and 2 (BOP1/2) controls internode length and homeotic changes of the barley inflorescence. *Plant Physiol.* **171**, 1113-1127. doi:10.1104/pp.16.00124
- Kellogg, E. A.** (2015). *Flowering Plants. Monocots*. Cham: Springer International Publishing AG.
- Khan, M., Ragni, L., Tabb, P., Salasini, B. C., Chatfield, S., Datla, R., Lock, J., Kuai, X., Despres, C., Proveniers, M. et al.** (2015). Repression of lateral organ boundary genes by PENNYWISE and POUND-FOOLISH is essential for meristem maintenance and flowering in Arabidopsis thaliana. *Plant Physiol.* **169**, 2166-2186. doi:10.1104/pp.15.00915
- Khanda, I., Yadav, S. R. and Vijayraghavan, U.** (2013). Rice LHS1/OsMADS1 controls floret meristem specification by coordinated regulation of transcription factors and hormone signaling pathways. *Plant Physiol.* **161**, 1970-1983. doi:10.1104/pp.112.212423
- Khanda, I., Das, S., Chongloi, G. L., Bansal, M., Grossniklaus, U. and Vijayraghavan, U.** (2016). Genome-wide targets regulated by the OsMADS1

- transcription factor reveals its DNA recognition properties. *Plant Physiol.* **172**, 372-388. doi:10.1104/pp.16.00789
- Krogan, N. T., Hogan, K. and Long, J. A.** (2012). APETALA2 negatively regulates multiple floral organ identity genes in Arabidopsis by recruiting the co-repressor TOPLESS and the histone deacetylase HDA19. *Development* **139**, 4180-4190. doi:10.1242/dev.085407
- Kunst, L., Klenz, J. E., Martinez-Zapater, J. and Haughn, G. W.** (1989). AP2 gene determines the identity of perianth organs in flowers of Arabidopsis thaliana. *Plant Cell* **1**, 1195-1208. doi:10.2307/3868917
- Kyozuka, J. and Shimamoto, K.** (2002). Ectopic expression of OsMADS3, a rice ortholog of AGAMOUS, caused a homeotic transformation of lodicules to stamens in transgenic rice plants. *Plant Cell Physiol.* **43**, 130-135. doi:10.1093/pcp/pcf010
- Lee, D.-Y. and An, G.** (2012). Two AP2 family genes, SUPERNUMERARY BRACT (SNB) and OsINDETERMINATE SPIKELET 1 (OsIDS1), synergistically control inflorescence architecture and floral meristem establishment in rice. *Plant J.* **69**, 445-461. doi:10.1111/j.1365-313X.2011.04804.x
- Lee, D. Y., Lee, J., Moon, S., Park, S. Y. and An, G.** (2007). The rice heterochronic gene SUPERNUMERARY BRACT regulates the transition from spikelet meristem to floral meristem. *Plant J.* **49**, 64-78. doi:10.1111/j.1365-313X.2006.02941.x
- Li, N. and Li, Y.** (2016). Signaling pathways of seed size control in plants. *Curr. Opin. Plant Biol.* **33**, 23-32. doi:10.1016/j.pbi.2016.05.008
- Li, N., Xu, R. and Li, Y.** (2019). Molecular networks of seed size control in plants. *Annu. Rev. Plant Biol.* **70**, 435-463. doi:10.1146/annurev-arplant-050718-095851
- Lombardo, F. and Yoshida, H.** (2015). Interpreting lemma and palea homologies: a point of view from rice floral mutants. *Front. Plant Sci.* **6**, 61. doi:10.3389/fpls.2015.00061
- Lu, J. and Magnani, E.** (2018). Seed tissue and nutrient partitioning, a case for the nucellus. *Plant Reprod.* **31**, 309-317. doi:10.1007/s00497-018-0338-1
- Lyu, J., Wang, D., Duan, P., Liu, Y., Huang, K., Zeng, D., Zhang, L., Dong, G., Li, Y., Xu, R. et al.** (2020). Control of grain size and weight by the GSK2-LARGE1/OML4 pathway in rice. *Plant Cell* **32**, 1905-1918. doi:10.1105/tpc.19.00468
- Ma, X., Zhang, Q., Zhu, Q., Liu, W., Chen, Y., Qiu, R., Wang, B., Yang, Z., Li, H., Lin, Y. et al.** (2015). A robust CRISPR/Cas9 system for convenient, high-efficiency multiplex genome editing in monocot and dicot plants. *Mol. Plant* **8**, 1274-1284. doi:10.1016/j.molp.2015.04.007
- Ma, X., Feng, F., Zhang, Y., Elesawi, I. E., Xu, K., Li, T., Mei, H., Liu, H., Gao, N., Chen, C. et al.** (2019). A novel rice grain size gene OsSNB was identified by genome-wide association study in natural population. *PLoS Genet.* **15**, e1008191. doi:10.1371/journal.pgen.1008191
- Malcomber, S. T. and Kellogg, E. A.** (2004). Heterogeneous expression patterns and separate roles of the *SEPALLATA* gene *LEAFY HULL STERILE1* in grasses. *Plant Cell* **16**, 1692-1706. doi:10.1105/tpc.021576
- Mascher, M., Gundlach, H., Himmelsbach, A., Beier, S., Twardziok, S. O., Wicker, T., Radchuk, V., Dockter, C., Hedley, P. E., Russell, J. et al.** (2017). A chromosome conformation capture ordered sequence of the barley genome. *Nature* **544**, 427-433. doi:10.1038/nature22043
- Modrusan, Z., Reiser, L., Feldmann, K. A., Fischer, R. L. and Haughn, G. W.** (1994). Homeotic transformation of ovules into carpel-like structures in Arabidopsis. *Plant Cell* **6**, 333-349. doi:10.2307/3869754
- Nair, S. K., Wang, N., Turuspekov, Y., Pourkheirandish, M., Sinsuwongwat, S., Chen, G., Sameri, M., Tagiri, A., Honda, I., Watanabe, Y. et al.** (2010). Cleistogamous flowering in barley arises from the suppression of microRNA-guided HvAP2 mRNA cleavage. *Proc. Natl. Acad. Sci. USA* **107**, 490-495. doi:10.1073/pnas.0909097107
- Nayar, S., Sharma, R., Tyagi, A. K. and Kapoor, S.** (2013). Functional delineation of rice MADS29 reveals its role in embryo and endosperm development by affecting hormone homeostasis. *J. Exp. Bot.* **64**, 4239-4253. doi:10.1093/jxb/ert231
- Nesi, N., Debeaujon, I., Jond, C., Stewart, A. J., Jenkins, G. I., Caboche, M. and Lepiniec, L.** (2002). The TRANSPARENT TESTA16 locus encodes the ARABIDOPSIS BSISTER MADS domain protein and is required for proper development and pigmentation of the seed coat. *Plant Cell* **14**, 2463-2479. doi:10.1105/tpc.004127
- Ohmori, S., Kimizu, M., Sugita, M., Miyao, A., Hirochika, H., Uchida, E., Nagato, Y. and Yoshida, H.** (2009). MOSAIC FLORAL ORGANS1, an AGL6-like MADS box gene, regulates floral organ identity and meristem fate in rice. *Plant Cell* **21**, 3008-3025. doi:10.1105/tpc.109.068742
- Ohto, M.-a., Fischer, R. L., Goldberg, R. B., Nakamura, K. and Harada, J. J.** (2005). Control of seed mass by APETALA2. *Proc. Natl. Acad. Sci. USA* **102**, 3123-3128. doi:10.1073/pnas.0409858102
- Ohto, M.-a., Floyd, S. K., Fischer, R. L., Goldberg, R. B. and Harada, J. J.** (2009). Effects of APETALA2 on embryo, endosperm, and seed coat development determine seed size in Arabidopsis. *Sex. Plant Reprod.* **22**, 277-289. doi:10.1007/s00497-009-0116-1
- Patil, V., McDermott, H. I., McAllister, T., Cummins, M., Silva, J. C., Mollison, E., Meikle, R., Morris, J., Hedley, P. E., Waugh, R. et al.** (2019). APETALA2 control of barley internode elongation. *Development* **146**, dev170373. doi:10.1242/dev.170373
- Paul, M. J., Watson, A. and Griffiths, C. A.** (2020). Linking fundamental science to crop improvement through understanding source and sink traits and their integration for yield enhancement. *J. Exp. Bot.* **71**, 2270-2280. doi:10.1093/jxb/erz480
- Pfaffl, M. W.** (2001). A new mathematical model for relative quantification in real-time RT-PCR. *Nucleic Acids Res.* **29**, e45. doi:10.1093/nar/29.9.e45
- Prasad, K., Sriram, P., Kumar, C. S., Kushalappa, K. and Vijayraghavan, U.** (2001). Ectopic expression of rice OsMADS1 reveals a role in specifying the lemma and palea, grass floral organs analogous to sepals. *Dev. Genes Evol.* **211**, 281-290. doi:10.1007/s004270100153
- Prasad, K., Parameswaran, S. and Vijayraghavan, U.** (2005). OsMADS1, a rice MADS-box factor, controls differentiation of specific cell types in the lemma and palea and is an early-acting regulator of inner floral organs. *Plant J.* **43**, 915-928. doi:10.1111/j.1365-313X.2005.02504.x
- Prasad, K., Zhang, X., Tobón, E. and Ambrose, B. A.** (2010). The Arabidopsis B-sister MADS-box protein, GORDITA, represses fruit growth and contributes to integument development. *Plant J.* **62**, 203-214. doi:10.1111/j.1365-313X.2010.04139.x
- Radchuk, V., Borisjuk, L., Radchuk, R., Steinbiss, H.-H., Rolletschek, H., Broeders, S. and Wobus, U.** (2006). Jekyll encodes a novel protein involved in the sexual reproduction of barley. *Plant Cell* **18**, 1652-1666. doi:10.1105/tpc.106.041335
- Radchuk, V., Weier, D., Radchuk, R., Weschke, W. and Weber, H.** (2011). Development of maternal seed tissue in barley is mediated by regulated cell expansion and cell disintegration and coordinated with endosperm growth. *J. Exp. Bot.* **62**, 1217-1227. doi:10.1093/jxb/erq348
- Ren, D., Rao, Y., Leng, Y., Li, Z., Xu, Q., Wu, L., Qiu, Z., Xue, D., Zeng, D., Hu, J. et al.** (2016). Regulatory Role of OsMADS34 in the determination of glumes fate, grain yield, and quality in rice. *Front. Plant Sci.* **7**, 1853. doi:10.3389/fpls.2016.01853
- Ren, D., Hu, J., Xu, Q., Cui, Y., Zhang, Y., Zhou, T., Rao, Y., Xue, D., Zeng, D., Zhang, G. et al.** (2018). FZP determines grain size and sterile lemma fate in rice. *J. Exp. Bot.* **69**, 4853-4866. doi:10.1093/jxb/ery264
- Ren, D., Li, Y., He, G. and Qian, Q.** (2020). Multifloret spikelet improves rice yield. *New Phytol.* **225**, 2301-2306. doi:10.1111/nph.16303
- Ripoll, J. J., Roeder, A. H. K., Ditta, G. S. and Yanofsky, M. F.** (2011). A novel role for the floral homeotic gene *APETALA2* during Arabidopsis fruit development. *Development* **138**, 5167-5176. doi:10.1242/dev.073031
- Ruan, B., Shang, L., Zhang, B., Hu, J., Wang, Y., Lin, H., Zhang, A., Liu, C., Peng, Y., Zhu, L. et al.** (2020). Natural variation in the promoter of *TGW2* determines grain width and weight in rice. *New Phytol.* **227**, 629-640. doi:10.1111/nph.16540
- Sakuma, S. and Schnurbusch, T.** (2020). Of floral fortune: tinkering with the grain yield potential of cereal crops. *New Phytol.* **225**, 1873-1882. doi:10.1111/nph.16189
- Schrager-Lavelle, A., Klein, H., Fisher, A. and Bartlett, M.** (2017). Grass flowers: an untapped resource for floral evo-devo. *J. Syst. Evol.* **55**, 525-541. doi:10.1111/jse.12251
- Schubert, R., Dobritsch, S., Gruber, C., Hause, G., Athmer, B., Schreiber, T., Marillonnet, S., Okabe, Y., Ezura, H., Acosta, I. F. et al.** (2019). Tomato myb21 acts in ovules to mediate jasmonate-regulated fertility. *Plant Cell* **31**, 1043-1062. doi:10.1105/tpc.18.00978
- Si, L., Chen, J., Huang, X., Gong, H., Luo, J., Hou, Q., Zhou, T., Lu, T., Zhu, J., Shangguan, Y. et al.** (2016). OsSPL13 controls grain size in cultivated rice. *Nat. Genet.* **48**, 447-456. doi:10.1038/ng.3518
- Simons, K. J., Fellers, J. P., Trick, H. N., Zhang, Z., Tai, Y.-S., Gill, B. S. and Faris, J. D.** (2006). Molecular characterization of the major wheat domestication gene Q. *Genetics* **172**, 547-555. doi:10.1534/genetics.105.044727
- Song, X.-J., Huang, W., Shi, M., Zhu, M.-Z. and Lin, H.-X.** (2007). A QTL for rice grain width and weight encodes a previously unknown RING-type E3 ubiquitin ligase. *Nat. Genet.* **39**, 623-630. doi:10.1038/ng2014
- Song, G., Sun, G., Kong, X., Jia, M., Wang, K., Ye, X., Zhou, Y., Geng, S., Mao, L. and Li, A.** (2019). The soft glumes of common wheat are sterile-lemmas as determined by the domestication gene Q. *Crop J.* **7**, 113-117. doi:10.1016/j.cj.2018.11.001
- Sormacheva, I., Golovnina, K., Vavilova, V., Kosuge, K., Watanabe, N., Blinov, A. and Goncharov, N. P.** (2015). Q gene variability in wheat species with different spike morphology. *Genet. Resour. Crop Evol.* **62**, 837-852. doi:10.1007/s10722-014-0195-1
- Sreenivasulu, N., Radchuk, V., Strickert, M., Miersch, O., Weschke, W. and Wobus, U.** (2006). Gene expression patterns reveal tissue-specific signaling networks controlling programmed cell death and ABA-regulated maturation in developing barley seeds. *Plant J.* **47**, 310-327. doi:10.1111/j.1365-313X.2006.02789.x
- Theißen, G., Melzer, R. and Rümpler, F.** (2016). MADS-domain transcription factors and the floral quartet model of flower development: linking plant development and evolution. *Development* **143**, 3259-3271. doi:10.1242/dev.134080
- Thiel, J., Weier, D., Sreenivasulu, N., Strickert, M., Weichert, N., Melzer, M., Czauderna, T., Wobus, U., Weber, H. and Weschke, W.** (2008). Different hormonal regulation of cellular differentiation and function in nucellar projection and endosperm transfer cells: a microdissection-based transcriptome study of young barley grains. *Plant Physiol.* **148**, 1436-1452. doi:10.1104/pp.108.127001

- Tsuchiya, T.** (1962). Annual report on breeding of malting barley. *Kihara Inst. Biol. Res., Japan* 28 pp. with 8 tables, Mimeo.
- Waddington, S. R., Cartwright, P. M. and Wall, P. C.** (1983). A quantitative scale of spike initial and pistil development in barley and wheat. *Ann. Bot.* **51**, 119-130. doi:10.1093/oxfordjournals.aob.a086434
- Wang, S., Wu, K., Yuan, Q., Liu, X., Liu, Z., Lin, X., Zeng, R., Zhu, H., Dong, G., Qian, Q. et al.** (2012). Control of grain size, shape and quality by OsSPL16 in rice. *Nat. Genet.* **44**, 950-954. doi:10.1038/ng.2327
- Wilkinson, L. G., Bird, D. C. and Tucker, M. R.** (2018). Exploring the role of the ovule in cereal grain development and reproductive stress tolerance. *Annu. Plant Rev. Online* **1**, 181-216. doi:10.1002/9781119312994.apr0609
- Wilkinson, L. G., Yang, X., Burton, R. A., Würschum, T. and Tucker, M. R.** (2019). Natural variation in ovule morphology is influenced by multiple tissues and impacts downstream grain development in barley. *Front. Plant Sci.* **10**, 1374. doi:10.3389/fpls.2019.01374
- Xie, Q., Mayes, S. and Sparkes, D. L.** (2015). Carpel size, grain filling, and morphology determine individual grain weight in wheat. *J. Exp. Bot.* **66**, 6715-6730. doi:10.1093/jxb/erv378
- Xie, Q., Li, N., Yang, Y., Lv, Y., Yao, H., Wei, R., Sparkes, D. L. and Ma, Z.** (2018). Pleiotropic effects of the wheat domestication gene Q on yield and grain morphology. *Planta* **247**, 1089-1098. doi:10.1007/s00425-018-2847-4
- Xu, W., Fiume, E., Coen, O., Pechoux, C., Lepiniec, L. and Magnani, E.** (2016). Endosperm and nucellus develop antagonistically in arabidopsis seeds. *Plant Cell* **28**, 1343-1360. doi:10.1105/tpc.16.00041
- Yamaguchi, T., Lee, D. Y., Miyao, A., Hirochika, H., An, G. and Hirano, H.-Y.** (2006). Functional diversification of the two C-class MADS box genes OSMADS3 and OSMADS58 in *Oryza sativa*. *Plant Cell* **18**, 15-28. doi:10.1105/tpc.105.037200
- Yang, X., Wu, F., Lin, X., Du, X., Chong, K., Gramzow, L., Schilling, S., Becker, A., Theißen, G. and Meng, Z.** (2012). Live and let die - The B_{sister} MADS-Box gene OsMADS29 controls the degeneration of cells in maternal tissues during seed development of rice (*Oryza sativa*). *PLoS ONE* **7**, e51435. doi:10.1371/journal.pone.0051435
- Yant, L., Mathieu, J., Dinh, T. T., Ott, F., Lanz, C., Wollmann, H., Chen, X. and Schmid, M.** (2010). Orchestration of the floral transition and floral development in Arabidopsis by the bifunctional transcription factor APETALA2. *Plant Cell* **22**, 2156-2170. doi:10.1105/tpc.110.075606
- Yin, L.-L. and Xue, H.-W.** (2012). The MADS29 transcription factor regulates the degradation of the nucellus and the nucellar projection during rice seed development. *Plant Cell* **24**, 1049-1065. doi:10.1105/tpc.111.094854
- Yoshida, H.** (2012). Is the lodicule a petal: molecular evidence? *Plant Sci.* **184**, 121-128. doi:10.1016/j.plantsci.2011.12.016
- You, X., Zhu, S., Zhang, W., Zhang, J., Wang, C., Jing, R., Chen, W., Wu, H., Cai, Y., Feng, Z. et al.** (2019). OsPEX5 regulates rice spikelet development through modulating jasmonic acid biosynthesis. *New Phytol.* **224**, 712-724. doi:10.1111/nph.16037
- Zhang, X., Wang, J., Huang, J., Lan, H., Wang, C., Yin, C., Wu, Y., Tang, H., Qian, Q., Li, J. et al.** (2012). Rare allele of OsPPKL1 associated with grain length causes extra-large grain and a significant yield increase in rice. *Proc. Natl. Acad. Sci. USA* **109**, 21534-21539. doi:10.1073/pnas.1219776110
- Zhao, L., Kim, Y., Dinh, T. T. and Chen, X.** (2007). miR172 regulates stem cell fate and defines the inner boundary of APETALA3 and PISTILLATA expression domain in Arabidopsis floral meristems. *Plant J.* **51**, 840-849. doi:10.1111/j.1365-313X.2007.03181.x
- Zhao, D.-S., Li, Q.-F., Zhang, C.-Q., Zhang, C., Yang, Q.-Q., Pan, L.-X., Ren, X.-Y., Lu, J., Gu, M.-H. and Liu, Q.-Q.** (2018). GS9 acts as a transcriptional activator to regulate rice grain shape and appearance quality. *Nat. Commun.* **9**, 1240. doi:10.1038/s41467-018-03616-y

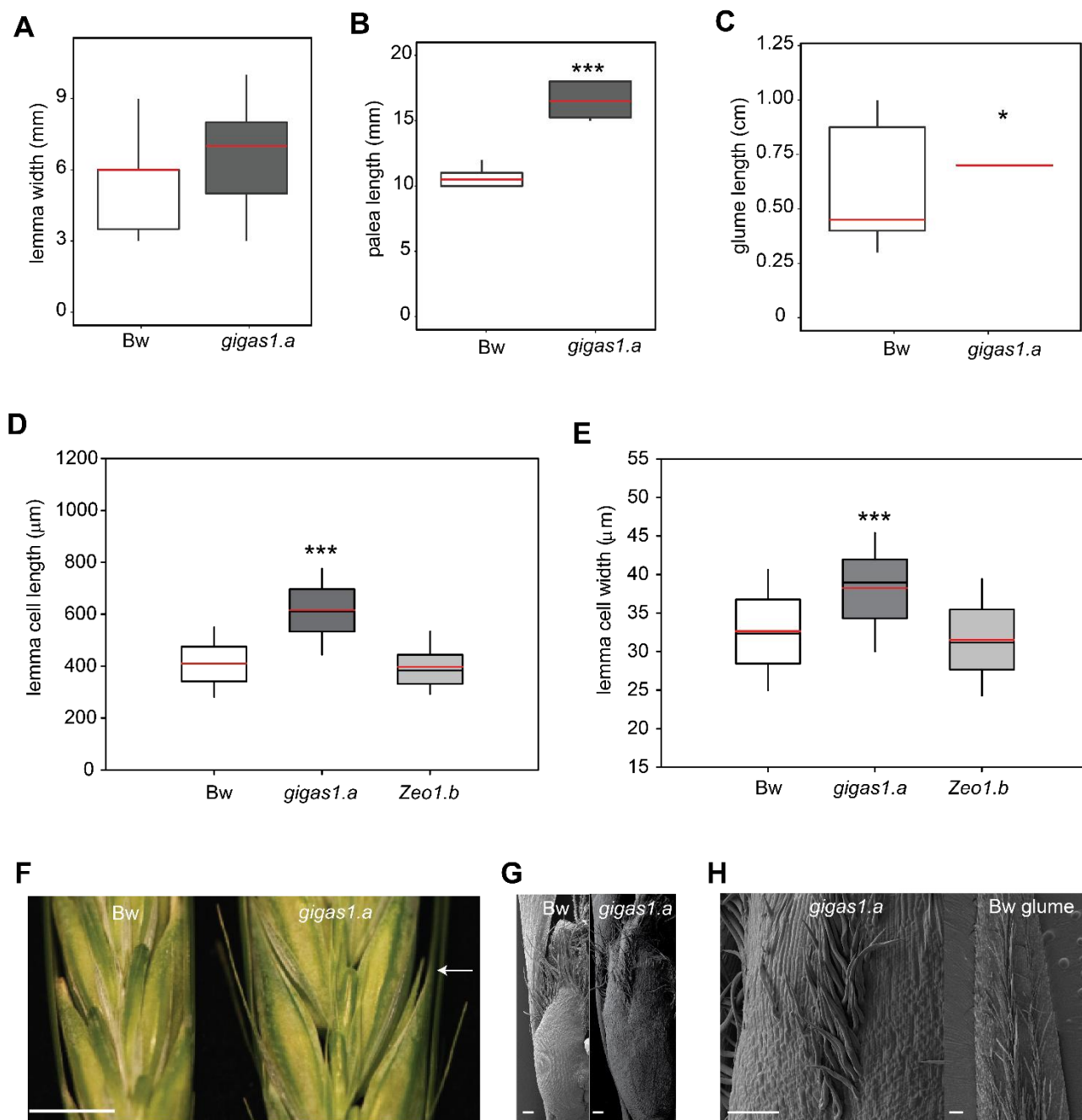


Fig. S1. Additional phenotypes of *gigas1.a*. (A-B) Phenotypes in *gigas1.a* compared to Bowman (Bowman) (n=8/ genotype). (A) Lemma width (mm). (B) Palea length (mm). (C) Glume length (cm). (D) Adaxial lemma cell length (μm). (E) Adaxial lemma cell width (μm). (F) Open-flowering in *gigas1.a* compared to Bowman. Arrow indicates gape between lemma and palea. (G) Scanning electron micrograph (SEM) of Bowman and *gigas1.a* lodicules. Note the central hairs on the distal end of *gigas1.a* lodicules. (H) Left panel shows SEM close up on the distal hairs of *gigas1.a* lodicules. Right panel shows Bowman glume with central hairs. Box plots show the median (red line) and 25th and 75th percentile and whiskers show 1.5* the interquartile range. Scale bars: F, 1mm; G,H 100 μm . *p<0.05; ***p<0.001 (t-test).

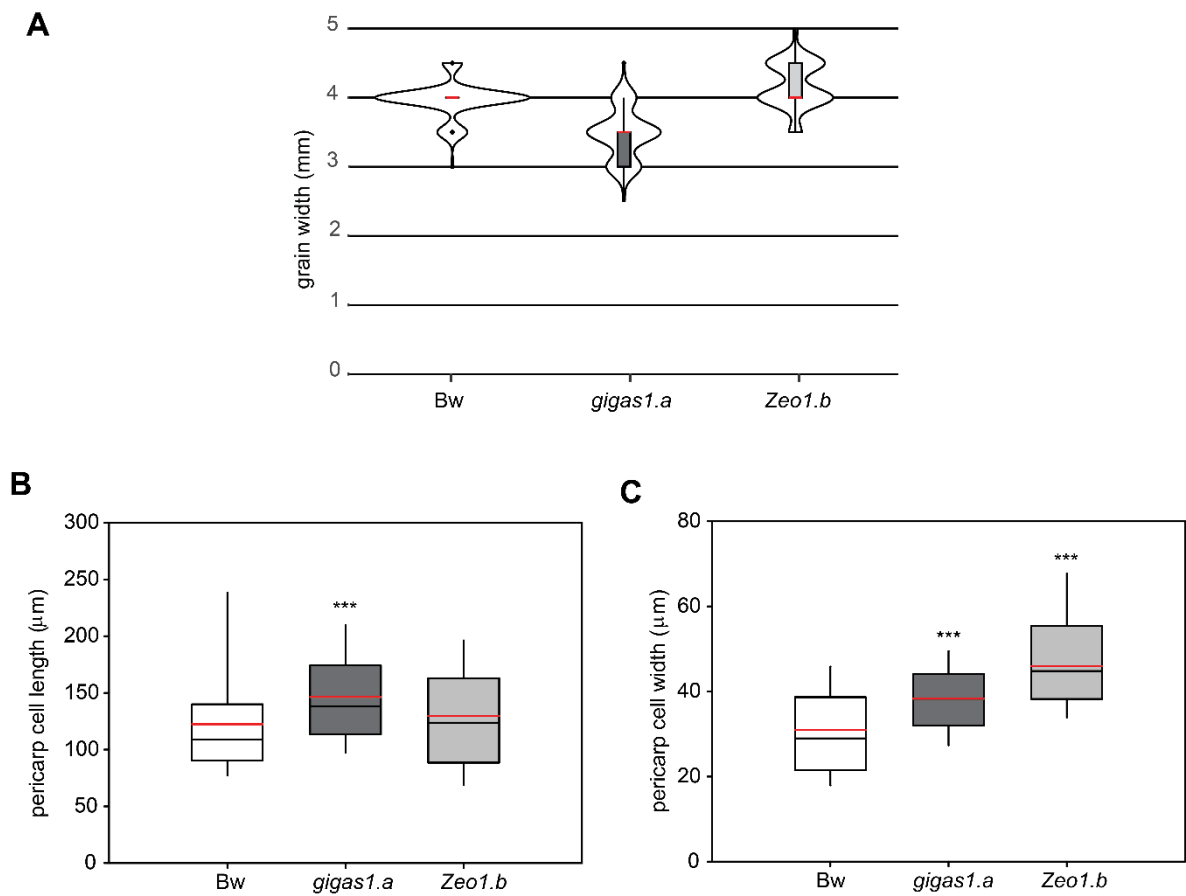


Fig. S2. Grain parameters of Bowman, *gigas1.a* and *Zeo1.b*. (A) Violin plots of grain width (cm). Grains of *gigas1.a* are narrower than Bowman (Bowman) and *Zeo1.b* ($p < 0.001$, Tukey HSD). *Zeo1.b* grains are wider than Bowman ($p < 0.001$, Tukey HSD). Bowman $n = 97$, *gigas1.a* $n = 69$, *Zeo1.b* $n = 72$. Violin plots show probability distribution of grain measurement. Box plots show the median (red line) and the 25th and 75th percentile ranges with whiskers as the 95% confidence interval and outliers as dots. (B) Pericarp lemma cell length (µm). (C) Pericarp lemma cell width (µm). *** $p \leq 0.001$ (*t*-test). $n \geq 3$ biological replicates.

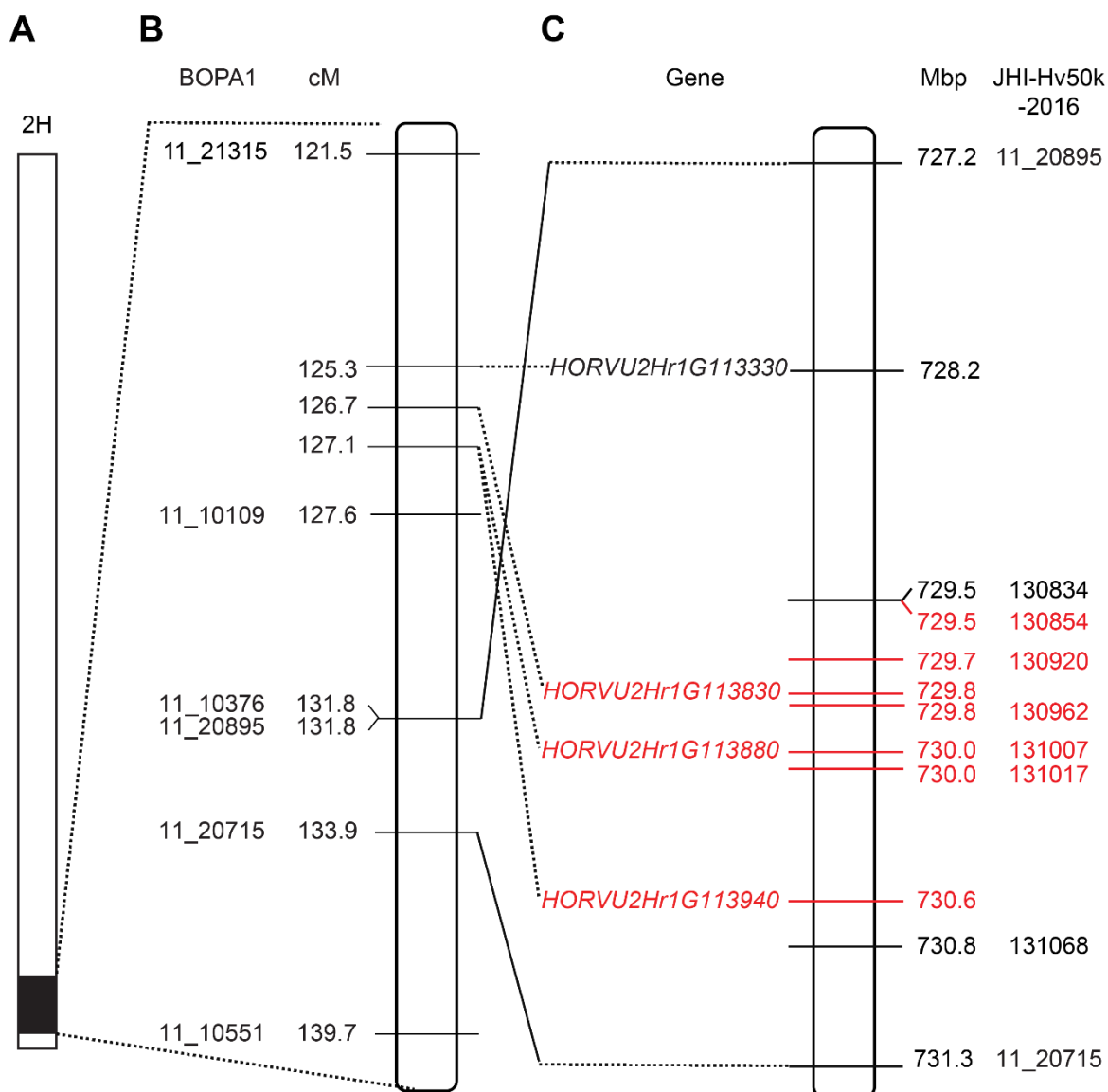


Fig. S3. Mapping detail of *gigas1.a*. (A) Schematic of section of chromosome 2HL. Black box marks the Golden Melon introgression in *gigas1.a* (BW381) (B) Golden Melon introgression markers in black from Druka et al. (2011) with cM taken from Close et al (2009). (C) Physical position of markers and selected genes. Markers in black were detected in all genotypes. Markers in red were missing in *gigas1.a* but present in Bowman and Golden Melon. PCR on *gigas1.a* genomic DNA amplified HORVU2Hr1G113330 but not HORVU2Hr1G11880 (*HvAP2*), HORVU2Hr1G11830 or HORVU2Hr1G113940. Genetic mapping data for HORVU gene models were derived from genetic mapping data linked to MLOC genes models: HORVU2Hr1G113330, MLOC_75110; HORVU2Hr1G11880, MLOC_3413; HORVU2Hr1G11830, MLOC_47968; HORVU2Hr1G113940, MLOC_81350. The deletion in *gigas1.a* spans 1.3Mbp.

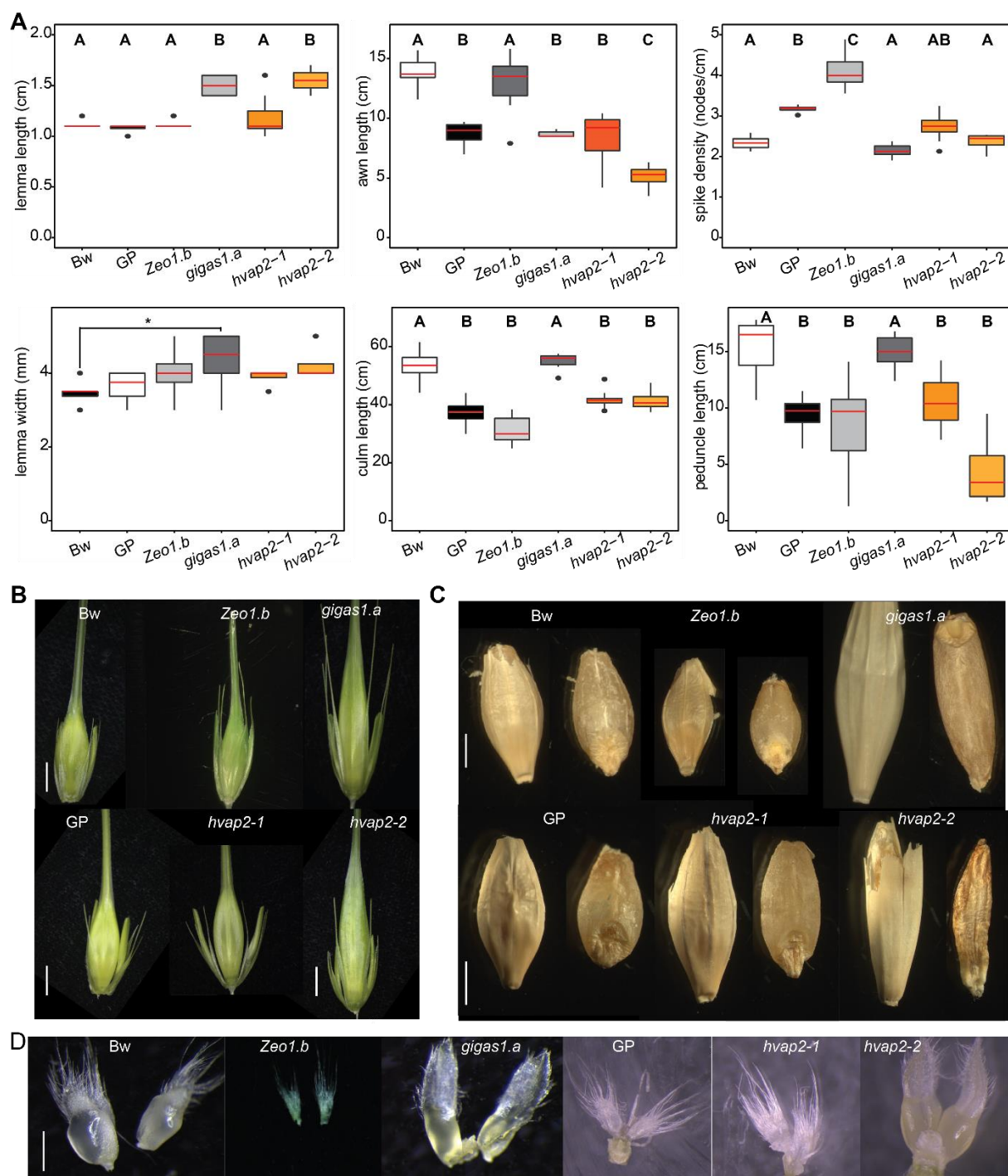


Fig. S4. *hvap2-2* phenocopies *gigas1.a*. (A) Growth phenotypes of Bowman, *Zeo1.b* and *gigas1.a* alleles and Golden Promise, *hvap2-1* and *hvap2-2* alleles. (B) Spikelets of Bowman, *Zeo1.b* and *gigas1.a* alleles and Golden Promise, *hvap2-1* and *hvap2-2* alleles. *hvap2-2* phenocopies *gigas1.a*. (C) Photos of Bowman, *Zeo1.b* and *gigas1.a* alleles and Golden Promise, *hvap2-1* and *hvap2-2* caryopses. Panels to the right of the label have had the hull peeled off. (D) Lodicule phenotypes of Bowman, *Zeo1.b* and *gigas1.a* alleles and Golden Promise, *hvap2-1* and *hvap2-2* alleles. Box plots show the median (red line) and 25th and 75th percentile, whiskers show 1.5* the interquartile range and outliers as dots. Letters indicate significant difference ($p < 0.05$) determined by ANOVA (Tukey HSD). For lemma width, the * shows the only significant difference. Scale bars: B, C, 2mm; D, 500µm.

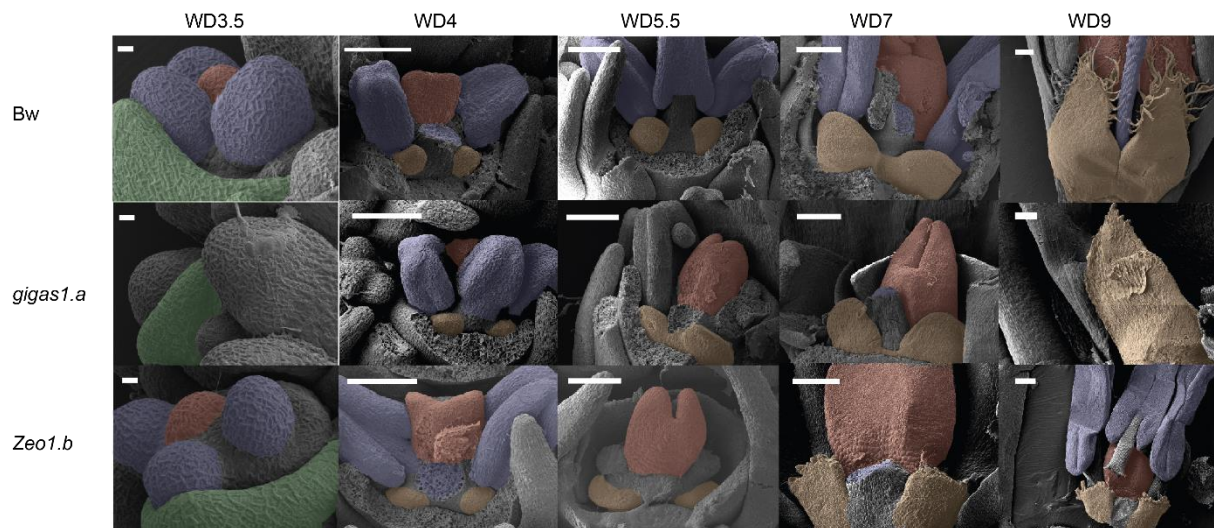


Fig. S5. Lodicule development in Bowman, *Zeo1.b* and *gigas1.a*. Scanning electron micrographs of Waddington stage 3.5 (WD4) to WD9 with lemmas removed and inner floret primordia false coloured: lodicules, yellow; stamens, blue; carpel, red.

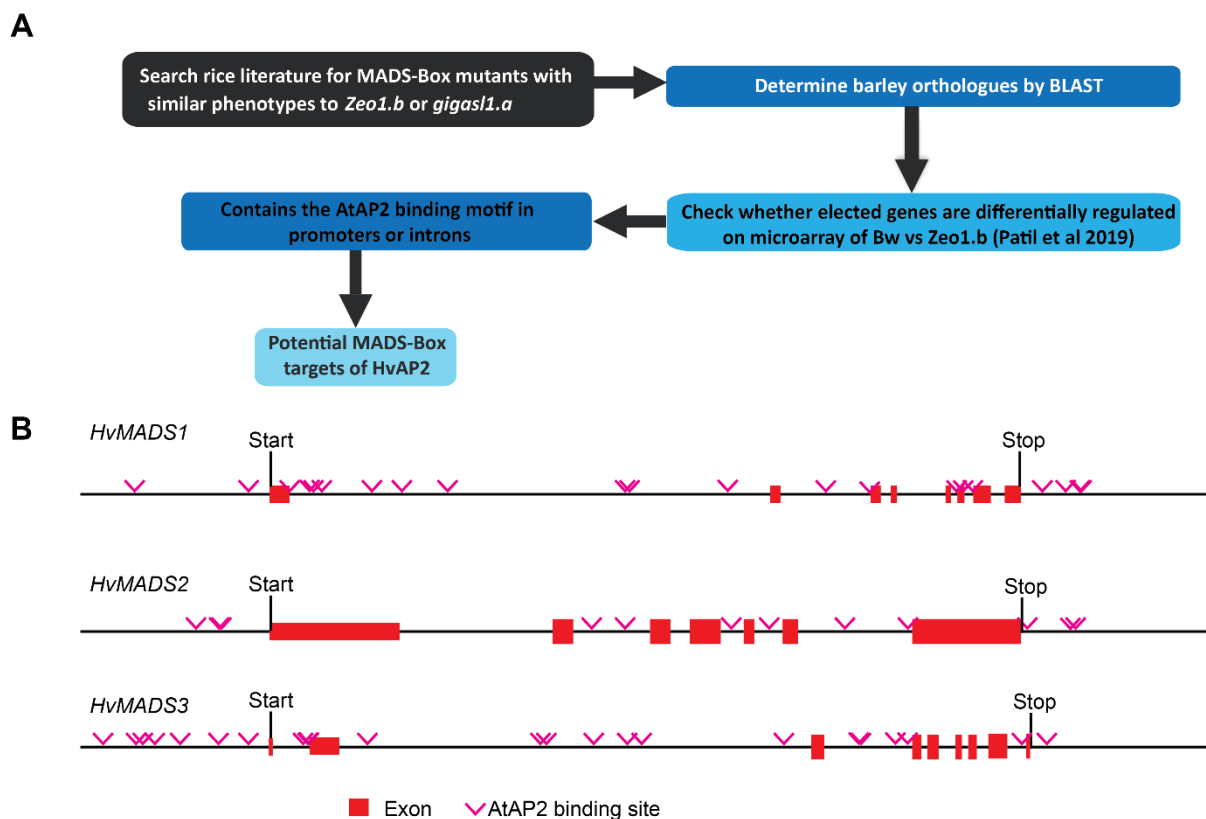


Figure S6. Pipeline to select potential targets of HvAP2. (A) Steps for choosing *MADS-box* genes as potential targets of HvAP2. (B) Schematic of the top three candidates showing putative *AtAP2* binding motifs (Dinh et al., 2012) in the promoters and introns, represented by pink “v” shapes. Bw, Bowman.

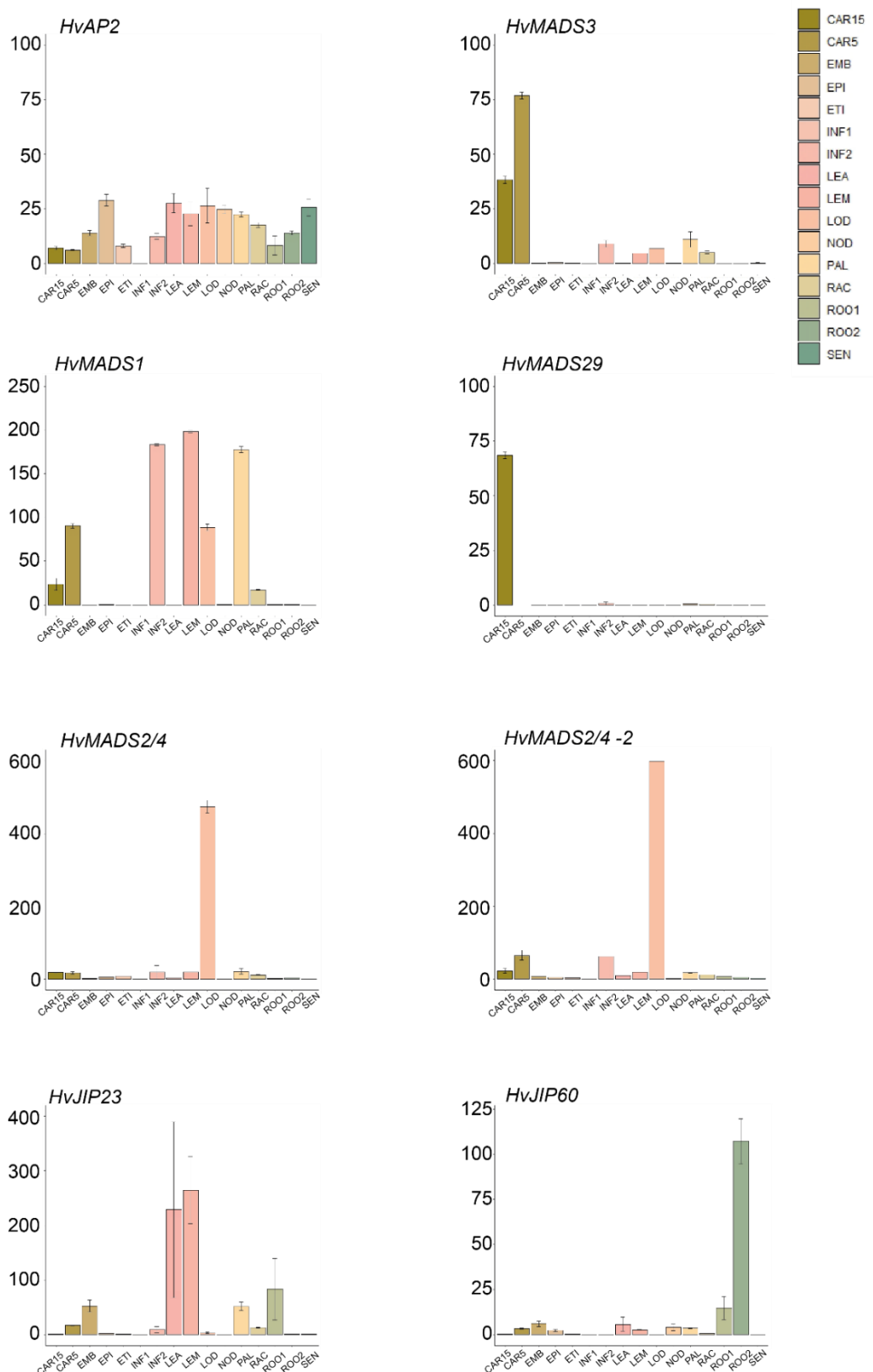


Figure S7. RNAseq data for selected *HvMADS* and *HvJIP* genes. Expression pattern for selected *HvMADS* and *HvJIP* genes in 16 different tissues/ developmental stages. The samples (3 replicates each) are: EMB, 4-day embryos dissected from germinating grains; ROO, Roots from the seedlings (10 cm shoot stage); ROO2, Root (4 weeks); LEA, Shoots from the seedlings (10 cm shoot stage); NOD, Developing tillers at six leaf stage, 3rd

internode; INF1, Young developing inflorescences (5mm); INF2, Developing inflorescences (1-1.5 cm); CAR5, Developing grain, bracts removed (5 DPA); CAR15, Developing grain, bracts removed (15 DPA); ETI, Etiolated (10 day old seedling); LEM, Lemma (6 weeks PA); LOD, Lodicule (6 weeks PA); PAL, Palea (6 weeks PA); RAC, Rachis (5 weeks PA); EPI, Epidermis (4 weeks); SEN, Senescing leaf (2 months). This expression data is derived from the publicly available RNAseq dataset BARLEX, <https://apex.ipk-gatersleben.de/apex/f?p=284:39>

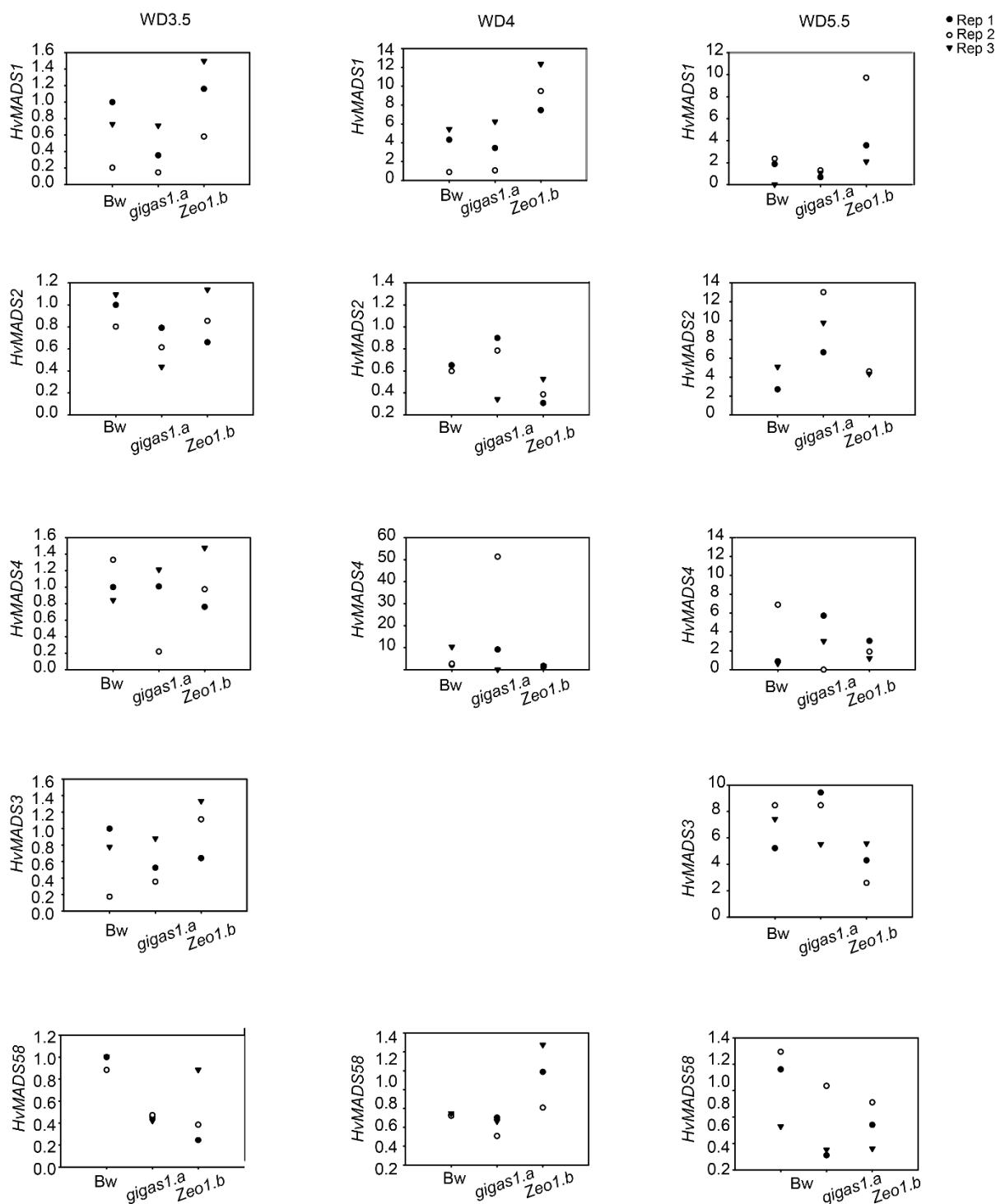


Fig. S8. qRT-PCR of MADS-box transcripts in developing spikes. Relative expression of *HvMADS1*, *HvMADS2*, *HvMADS4*, *HvMADS3*, *HvMADS58* in Bowman (Bw), *gigas1.a* and *Zeo1.b* developing spikes. Corresponding Waddington (WD) stage indicated at top. Individual points are independent biological replicates.

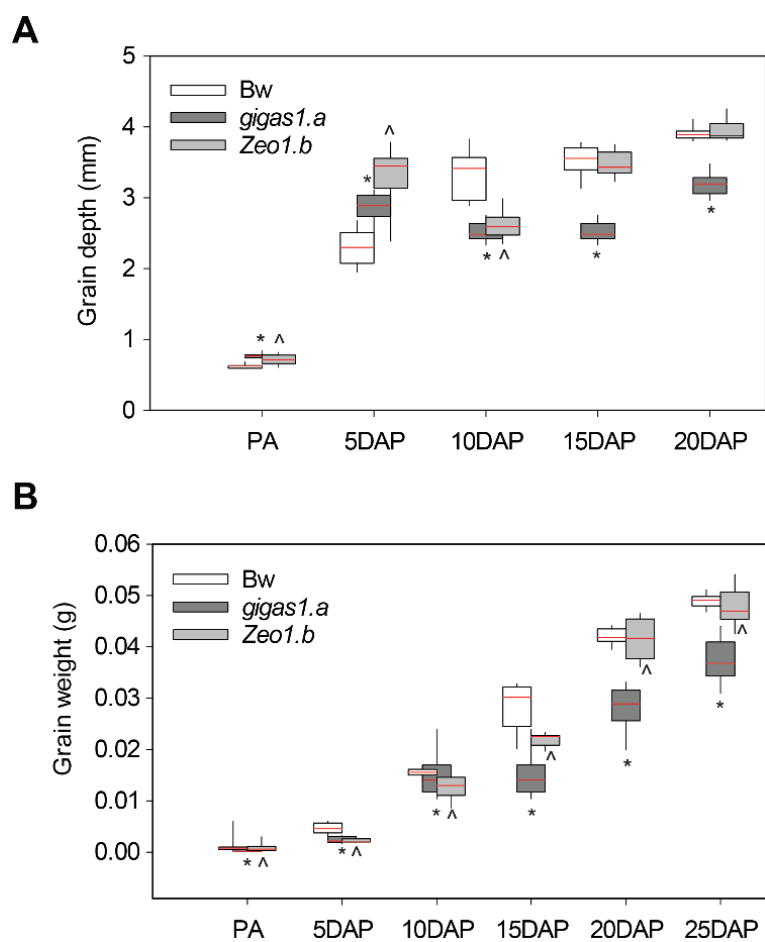


Figure S9. Ovary and caryopsis depth and weight in Bowman, *gigas1.a* and *Zeo1.b*. (A) Depth (cm) and (B) weight (g) of pre-anthesis ovary (PA) and caryopses were measured at five-day intervals at defined days after anthesis (DAP). Box plots show the median (red line), 25th and 75th percentile, whiskers show 1.5* the interquartile range. * indicates significant differences in *gigas1.a* versus Bowman and ^ indicates significant differences in *Zeo1.b* versus Bowman ($p < 0.01$ Tukey post-hoc). Depth: $n = 4$ to 11 per genotype; Weight: $n = 5$ to 10 per genotype.

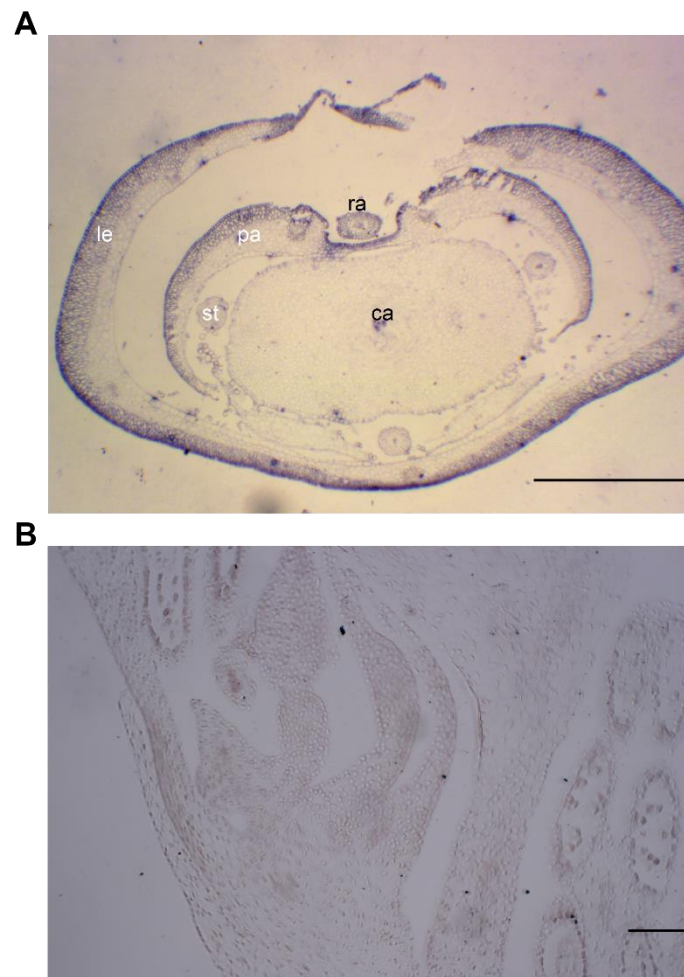


Figure S10. *HvAP2* in situ and *HvMADS1* sense in situ hybridisation. (A) Anti-*HvAP2* probe *in situ* hybridisation shows signal in lemma, palea and rachilla. (B) *HvMADS1* sense probe *in situ* hybridisation. le, lemma; pa, palea; ra, rachilla; st, stamen; ca, carpel. Scale bar: A,B 50 μ m.

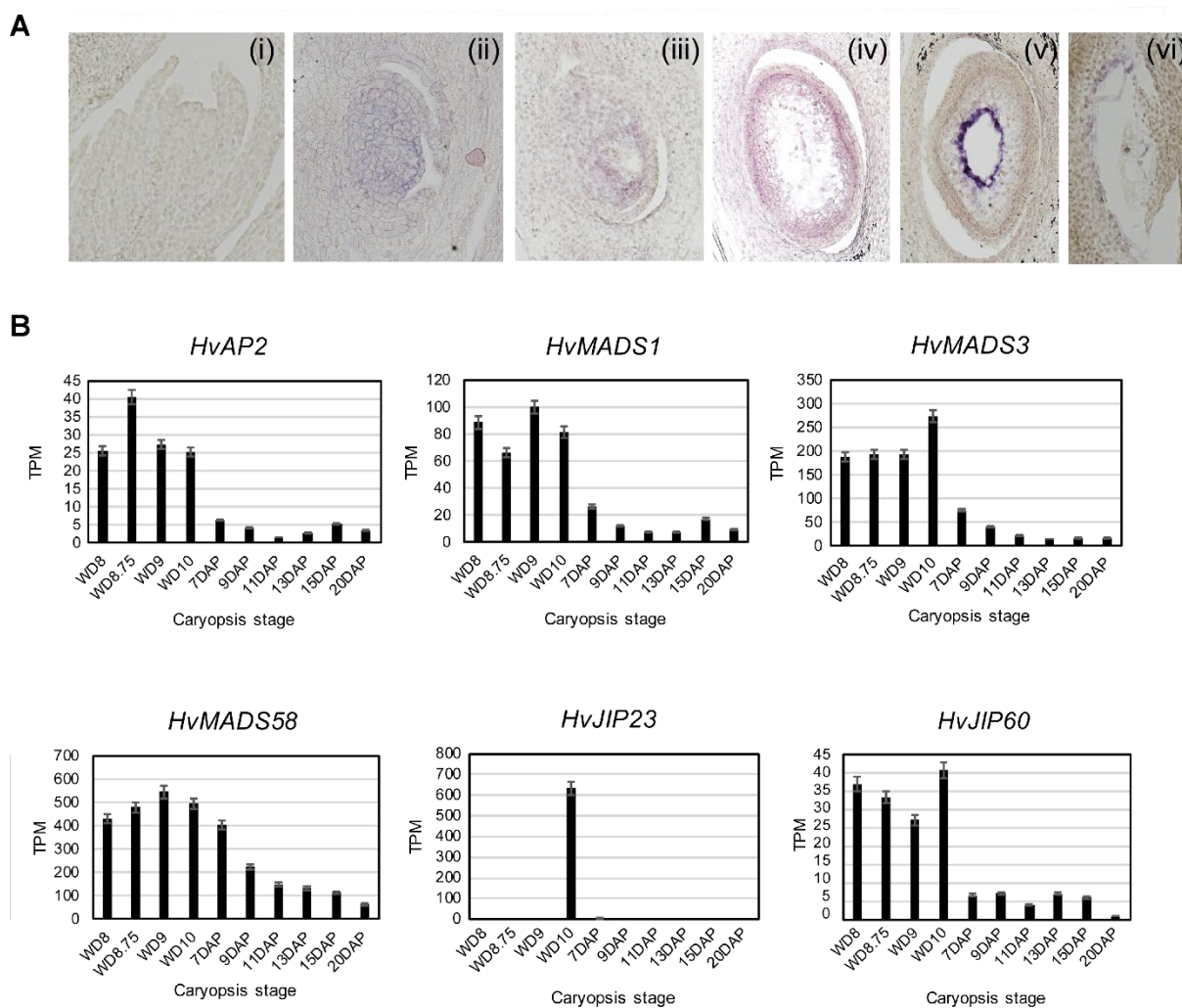


Fig. S11 *HvMADS-box* expression dynamics. (A) *HvMADS29* in situ hybridisation on pre-fertilisation carpels. Anti-sense *HvMADS29* probe (i) MMC; (ii) FGmit; (iii) FGexp; (iv, v); sense *HvMADS29* probe (vi) (B) Whole pistil/caryopsis RNAseq extracted from Aubert et al., (2018). TPM = transcripts per million, WD = Waddington stage, DAP = days after pollination.

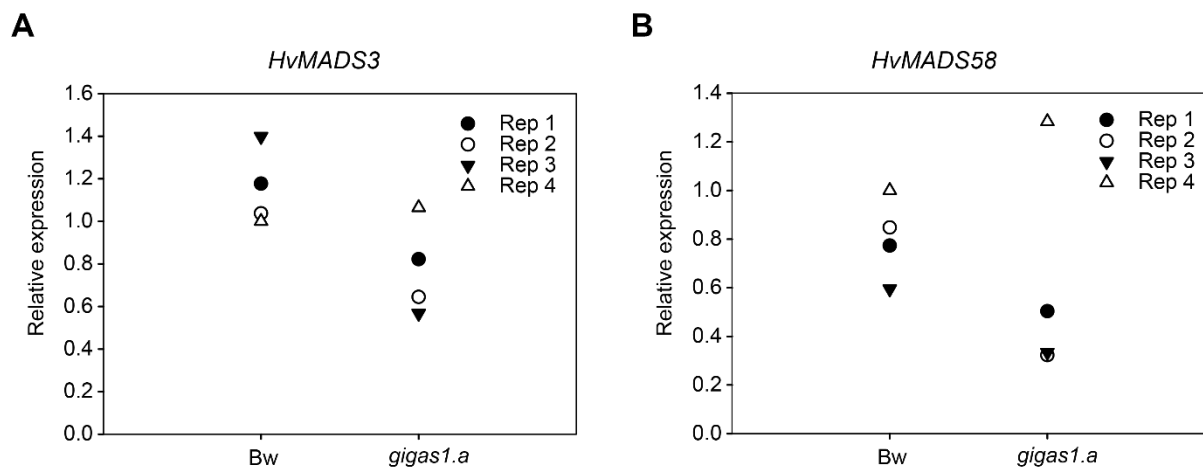


Fig. S12 *HvMADS58* and *HvMADS3* expression in *gigas1.a*. qRT-PCR of *HvMADS3* and *HvMADS58* to show relative expression in 5 days post-anthesis caryopses. Data points show individual biological replicates.

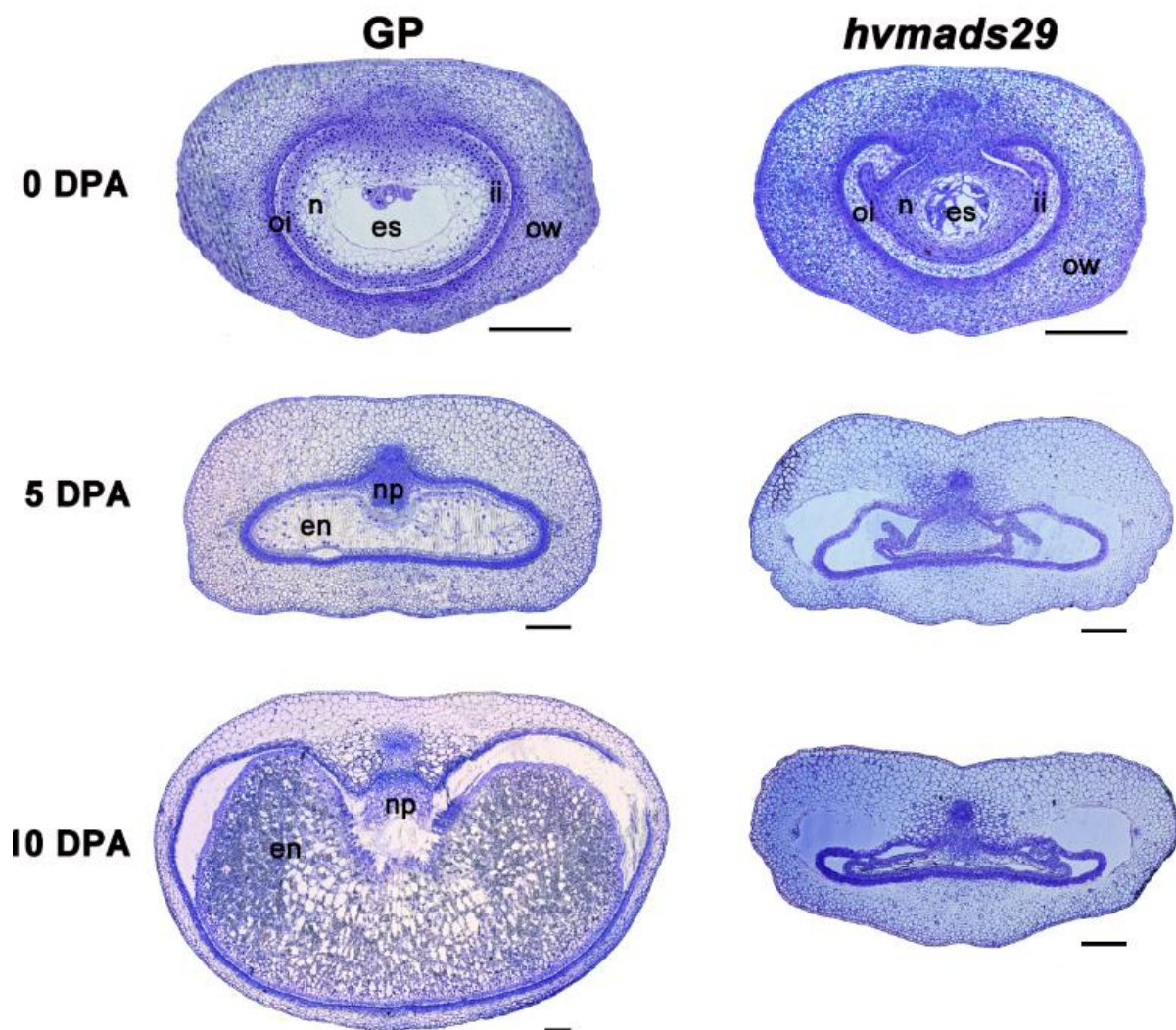


Fig. S13. Wholegrain phenotypes of *hvmads29-2* compared to cv. Golden Promise. Toluidine-stained sections are shown from the midpoint of each caryopsis. Compared to Golden Promise (GP), *hvmads29-2* ovules at anthesis show defects, particularly in the nucellus and integuments. The two layers of *hvmads29-2* inner integument cells show similar morphology to Golden Promise but have an abnormally convoluted structure, possibly due to abnormal nucellus growth. The outer integument cells are abnormally enlarged and occasionally show more than two cell layers. es, embryo sac; en, endosperm; ii, inner integument; n, nucellus; np, nucellar projection; oi, outer integument; ow, ovary wall. Scale bar: 200um.

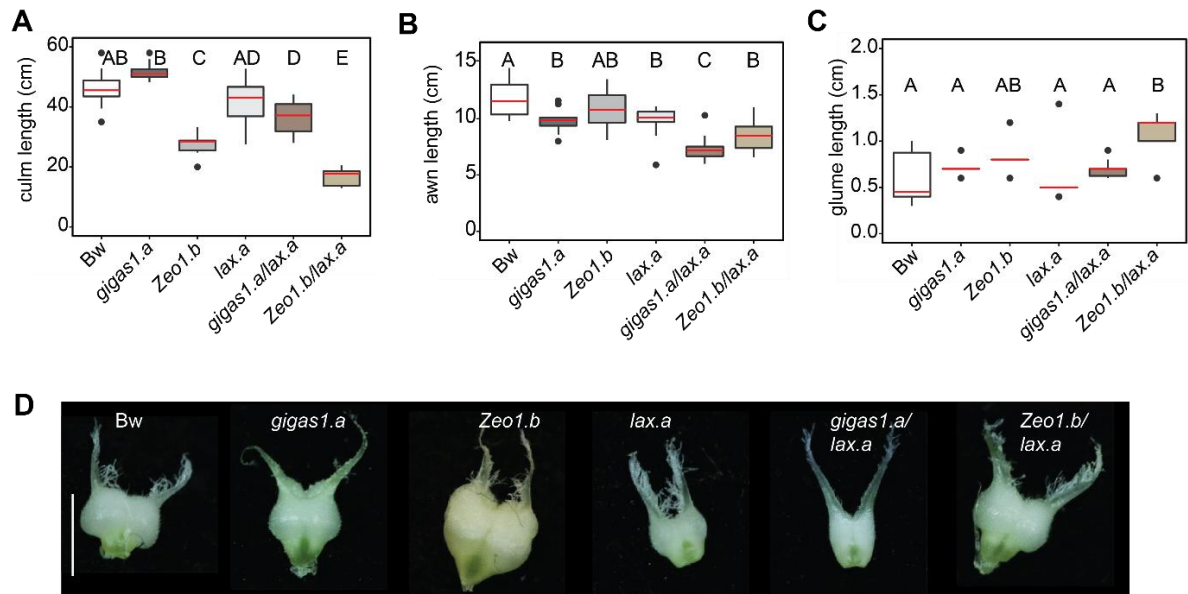


Fig. S14. Additional phenotypes of *gigas1.a/lax.a* and *Zeo1.b/lax.a*, compared to single mutant parents and Bowman. (A) Culm length (cm). (B) awn length (cm). (C) glume length (cm). $n = 8/$ genotype. (D) Stigmatic papillae branches are reduced in *gigas1.a* and in the *gigas1.a/lax.a* double mutant carpels. Box plots show the median (red line), 25th and 75th percentile, whiskers show $1.5 \times$ the interquartile range and outliers as dots. Letters indicate significant difference ($p < 0.05$) determined by ANOVA (Tukey HSD). Bw, Bowman. Scale bar: D, 2mm.

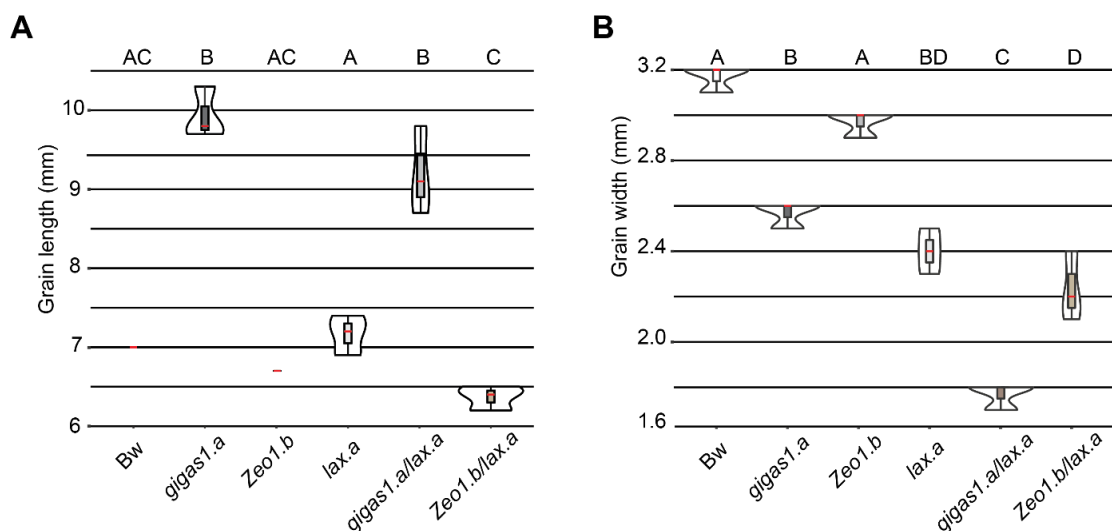


Fig. S15. Grain parameters of Bowman, *gigas1.a*, *Zeo1.b*, *lax.a*, *gigas1.a lax.a* and *Zeo1.b lax.a*. (A-B) Violin plots of grain width (A, mm) and length (B, mm). Bowman n=150, *gigas1.a* n=150, *Zeo1.b* n=150, *lax.a* n =144, *Zeo1.b lax.a* n=75, *gigas1.a lax.a* n=131. Violin plots show probability distribution of grain measurement. Box plots show the median (red line) and the interquartile ranges with whiskers 95% confidence interval. Bw, Bowman. Statistically significant differences shown by different letters (Tukey HSD, $p \leq 0.05$).



Fig. S16. *Zeo1.b* dosage on *lax.a* floret phenotypes. Top panel: *Zeo1.b/+ lax.a* (heterozygous *Zeo1.b* and homozygous *lax.a*) florets develop intermediate stamen-lobed organs in the lodicule position while *Zeo1.b lax.a* double mutant shows *Zeo1.b*-like lodicules. Bottom panel: lemmas of *Zeo1.b/+ lax.a* are also intermediate between *lax.a* and *Zeo1.b*. Scale bar, 1 mm.

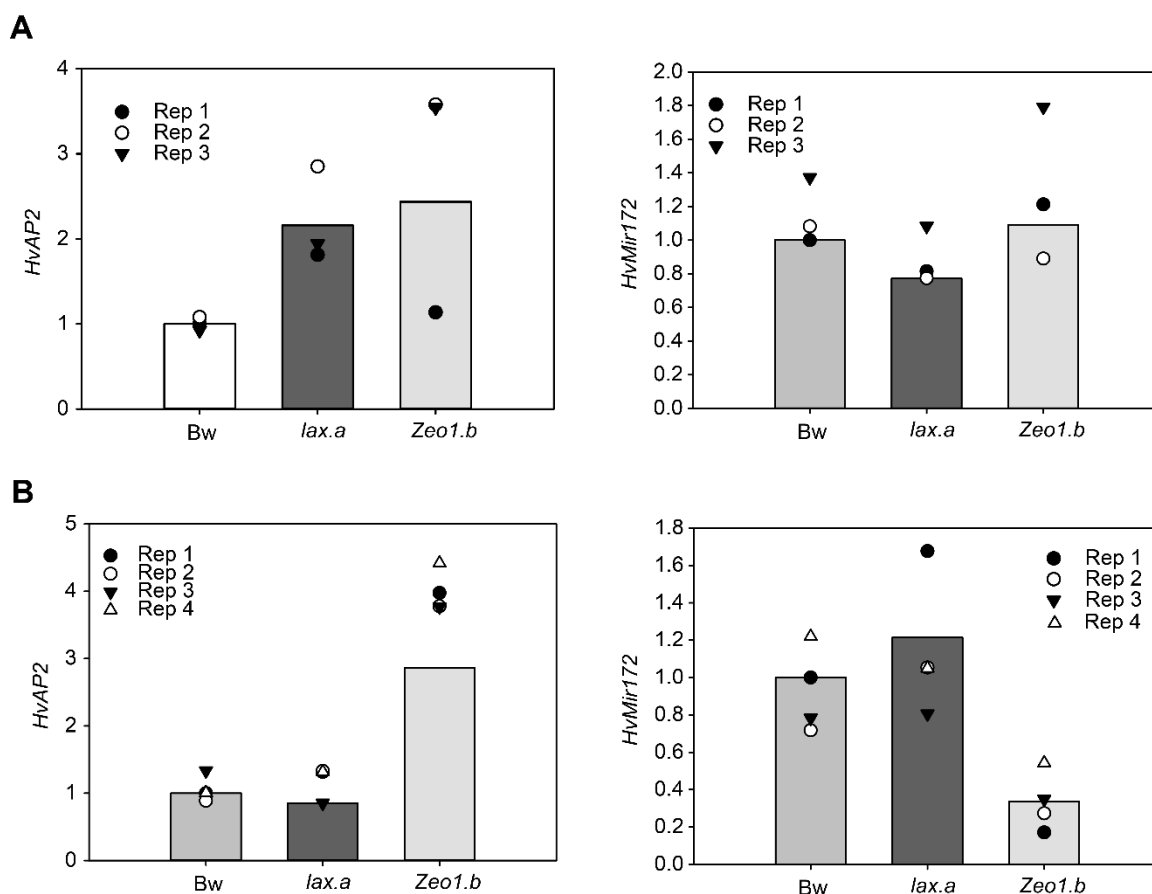


Fig. S17. qRT-PCR of *HvAP2* transcripts and *HvMir172* in whole seedlings and developing spikes. (A) Relative expression of *HvAP2* transcripts and *HvMir172* in Bowman, *lax.a* and *Zeo1.b* whole seedlings at 14 days post anthesis. (B) Relative expression of *HvAP2* transcripts and *HvMir172* in Bowman, *lax.a* and *Zeo1.b* spikes at Waddington (WD) stage 3-3.5. Individual points represent independent biological replicates and bars average expression across replicates. Each seedling replicate pooled 3-4 individuals and each spike replicate pooled 8-10 individuals. Bw, Bowman.

Table S1 Germplasm used in this study

Allele	Mutagen	Cultivar	Molecular nature	Bowman Near Isogenic Line (backcross#)	Phenotype	Gene name, HORVU gene model
<i>gigas1.a</i>	X-ray	Golden Melon	1.3Mbp deletion	BWNIL381 (BC7)	Long lemmas, lax spike, short awns, enlarged lodicules	<i>HvAP2</i> , HORVU2Hr1G113880
<i>Zeo1.b</i>	X-ray	Donaria	SNP a-g in mir172 binding site (Houston et al., 2013)	BWNIL938 (BC5)	Dense spike, non-swelling lodicules	<i>HvAP2</i> , HORVU2Hr1G113880
<i>lax.a</i>	Gamma-ray	Bonus	450-Kbp deletion	BWNIL457 (BC7)	Lax spike, lodicules transformed to stamens	<i>HvBOP2</i> , HORVU5Hr1G043230
<i>hvap2-1</i>	CRISPR-Cas9	Golden Promise	39bp deletion in exon 1	n/a	Not detected	<i>HvAP2</i> , HORVU2Hr1G113880
<i>hvap2-1</i>	CRISPR-Cas9	Golden Promise	40bp deletion in exon 1	n/a	Long lemmas, short awns, enlarged, bract-like lodicules	<i>HvAP2</i> , HORVU2Hr1G113880
<i>hvmads2-2</i>	CRISPR-Cas9	Golden Promise	1bp deletion in exon 1	n/a	Shrivelled aborted seeds, abnormal ovules	<i>HvMADS29</i> , HORVU6Hr1G32220

Table S2 Whole plant phenotypes. Phenotype table for single mutant † (Summer 2018; Bowman n=8; Golden Promise n=4; *Zeo1.b* n=7; *gigas1.a* n=7; *hvap2-1* n=8; *hvap2-2* n=4; ‡ (Autumn 2018, n = 10/ genotype) ¯ (Winter 2016; grain weight Bowman, n=62; *Zeo1.b*, n=79) *p≤0.05, ***p≤0.001 compared to Bowman; Letters indicate significant difference (p<0.05) determined by ANOVA (Tukey HSD).

Line	Spike density (nodes/cm)	Lemma length (mm)	Palea length (mm)	Glume length (mm)	Glume awn length (mm)	Lemma awn length (cm)	Spikelet width (mm)	Plant height (cm)	Peduncle length (cm)	Grain width (mm)	Grain length (mm)	Thousand grain weight (g)
Bowman	1.4±0.07‡	11.3±1.03‡	10.6±0.7‡	5.9±3‡	3.7±1‡	13.9±1.3‡	5.3±2‡	64.4±4.1‡	16.95±3.4‡	n/a	n/a	n/a
<i>gigas1.a</i>	1.3±0.08‡***	17.4±2.3‡***	16.6±1.4‡***	7.2±1‡*	7.6±1.3‡***	10.7±1.9‡***	6.5±2‡	67±5.4‡	16.9±3.8‡	n/a	n/a	n/a
Bowman	2.3±0.16†a	11.1±0.3†a	n/a	n/a	n/a	13.9±1.2†a	3.4±0.3†	53.3±5.1†a	16.95±3.4†a	3.9±0.3 a	7.7±0.7 a	49.27
<i>gigas1.a</i>	2.2±0.17†a	15±1†b	n/a	n/a	n/a	8.7±0.3†b	4.4±0.7†*	54.9±2.9a	16.9±3.7†a	3.5±0.4 b	11.2±0.8 b	55.71
<i>Zeo1.b</i>	4.1±0.5†c	11.1±0.38†a	n/a	n/a	n/a	12.8±2.7†a	4±0.7†	31.4±5†b	8.4±4.3†b	4.2±0.3 c	8.1±0.6	52.65
<i>hvap2-1</i>	2.7±0.4†ab	11.9±2.1†a	n/a	n/a	n/a	8.3±2.2†b	3.9±0.2†	41.9±3.4†b	10.6±2.4†b	n/a	n/a	n/a
<i>hvap2-2</i>	2.4±0.2†a	15.5±1.3†b	n/a	n/a	n/a	5.1±1.2†c	4.3±0.5†	41.6±4.3†b	4.5±3.5†b	n/a	n/a	n/a
Golden Promise	3.2±0.1†b	10.8±0.5†a	n/a	n/a	n/a	8.7±1.2†b	3.6±0.5†	37.3±5.7†b	9.4±2.1†b	n/a	n/a	n/a

Table S3 Genotyping data (excel file). Green SNP called is different to Golden Melon (GM), Yellow SNP called is different in *gigas1.a* compared to Bowman (Bowman), Blue GM and Bowman are the same and *gigas1.a* is different, Purple SNP called is the same in *gigas1.a* and GM but different from Bowman. Red all SNPs called are different in each genotype.

[Click here to Download Table S3](#)

Table S4 Gene models deleted in *gigas1.a*

Gene model	AGP start	AGP end	Gene model confidence	Annotation	Gene Ontology Terms
HORVU2Hr1G113720.2	729529945	729530581	LC_u	undescribed protein	none
HORVU2Hr1G113730.1	729530473	729531038	HC_U	unknown function	none
HORVU2Hr1G113740.1	729542559	729543898	LC_u	undescribed protein	none
HORVU2Hr1G113750.1	729542812	729543654	LC_u	undescribed protein	none
HORVU2Hr1G113760.1	729615037	729615558	LC_u	undescribed protein	none
HORVU2Hr1G113770.1	729726871	729727432	LC_u	undescribed protein	none
HORVU2Hr1G113780.1	729743163	729743624	LC_u	undescribed protein	none
HORVU2Hr1G113790.1	729744151	729744936	LC_u	undescribed protein	none
HORVU2Hr1G113810.2	729750668	729751329	LC_u	undescribed protein	none
HORVU2Hr1G113800.4	729750728	729751655	LC_u	undescribed protein	none
HORVU2Hr1G113820.5	729806528	729807892	HC_G	WUSCHEL related homeobox 4	GO:0003677
HORVU2Hr1G113830.11	729840906	729846418	HC_G	Filament-like plant protein 7	none
HORVU2Hr1G113840.1	729845136	729845473	LC_u	undescribed protein	none
HORVU2Hr1G113850.1	729917309	729917909	LC_u	undescribed protein	none
HORVU2Hr1G113860.1	729967615	729968783	LC_TE	unknown function	none
HORVU2Hr1G113870.1	730018206	730019081	LC_u	undescribed protein	none
HORVU2Hr1G113880.23	730027508	730030208	HC_G	AP2-like ethylene-responsive transcription factor	GO:0003677, GO:0003700, GO:0006355
HORVU2Hr1G113890.1	730352263	730353299	LC_u	undescribed protein	none
HORVU2Hr1G113900.1	730450598	730451268	LC_u	undescribed protein	none
HORVU2Hr1G113910.1	730461449	730462605	LC_u	undescribed protein	none
HORVU2Hr1G113920.1	730538427	730539037	LC_u	undescribed protein	none
HORVU2Hr1G113930.2	730544261	730547900	HC_G	RING/U-box superfamily protein	GO:0005515, GO:0008270
HORVU2Hr1G113940.4	730619045	730619834	HC_G	Dehydration responsive element binding protein	none
HORVU2Hr1G113950.1	730626720	730627002	LC_u	undescribed protein	none
HORVU2Hr1G113960.1	730632982	730633361	LC_u	undescribed protein	none
HORVU2Hr1G113970.2	730823581	730827301	HC_G	RING/U-box superfamily protein	GO:0005515, GO:0008270
HORVU2Hr1G113980.1	730847771	730848860	LC_u	undescribed protein	none

AGP, A Golden Path; LC, low confidence; HC, high confidence

Table S5. Potential binding targets of HvAP2

Gene	Phenotype of allele	Reference	Barley homologue	Arabidopsis homologue	Gene class
<i>OsMADS1</i>	Elongated lodicules	(Prasad et al., 2005, Jeon et al., 2000)	HORVU4Hr1G067680.2 HORVU7Hr1G025700.6	<i>SEP3/AGL9</i>	C
<i>OsMADS3</i>	Lodicules to stamens	(Kyoizuka and Shimamoto, 2002)	HORVU3Hr1G026650.1	<i>AGAMOUS</i>	C
<i>OsMADS2</i> and 4	Lodicule identity	(Yao et al., 2008)	HORVU3Hr1G091000.8 HORVU1Hr1G063620.2	<i>PISTILLATA</i>	B
<i>OsMADS37</i>	Flowering time		HORVU7Hr1G054390.1 HORVU7Hr1G054320.1		
<i>OsMADS58</i>	Ectopic lodicules Stamens to lodicules Abnormal carpels	(Yamaguchi et al., 2006)	HORVU1Hr1G029220.1 (top hit) HORVU3Hr1G026650.1	<i>AGL1 SHP1</i>	C
<i>OsMADS6</i>	Floral organ and meristem identity	(Li et al., 2010)	HORVU0Hr1G032300.1 HORVU6Hr1G066140.9	<i>AGL6/RSB1</i>	C
<i>OsMADS16</i>	Stamens to carpels lodicules to lemma/ palea	(Xiao et al., 2003, Yun et al., 2013, Lee et al., 2003)	HORVU7Hr1G091210.4	<i>SPW/AP3</i>	B
<i>OsMADS50/56</i>	Late flowering more internodes	(Lee et al., 2004)	HORVU1Hr1G051660.8	<i>AGL20/SOC1</i>	
<i>OsMADS8/7</i>	Floral organs to lemma palea	(Cui et al., 2010)	HORVU5Hr1G076400.1	<i>SEP3/AGL9</i>	E
<i>OsMADS22</i>	Floral morphogenesis sterility	(Sentoku et al., 2005, Lee et al., 2008)	HORVU6Hr1G077300.1	<i>SVP/AGL22</i>	?
<i>OsMADS32</i>	Elongated lodicules	(Wang et al., 2015)	HORVU3Hr1G068900.3	<i>AP3/SPW</i>	B
<i>OsMADS26</i>	Stress response	(Khong et al., 2015)	HORVU7Hr1G076310.14	<i>AGL12/XAL1</i>	
<i>OsMADS29</i>	Grain development hormone control	(Nayar et al., 2013)	HORVU6Hr1G032220.8	<i>AGL32/ ABS</i>	
<i>OsMADS55</i>	Reduction in elongated internodes	(Lee et al., 2008)	HORVU7Hr1G036130.1	<i>SVP/AGL22</i>	
<i>OsMADS34</i>	Elongated sterile lemmas functions with <i>OsMADS1</i> to specify floral organ identity	(Gao et al., 2010)	HORVU5Hr1G095710.1	<i>SEP/PAP2/AGL1/2/4</i>	E
<i>OsMADS15</i>	Tillering, panicle branching internode elongation	(Lu et al., 2012)	HORVU2Hr1G063800.7	<i>AP1</i>	A

Table S6 Dimensions and weight of Bowman, *gigas1.a* and *Zeo1.b* pre-anthesis ovaries and caryopses. Length, width, depth and weight (g) of preanthesis ovary (PA) and caryopses were measured at five-day intervals at defined days post anthesis (DPA). Length, width, depth, n = 4 to 11; weight: n = 5-10. Dunn's Post-hoc test different from Bowman *P<0.05 **P<0.01 ***P<0.001

Trait	stage	Bowman	se	<i>Zeo1.b</i>	se	<i>gigas1.a</i>	se
length (cm)	PrAsOv	1.60	0.06	1.52***	0.05	1.87***	0.08
	5 DPA	8.59	0.29	6.04*	0.10	7.29***	0.31
	10 DPA	9.13	0.18	9.78***	0.18	12.58***	0.14
	15 DPA	9.10	0.05	9.91*	0.11	14.13***	0.14
	20 DPA	9.54	0.09	9.61**	0.06	13.69***	0.19
	25 DPA	9.32	0.04	9.35	0.17	15.14***	0.10
	30 DPA	8.57	0.06	9.44*	0.06	13.16***	0.23
width (cm)	PrAsOv	0.98	0.02	0.98	0.02	1.18***	0.02
	5 DPA	2.84	0.05	3.76***	0.16	2.66	0.22
	10 DPA	3.97	0.06	3.65*	0.03	3.35*	0.05
	15 DPA	4.57	0.03	4.65	0.03	4.31***	0.03
	20 DPA	4.96	0.01	4.99	0.04	4.34***	0.04
	25 DPA	4.94	0.01	5.07	0.06	4.63***	0.04
	30 DPA	4.22	0.04	5.14***	0.04	4.37*	0.05
depth (cm)	PrAsOv	0.62	0.01	0.72***	0.02	0.77***	0.01
	5 DPA	2.30	0.08	3.32*	0.13	2.83***	0.09
	10 DPA	3.31	0.11	2.62**	0.06	2.51*	0.04
	15 DPA	3.52	0.07	3.47*	0.06	3.19	0.05
	20 DPA	3.91	0.03	3.94**	0.04	3.26	0.03
	25 DPA	3.94	0.04	3.80**	0.07	3.38	0.02
	30 DPA	3.69	0.17	4.07*	0.06	3.33	0.04
weight (cm)	PrAsOv	0.0336	0.0083	0.0009**	0.0003	0.0004**	0.0001
	5 DPA	0.0047	0.0003	0.0022**	0.0002	0.0024**	0.0002
	10 DPA	0.0155	0.0003	0.0129**	0.0007	0.0150**	0.0014
	15 DPA	0.0286	0.0014	0.0220**	0.0004	0.0283**	0.0014
	20 DPA	0.0420	0.0005	0.0415**	0.0013	0.0374**	0.0013
	25 DPA	0.0490	0.0004	0.0478**	0.0011	0.0502**	0.0012
	30 DPA	0.0478	0.0004	0.0531**	0.0017	0.0521**	0.0021

PrAnOv: preanthesis ovary; DPA; days post anthesis

Table S7 Phenotypes of Bowman, single mutant parents and double mutants. Measurements taken in summer 2018. Letters indicate significant difference ($p < 0.05$) determined by ANOVA (Tukey HSD). $n = 10$ / genotype.

Line	Spike density (nodes/cm)	Lemma length (mm)	Palea length (mm)	Glume length (mm)	Glume awn length (mm)	Lemma awn length (cm)	Spikelet width (mm)	Culm height (cm)	TGW (g)
Bowman	1.4±0.1a	9.8±0.4a	10.5±0.5	5.9±2.9a	3.7±0.9a	11.8±1.7a	3.7±0.a	46.1±6.5ab	38±0.7
<i>Zeo1.b</i>	2.4±0.2b	10.5±0.5ac	10.5±0.8	8.3±1.9ab	6.3±1.4ac	10.8±2ab	3.8±0.4a	27.2±3.7c	28.7±0.5
<i>gigas1.a</i>	1.4±0.1a	14.2±0.9bc	9.3±0.9	7.2±1a	7.6±1.4b	9.8±1.1b	4.6±0.8b	53.4±5.7b	33.0±0.78
<i>lax.a</i>	1.3±0.1a	17.3±4b	11.9±7	5.7±2.9a	5.8±2.9a	9.7±1.5b	3±0.4ac	41.6±7.3ad	23.6±1.4
<i>gigas1.a</i> / <i>lax.a</i>	1.4±0.2a	17.6±4b	11.2±3	7±0.9a	7.7±1.5bc	7.4±1.3c	2.7±0.6c	36.4±5.9d	15.5±1.1
<i>Zeo1.b</i> / <i>lax.a</i>	2.1±0.3b	1.4±2.5bc	12.3±0.7	10.8±2.1b	43.7±23d	8.6±1.4b	2.8±0.7ac	16.8±3e	16.0±1.9

TGW, thousand grain weight

Table S8 Spike lengths, ages and stages for developmental analysis and RNA isolation

Days after sowing	Spike length (mm)			Stage*
	Bowman	<i>Zeo1.b</i>	<i>gigas1.a</i>	
21	2.2±0.11 [^]	1.7±0.06	1.7±0.07	3.5
23	3.4±0.1 [^]	2.7±0.07	2.7±0.06	4
25	4.8±0.19 [^]	3.2±0.13 [^]	3.9±0.09 [^]	5.5
30	12.7±0.72 [^]	5.9±0.27	6.3±0.32	7
35	18.4±2.3 [^]	10.9±0.75	12.5±0.91	9

*Stages according to Waddington et al (1983)

[^] significantly different

Table S9. Primers used to synthesise probes for in situ hybridisation

Primer	Sequence 5'-3'
HvAP2_12_F2	TCTTCCACCACTCCATCTCC
HvAP2_12_RT7	GAATTGTAATACGACTCACTATAGGGGCTCCACCACAAACACACAC
HvMADS1-AF	CCCTCATCATCTTCTCCGGC
HvMADS1-RF	CAT AAT ACG ACT CAC TAT AGGCCCTCATCATCTTCTCCGGC
HvMADS1-SF	CAT AAT ACG ACT CAC TAT AGG GACGATCCAGGATGTCCACC
HvMADS1-SR	GACGATCCAGGATGTCCACC
HvM29-ISH-AF	ACGTCGCAAGGAGCATATCT
HvM29-ISH-AR	TAATACGACTCACTATAGGGTTACCAGAGGTGGAGGCCGT
HvM29-ISH-SF	TAATACGACTCACTATAGGGACGTCGCAAGGAGCATATCT
HvM29-ISH-SR	TTACCAGAGGTGGAGGCCGT

Table S10. Primers used to clone gRNAs

gRNA	primers	Sequence 5'-3'
HvAP2-3	CRISPR-F1 HvAP2	ACGCGACCAACTTATAAACCCGCGCGCTGTCGCTTGTGTTGCCGGCCAG GCGGAGCCACG
	CRISPR-R1 HvAP2	GACTAGCCTTATTTTAACTTGCTATTCTAGCTCTAAAACCGTGGCTCCGC CTGGCCGGC
HvAP2-2	C- CRISPR_F2_Hv AP2	ACGCGACCAACTTATAAACCCGCGCGCTGTCGCTTGTGTTGGGTATCTC GACCACCGCGG
	C- CRISPR_R2_Hv AP2	GACTAGCCTTATTTTAACTTGCTATTCTAGCTCTAAAACCGCGGTGGT CGAGATACCC
HvMADS 29	M29T1-sgF	TGACCTTCTCCAAGCGCCGGTTTTAGAGCTAGAAAT
	M29T1-U6aR	CGGCGCTTGGAGAAGGTCACGGCAGCCAAGCCAGCA
	U-F	CTCCGTTTTACCTGTGGAATCG
	gR-R	CGGAGGAAAATTCCATCCAC
	Pps-GGL	TTCAGAGGTCTCTCTCGACTAGTATGGAATCGGCAGCAAAGG
	Pgs-GGR	AGCGTGGGTCTCGACCGACGCGTATCCATCCACTCCAAGCTC

Blue text indicates Gibson Assembly sequence and green text indicate the *HvAP2* guide sequence

Table S11. Primers for CRISPR-Cas9 screening

Primer	Forward Primer 5'-3'	Reverse Primer 5'-3'
Cas9	ACGACTCCCTGACCTTCAAG	AGCTTGCTCTTGAGGGTGAT
<i>HvAP2</i> CRISPR screening external primers	GCGCTCCTAGGTTAAGAAGAGG	GTAAAAGGAGCAGAGGCATGG
<i>HvAP2</i> CRISPR screening internal primers	CAATTTTGCTGCCGGTCAGCTAAGGGAAGGGAAGGGAAGGA	AGGAAAGGAAAGGAGCGGAG
<i>lax.a</i> screening primers	TCTCTGCCGCATCAACAG	CCGCATGGATACTCACTTCTT
<i>gigas1.a</i> screening primers	GGAGCAGAGAGGGGTGAATG	AGTGCCTACAAATTGCCGTC
<i>mads29</i> genotyping primers	GCTGTTGGATCAGATCCAGTTGA	GACAATACTGTACAAGGTAGAG

Table S12. qRT-PCR primers

Target	Forward	Reverse	Amplicon length	UP#	Efficiency	R ²
<i>HvMADS1#2</i>	GGACATATGGACCGCATTCT	AGCAAGAATTGCAGGATGAAA	92	77	102	0.995
<i>HvMADS2#2</i>	TGGTCTGGTACTTCTCCAAGAT T	GAAGGCCAAGGAGATCAGC	131	32	99.5	0.998
<i>HvMADS3#1</i>	TCAGCATACATCAGCTCATTCT T	ACCCTGAGGGATCTTAAGCAG	89	19	100.3	0.985
<i>HvMADS4#1</i>	AGCTCCATCTCCCTCATGC	GCTGGAGGAGGAGCACAA	78	21	101.8	0.998
<i>HvMADS37#3</i>	GGAGGGTATGGGGAGGAGT	GCCGTCTTCAAATGCTCATC	72	18	102.7	0.998
<i>HvMADS58#3</i>	CTCAATGGTTGCCCTTGACG	GAGCTCTCGGTGCTCTGC	102	28	108	0.997
<i>HvMADS29#2</i>	AGTTCTCCGTCGCCAAAGT	CGACGTAAATTGTCGAGCTG		17		
<i>HvJIP23</i> [^]	ATCACAGTGTGTGTGCAAAG	ACTTTTGC GCGTTAACATCC			100	0.98
<i>HvJIP60</i> [^]	CAGCAGCGACTTCATTTACA	ATGGTGTGCGAGACTATCCT			128	0.99
<i>HvMiR172</i> reverse transcription ^{**^}	<i>Uni_MIRs</i> - TGGTGCAGGGTCCGAGGTATT	RTmiR172a – GGCGGAGAATCTTGATGATG				
<i>HvMiR172</i> qPCR ^{**^}	SLOmiR172- GTCTCCTCTGGTGCAGGGTCC GAGGTATTCGCACcagaggagAC ATGCAG	RTmiR172a – GGCGGAGAATCTTGATGATG				
<i>HvsnoR101</i>	GATGTCTTACACTTGATCTCTG AACTT	TGCATCAGGATTGATATAGTGTC C				

UP, Universal Probe

*Davis (2011) PhD Thesis Glasgow University.

**From Debernardi et al (2017)

^SYBER Green Power UP chemistry

Table S13. *Zeo1.b/lax.a* F2 segregation analysis.

	wild type	<i>Zeo1.b</i> +	<i>Zeo1.b</i>	<i>lax.a</i>	<i>Zeo1.b</i> + <i>lax.a</i>	<i>Zeo1.b lax.a</i>	total number
Expected	3	6	3	1	2	1	16
Expected normalised	4.875	9.75	4.875	1.625	3.25	1.625	26
Observed	4	10	3	2	3	1	26

 $\chi^2 = (5, n = 16) = 0.94, p > 0.05.$

Supplemental Methods

***gigas1.a lax.a* double mutant genotyping**

The *lax.a* marker (2_0524) was described (Jost et al., 2016). The *gigas1.a* marker (131068) was derived from the 50 iSelect SNP Chip (Bayer et al., 2017). The *gigas1.a* genotyping reaction (7.5µl OneTaq 2x mastermix with standard buffer (NEB), 0.5µl of each primer, 1µl genomic RNA, and 5.5µl of nuclease-free water) was run for an initial denaturation of 94°C for 5 minutes, followed by 35 cycles of 94°C for 30 seconds, 51°C for 30 seconds and 68°C for 30 seconds and a final extension of one minute at 68°C. PCR products were digested using TaqI (ThermoFisher) in a reaction of 7µl nuclease-free water, 2µl of 10x TaqI buffer, 10µl of PCR product and 1µl of TaqI. Digests were incubated overnight at 65°C and deactivated for 20 minutes at 80°C. Primers listed in Tables S10.

CRISPR-Cas9 genotyping and mutation screening

Transgenic lines were screened for the presence of the *bcoCas9* gene by PCR. PCR reactions (7.5µl OneTaq 2x mastermix with standard buffer (NEB), 0.5µl of each primer, 1µl of genomic DNA, and 5.5µl of nuclease-free water) were run for an initial denaturation at 94°C for two minutes, followed by 35 cycles of 94°C for 30 seconds, 54°C for 30 seconds, 68°C for one minute, with a final extension of 68°C for five minutes.

Screening for mutations in *HvAP2* involved an external and internal PCR reaction. The external PCR (10µl of OneTaq polymerase 2x mastermix with GC buffer (NEB), 2.5µl of GC enhancer (NEB), 0.5µl of each primer and 1µl of genomic DNA) was run with an initial denaturation of 94°C for one minute and then 35 cycles of 94°C for 30 seconds, 55°C for 30 seconds, 68°C for one minute, with a final extension of 68°C for five minutes. Internal PCR reactions (identical recipe as the external PCR but using the external PCR reaction as template) were run with an initial denaturation of 94°C for one minute and then 35 cycles of 94°C for 30 seconds, 58°C for 30 seconds, 68°C for 30 seconds and a final extension at 68°C for five minutes. For indel analysis, internal PCR products were added to a mix of 8.9µl of HiDi formamide, 0.1µl of Liz500 (ThermoFischer) and 1µl of each PCR product. Indel Detection by Amplicon Analysis (IDAA) (Yang et al., 2015) All primers listed in Table S10.

Supplemental References

- BAYER, M. M., RAPAZOTE-FLORES, P., GANAL, M., HEDLEY, P. E., MACAULAY, M., PLIESKE, J., RAMSAY, L., RUSSELL, J., SHAW, P. D., THOMAS, W. & WAUGH, R. 2017. Development and Evaluation of a Barley 50k iSelect SNP Array. *Frontiers in Plant Science*, 8.
- CLOSE, T.J., BHAT, P.R., LONARDI S *et al.* 2009 Development and implementation of high-throughput SNP genotyping in barley. *BMC Genomics* 10, 582
- CUI, R., HAN, J., ZHAO, S., SU, K., WU, F., DU, X., XU, Q., CHONG, K., THEIßEN, G. & MENG, Z. 2010. Functional conservation and diversification of class E floral homeotic genes in rice (*Oryza sativa*). *The Plant Journal*, 61, 767-781.
- DEBERNARDI JM, LIN H, CHUCK G, FARIS JD, DUBCOVSKY J. 2017. microRNA172 plays a crucial role in wheat spike morphogenesis and grain threshability. *Development* 144: 1966–1975
- DINH, T. T., GIRKE, T., LIU, X., YANT, L., SCHMID, M. & CHEN, X. 2012. The floral homeotic protein APETALA2 recognizes and acts through an AT-rich sequence element. *Development*, 139, 1978-1986.
- DRUKA, A., FRANCKOWIAK, J., LUNDQVIST, U., BONAR, N., ALEXANDER, J., HOUSTON, K., RADOVIC, S., SHAHINNIA, F., VENDRAMIN, V., MORGANTE, M., STEIN, N. & WAUGH, R. 2011. Genetic Dissection of Barley Morphology and Development. *Plant Physiology*, 155, 617-627.

- GAO, X., LIANG, W., YIN, C., JI, S., WANG, H., SU, X., GUO, C., KONG, H., XUE, H. & ZHANG, D. 2010. The *SEPALLATA*-Like Gene *OsMADS34* Is Required for Rice Inflorescence and Spikelet Development. *Plant Physiology*, 153, 728-740.
- HOUSTON, K., MCKIM, S. M., COMADRAN, J., BONAR, N., DRUKA, I., UZREK, N., CIRILLO, E., GUZY-WROBELSKA, J., COLLINS, N. C., HALPIN, C., HANSSON, M., DOCKTER, C., DRUKA, A. & WAUGH, R. 2013. Variation in the interaction between alleles of *HvAPETALA2* and *microRNA172* determines the density of grains on the barley inflorescence. *Proc Natl Acad Sci U S A*, 110, 16675-80.
- JEON, J.-S., JANG, S., LEE, S., NAM, J., KIM, C., LEE, S.-H., CHUNG, Y.-Y., KIM, S.-R., LEE, Y. H., CHO, Y.-G. & AN, G. 2000. *leafy hull sterile1* Is a Homeotic Mutation in a Rice MADS Box Gene Affecting Rice Flower Development. *The Plant Cell*, 12, 871-884.
- JOST, M., TAKETA, S., MASCHER, M., HIMMELBACH, A., YUO, T., SHAHINNIA, F., RUTTEN, T., DRUKA, A., SCHMUTZER, T., STEUERNAGEL, B., BEIER, S., TAUDIEN, S., SCHOLZ, U., MORGANTE, M., WAUGH, R. & STEIN, N. 2016. A Homolog of *Blade-On-Petiole 1 and 2 (BOP1/2)* Controls Internode Length and Homeotic Changes of the Barley Inflorescence. *Plant Physiol*, 171, 1113-27.
- KHONG, G. N., PATI, P. K., RICHAUD, F., PARIZOT, B., BIDZINSKI, P., MAI, C. D., BÈS, M., BOURRIÉ, I., MEYNARD, D., BEECKMAN, T., SELVARAJ, M. G., MANABU, I., GENGA, A.-M., BRUGIDOU, C., NANG DO, V., GUIDERDONI, E., MOREL, J.-B. & GANTET, P. 2015. *OsMADS26* Negatively Regulates Resistance to Pathogens and Drought Tolerance in Rice. *Plant Physiology*, 169, 2935-2949.
- KYOZUKA, J. & SHIMAMOTO, K. 2002. Ectopic expression of *OsMADS3*, a rice ortholog of *AGAMOUS*, caused a homeotic transformation of lodicules to stamens in transgenic rice plants. *Plant and Cell Physiology*, 43, 130-135.
- LEE, S., CHOI, S. C. & AN, G. 2008. Rice SVP-group MADS-box proteins, *OsMADS22* and *OsMADS55*, are negative regulators of brassinosteroid responses. *Plant Journal*, 54, 93-105.
- LEE, S., JEON, J. S., AN, K., MOON, Y. H., LEE, S., CHUNG, Y. Y. & AN, G. 2003. Alteration of floral organ identity in rice through ectopic expression of *OsMADS16*. *Planta*, 217, 904-911.
- LEE, S., KIM, J., HAN, J.-J., HAN, M.-J. & AN, G. 2004. Functional analyses of the flowering time gene *OsMADS50*, the putative *SUPPRESSOR OF OVEREXPRESSION OF CO 1/AGAMOUS-LIKE 20 (SOC1/AGL20)* ortholog in rice. *The Plant Journal*, 38, 754-764.
- LI, H., LIANG, W., JIA, R., YIN, C., ZONG, J., KONG, H. & ZHANG, D. 2010. The *AGL6*-like gene *OsMADS6* regulates floral organ and meristem identities in rice. *Cell Res*, 20, 299-313.
- LU, S.-J., WEI, H., WANG, Y., WANG, H.-M., YANG, R.-F., ZHANG, X.-B. & TU, J.-M. 2012. Overexpression of a Transcription Factor *OsMADS15* Modifies Plant Architecture and Flowering Time in Rice (*Oryza sativa* L.). *Plant Molecular Biology Reporter*, 30, 1461-1469.
- NAYAR, S., SHARMA, R., TYAGI, A. K. & KAPOOR, S. 2013. Functional delineation of rice *MADS29* reveals its role in embryo and endosperm development by affecting hormone homeostasis. *Journal of Experimental Botany*, 64, 4239-4253.
- PRASAD, K., PARAMESWARAN, S. & VIJAYRAGHAVAN, U. 2005. *OsMADS1*, a rice MADS-box factor, controls differentiation of specific cell types in the lemma and palea and is an early-acting regulator of inner floral organs. *The Plant Journal*, 43, 915-928.
- SENTOKU, N., KATO, H., KITANO, H. & IMAI, R. 2005. *OsMADS22*, an *STMADS11*-like MADS-box gene of rice, is expressed in non-vegetative tissues and its ectopic expression induces spikelet meristem indeterminacy. *Molecular Genetics and Genomics*, 273, 1-9.

- WANG, H., ZHANG, L., CAI, Q., HU, Y., JIN, Z., ZHAO, X., FAN, W., HUANG, Q., LUO, Z., CHEN, M., ZHANG, D. & YUAN, Z. 2015. OsMADS32 interacts with PI-like proteins and regulates rice flower development. *Journal of Integrative Plant Biology*, 57, 504-513.
- XIAO, H., WANG, Y., LIU, D. F., WANG, W. M., LI, X. B., ZHAO, X. F., XU, J. C., ZHAI, W. X. & ZHU, L. H. 2003. Functional analysis of the rice AP3 homologue OsMADS16 by RNA interference. *Plant Molecular Biology*, 52, 957-966.
- YAMAGUCHI, T., LEE, D. Y., MIYAO, A., HIROCHIKA, H., AN, G. H. & HIRANO, H. Y. 2006. Functional diversification of the two C-class MADS box genes OSMADS3 and OSMADS58 in *Oryza sativa*. *Plant Cell*, 18, 15-28.
- YANG, Z., STEENTOFT, C., HAUGE, C., HANSEN, L., THOMSEN, A. L., NIOLA, F., VESTER-CHRISTENSEN, M. B., FRÖDIN, M., CLAUSEN, H., WANDALL, H. H. & BENNETT, E. P. 2015. Fast and sensitive detection of indels induced by precise gene targeting. *Nucleic Acids Res*, 43, e59.
- YAO, S. G., OHMORI, S., KIMIZU, M. & YOSHIDA, H. 2008. Unequal genetic redundancy of rice PISTILLATA orthologs, OsMADS2 and OsMADS4, in lodicule and stamen development. *Plant and Cell Physiology*, 49, 853-857.
- YUN, D. P., LIANG, W. Q., DRENI, L., YIN, C. S., ZHOU, Z. G., KATER, M. M. & ZHANG, D. B. 2013. OsMADS16 Genetically Interacts with OsMADS3 and OsMADS58 in Specifying Floral Patterning in Rice. *Molecular Plant*, 6, 743-756.